

# COMPUTED POTENTIAL ENERGY SURFACES FOR CHEMICAL REACTIONS

P-160

Semi-Annual Report  
for the period  
January 1, 1990 - June 30, 1990

and  
Three-Year Summary Report  
for the award period  
July 1, 1987 - June 30, 1990

for  
Cooperative Agreement NCC2-478

Submitted to

National Aeronautics and Space Administration  
Ames Research Center  
Moffett Field, California 94035

Computational Chemistry Branch  
Dr. David Cooper, Chief and Technical Monitor

Thermosciences Division  
Dr. Jim Arnold, Chief

Prepared by

ELORET INSTITUTE  
1178 Maraschino Drive  
Sunnyvale, CA 94087  
Phone: 408 730-8422 and 415 493-4710  
Telefax: 408 730-1441

K. Heinemann, President and Grant Administrator  
Stephen P. Walch, Principal Investigator  
26 July 1990

N91-13506

Uncl us  
0296149

H1/25

CSCL 21B

(NASA-CR-186377) COMPUTED POTENTIAL ENERGY  
SURFACES FOR CHEMICAL REACTIONS Semiannual  
Report, 1 Jan. - 30 Jun. 1990 (Eloret  
Corp.) 160 p



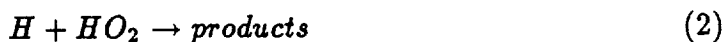
The objective of this grant was to obtain accurate potential energy surfaces (PES's) for a number of reactions which are important in the H/N/O combustion process. The interest in this at NASA centered around the design of the SCRAM jet engine for the National Aerospace Plane (NASP), which was envisioned as an air-breathing hydrogen-burning vehicle capable of reaching velocities as large as Mach 25. Preliminary studies indicated that the supersonic flow in the combustor region of the scram jet engine required accurate reaction rate data for reactions in the H/N/O system, some of which was not readily available from experiment.

Among reactions which are important in the H/N/O system, the following reactions were selected as being critical and were studied in this grant. (The following discussion is organized by class of reaction, while the publications are in chronological order.)

The first class of reactions which were studied are initiation reactions. The dominant initiation reaction in H<sub>2</sub> combustion is thought to be the reaction



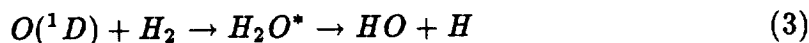
The rate for this reaction has been inferred from the rate of the reverse reaction



This analysis is complex because the reactants give rise to both a triplet surface which leads to H<sub>2</sub> + O<sub>2</sub> as products and a singlet surface which correlates with H<sub>2</sub>O<sub>2</sub> and gives OH as product. The experimental rate is derived from the difference in the rate of disappearance of HO<sub>2</sub> and the rate of appearance of OH. There are considerable uncertainties in the experimental result. Also kinetic models used at Lewis and Langley were not in agreement on the rate of this reaction. In Ref. 14 the saddle point on the triplet surface for reaction (2) was characterized in sufficient detail to permit computation of the rate constant as a function of temperature using transition state theory plus an estimate of tunneling through an Eckart barrier. This computed rate is believed to be the most accurate estimate available for the rate of reaction (2).

Another initiation reaction which was studied is the reaction





This reaction was of interest because the  $^1D$  excited state of O atom reacts with  $H_2$  with no barrier, while the  $^3P$  ground state has an  $\approx 12.5$  kcal/mol barrier. Thus, the excited state might be used to initiate combustion in the SCRAM jet. This study focused on the long range portion of the potential, in particular on the relative barriers to end-on and edge-on insertion of O atom into  $H_2$ . These features of the surface are relevant to difficulties in reproducing, from calculations, the isotopic ratios in the reaction of  $O(^1D)$  with HD. This work is discussed in Ref. 4.

The most important chain propagation mechanism in  $H_2$  combustion is the reaction



A detailed study has been made of this reaction. Ref. 3 focused on the minimum energy path (MEP) region of this surface. Ref. 8 studied the potential for exchanging the H between the two oxygens via a T-shaped  $HO_2$  saddle point. This exchange process is important in the reaction of  $H + O_2$ , since the saddle point is  $\approx 13$  kcal/mol below  $H + O_2$ . The study of this system has culminated in the last year in the generation of enough computed points to provide a global PES for  $H + O_2$ . The  $H + O_2$  and  $HO_2$  portions of the global potential are described in Ref. 13, while the  $OH + O$  portion of the potential is nearly complete and will be published later. At the current time the plan is to collaborate with A.F. Wagner (Argonne National Laboratory) to develop an analytical representation of the computed points and carry out dynamics calculations for reaction (4). Fig. 1 shows a perspective plot of the  $H + O_2$  PES.

The most important class of combustion reactions from the standpoint of the NASP project are radical recombination reactions, since these reactions result in most of the heat release in the combustion process. These processes involve recombination of two radicals (A and B) with a third body (C) to remove enough energy that the resulting AB fragment remains bound. This process is thought

## THE H + O<sub>2</sub> SURFACE

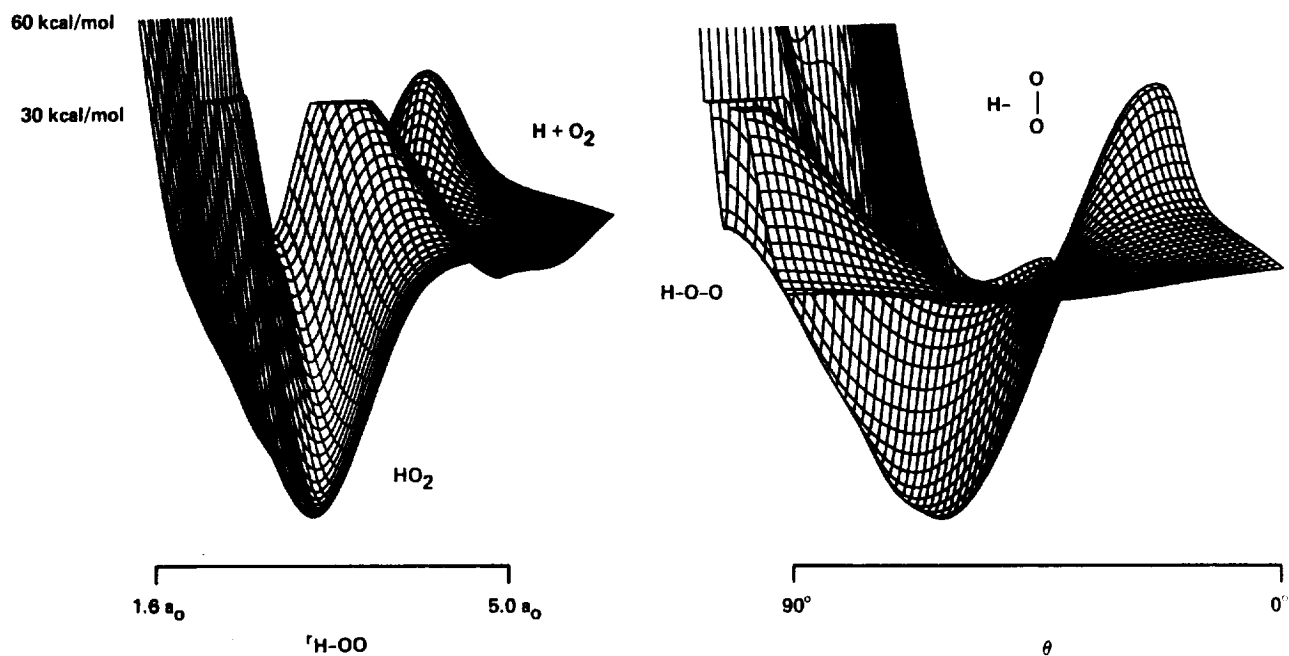


Fig. 1: Global Potential for H + O<sub>2</sub>. See ref. 13. for a detailed discussion.

to involve either i) formation of a metastable AB\* species which transfers energy to C or ii) formation of an intermediate complex AC which subsequently reacts with B to yield AB. An example of the latter process, referred to as a chaperone mechanism, is illustrated by the series of reactions.



The net result of reactions (5) and (6) is recombination of two H atoms with N<sub>2</sub> as a third body.

Calculations described in Refs. 5 and 10 indicate that the  $\text{HN}_2$  molecule is unstable with respect to  $\text{H} + \text{N}_2$  by 3-4 kcal/mol but is quasi-bound due to an  $\approx 12$  kcal/mol barrier to dissociation. The  $\text{HN}_2$  well is able to support 6 vibrational levels and in Ref. 5 the lifetimes for dissociation were estimated using a method which utilizes an Eckart barrier to compute one-dimensional tunneling effects. In Ref. 10 computed points which define a global potential for reaction (5) were reported. The PES for this reaction is shown in Fig. 2. G.S. Schatz (Northwestern) has obtained an analytic representation of the global  $\text{H} + \text{N}_2$  potential and will be carrying out quantum calculations which will determine the rate of formation and decay of  $\text{HN}_2$ . Calculations for reaction (6) are described in Ref. 7. The important conclusion for the recombination process is that reaction (6) has no barrier and thus should proceed at close to the gas kinetic collision frequency. Combining this information it should be possible to obtain estimates of the rate for the overall recombination process.

Another species which may be important in H atom recombination is HNO.



The sequence of reactions (7) and (8) may be important in SCRAM jet simulation studies due to  $\text{NO}_x$  formation by the Zeldovich mechanism. The lowest  $^1\text{A}'$ ,  $^1\text{A}''$ , and  $^3\text{A}''$  surfaces for HNO and HON have been characterized in the minimum energy path regions as discussed in Ref. 9. In a related study, described in Ref. 11, the rate constant for the reaction,



which is an important reaction in nitramine combustion, was computed using transition state theory with a one-dimensional tunneling correction based on an Eckart barrier. While a recommended rate constant expression for reaction (9) existed prior to this work, it was only an estimate based on no data and therefore the computed rate constant is believed to be much more reliable. Fig. 3 shows the computed rate constant for reaction (9).

## THE H + N<sub>2</sub> SURFACE

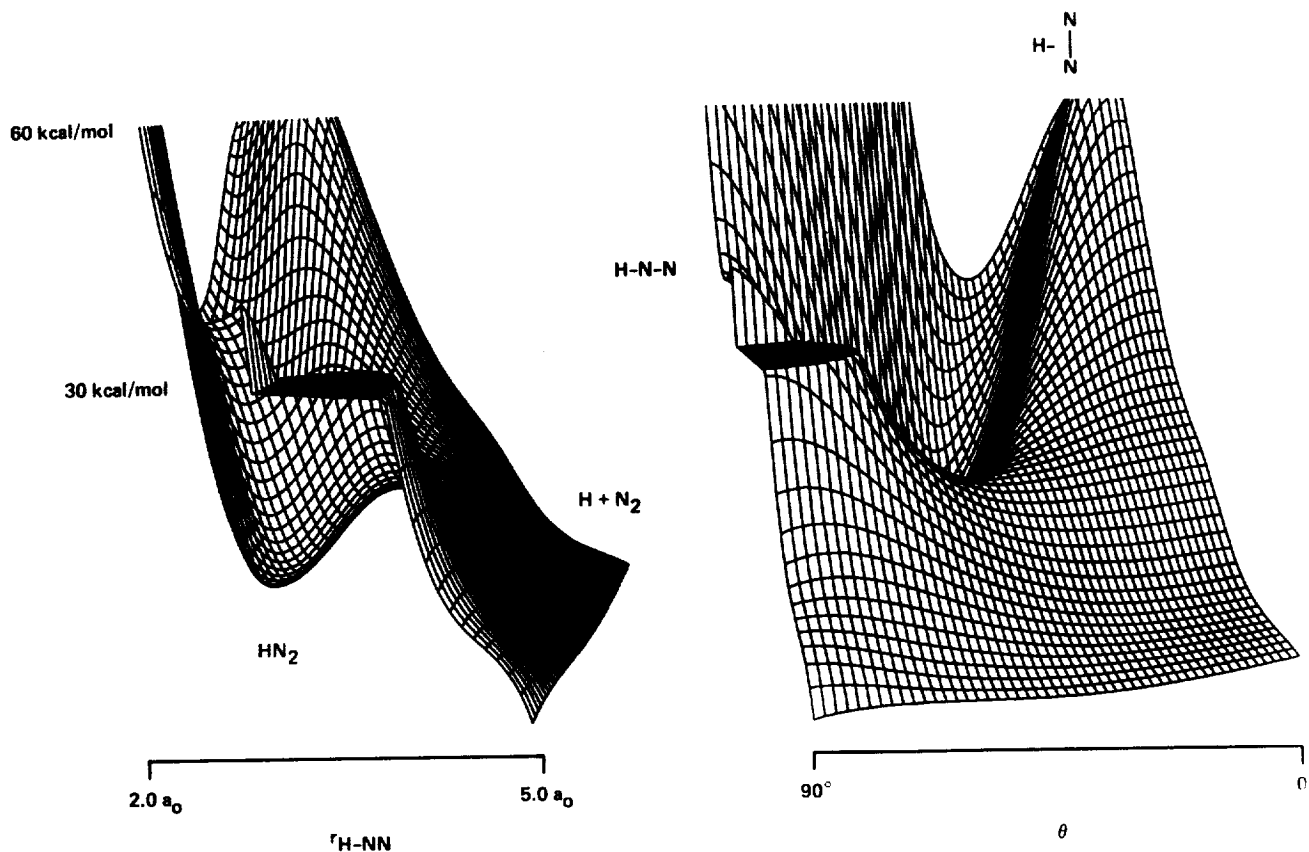


Fig. 2: Global Potential for H + N<sub>2</sub>. See ref. 10. for a detailed discussion.

The last recombination reaction which was considered is



An analytic function has been developed which consists of the known H<sub>2</sub> and H<sub>2</sub>O potentials plus a term which describes the interaction. The interaction term is expanded in terms of OH and OO two body interactions, which were obtained from computed H + H<sub>2</sub>O interactions, and a correction term which was fit based on H<sub>2</sub> + H<sub>2</sub>O interactions. This potential has an overall root-mean-square error of 0.64 mE<sub>h</sub>. This work is described in Ref. 12.

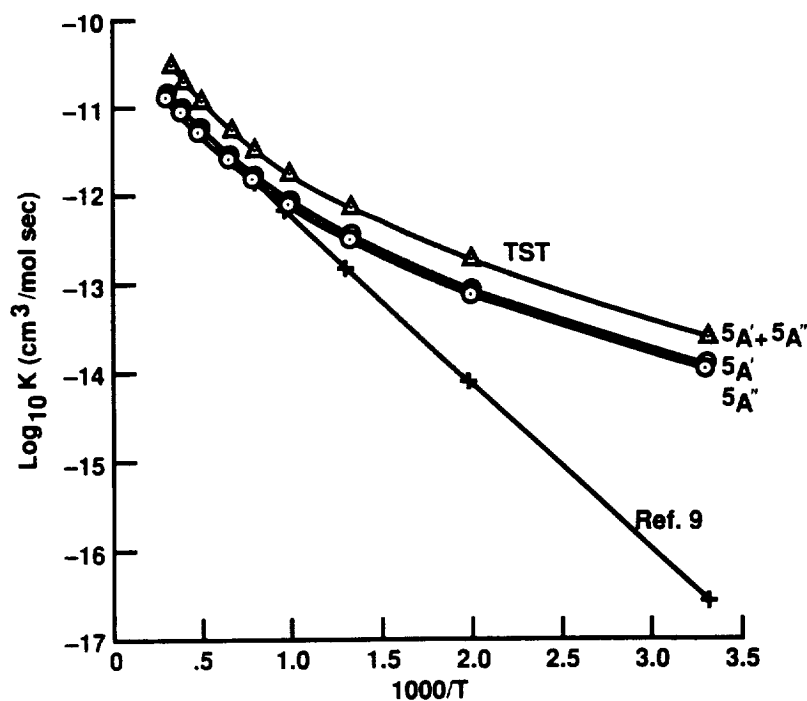


Fig. 3: Computed (transition state theory) rate constant for  $\text{NH} + \text{O} \rightarrow \text{N} + \text{OH}$ . See Ref 11. for a detailed discussion.

#### Publications Resulting from this Grant

1. A Theoretical Study of the Excited States of  $\text{Ag}_3$ , S.P. Walch, J. Chem. Phys., **87**, 6776(1987).
2. Theoretical Studies of the Potential Surface for the  $\text{F} + \text{H}_2 \rightarrow \text{FH} + \text{H}$  Reaction, C.W. Bauschlicher, Jr., S.P. Walch, S.R. Langhoff, P.R. Taylor, and R.L. Jaffe, J. Chem. Phys., **88**, 1743(1988).
3. Theoretical Characterization of the Minimum Energy Path for the Reaction  $\text{H} + \text{O}_2 \rightarrow \text{HO}_2^* \rightarrow \text{HO} + \text{O}$ , S.P. Walch, C.M. Rohlfiing, C.F. Melius, and C.W. Bauschlicher, Jr., J. Chem. Phys., **88**, 6273(1988)
4. An Improved Long Range Potential for  $\text{O}(^1\text{D}) + \text{H}_2$ , S.P. Walch and L.B. Harding, J. Chem. Phys., **88**, 7653(1988)
5. Theoretical Characterization of the Minimum Energy Path for Hydrogen Atom Addition to  $\text{N}_2$ : Implications for the Unimolecular Lifetime of  $\text{HN}_2$ , S.P. Walch, R.J. Duchovic, and C.M. Rohlfiing, J. Chem. Phys., **90**, 3230(1989).

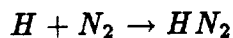
6. Computed Potential Energy Surfaces for Chemical Reactions, S.P. Walch and C.M. Rohlfiing, in Supercomputer Algorithms for Reactivity, Dynamics, and Kinetics of Small Molecules, ed. by A. Lagana (Kluwer Academic Publishers, Dordrecht, 1989).
7. Theoretical Characterization of Selected Regions of the Ground State Potential Surface of  $N_2H_2$ ., S.P. Walch, J. Chem. Phys., **91**, 389(1989).
8. Theoretical Characterization of the Potential Energy Surface for  $H + O_2 \rightarrow HO_2^* \rightarrow HO + O$ , II. The Potential for H Atom Exchange in  $HO_2$ ., S.P. Walch and C.M. Rohlfiing, J. Chem. Phys., **91**, 2373(1989).
9. Theoretical Characterization of the Lowest Three Potential Surfaces of  $HNO$ , I. The Potential for H Atom Addition to  $NO$ ., S.P. Walch and C.M. Rohlfiing, J. Chem. Phys., **91**, 2939(1989).
10. Theoretical Characterization of the Potential Energy Surface for  $H + N_2 \rightarrow HN_2$ , II. Computed Points to Define a Global Potential., S.P. Walch, J. Chem. Phys., in press.
11. Theoretical Characterization of the  $^5\Pi$  and  $^3\Pi$  Potential Energy Surfaces for  $NH + O \rightarrow N + OH$ ., S.P. Walch, J. Chem. Phys., submitted.
12. A Potential Energy Surface for  $H_2 + H_2O$ : ab initio calculations and analytical representation., D.W. Schwenke, S.P. Walch, and P.R. Taylor, J. Chem. Phys., in preparation.
13. Theoretical Characterization of the Potential Energy Surface for  $H + O_2 \rightarrow HO_2^* \rightarrow HO + O$ , III. Computed Points to Define a Global Potential for  $H + O_2$ ., S.P. Walch and R.J. Duchovic, J. Chem. Phys., in preparation.
14. Computed Reaction Rate for  $H + HO_2 \rightarrow H_2 + O_2$ ., S.P. Walch and R.L. Jaffe, J. Chem. Phys., in preparation.

## **Appendix**

The appendix contains copies of Ref's 10-14 which have not yet appeared as journal articles.



**Theoretical Characterization of the Potential Energy Surface  
for**



**II. Computed Points to Define a Global Potential**

Stephen P. Walch<sup>a</sup>  
ELORET Institute  
Sunnyvale, Ca. 94087

Abstract. A previous calculation for  $H + N_2$  [Walch, Duchovic, and Rohlfing, J. Chem. Phys, 90, 3230(1989)] focused on the minimum energy path (MEP) region of the potential energy surface and on estimates of the lifetime of the  $HN_2$  species. In this paper, we report energies computed at geometries selected to permit a global representation of the potential energy surface (PES). As in the previous work, the calculations were performed using the complete active space self consistent field / externally contracted configuration interaction (CASSCF/CCI) method. The surface was characterized using the same basis set as in the previous paper except that an improved contraction of the H s basis is used. Calculations with a larger basis set were carried out along an approximate MEP obtained with the smaller basis set. The new PES exhibits a sharp curvature, which was not present in the previous calculations, and has a slightly narrower and smaller barrier to dissociation. Saddle points for H atom exchange via collinear and T-shaped  $HN_2$  complexes are also reported.

<sup>a</sup>Mailing Address: NASA Ames Research Center, Moffett Field, CA 94035.

## I. Introduction

The  $\text{HN}_2$  species has been postulated as an important intermediate in thermal De- $\text{NO}_x$  processes [1-4]. Indirect evidence for the existence of this species has been obtained from experimental studies of the reaction:



Studies of reaction (1) have considered three possible product channels [5]:



While the experimental studies varied widely as to the branching ratio for OH production, none of the experiments observed H atoms [5]. This result, along with the product channels assumed here, argues for the existence of the  $\text{HN}_2$  species.

Given the possible importance of the  $\text{HN}_2$  species in combustion processes, there have been several theoretical and experimental studies directed toward estimating its lifetime. A recent ab-initio study [6] (hereafter referred to as I) of the minimum energy path (MEP) region of the  $\text{HN}_2$  surface found the  $\text{HN}_2$  species to be unstable with respect to  $\text{H} + \text{N}_2$  by 3.0 kcal/mol, but to be quasi-bound due to a 12.2 kcal/mol barrier to dissociation (before zero-point correction). In I the lifetime of the  $\text{HN}_2$  species was estimated using a method which utilizes an Eckart barrier to compute one-dimensional tunneling effects. The lifetime of the lowest vibrational level was estimated to be between  $8.8 \times 10^{-11}$  and  $5.8 \times 10^{-9}$  sec. This lifetime is somewhat longer than the value of  $5 \times 10^{-11}$  obtained theoretically by Curtiss et al. [7]. The short lifetime of  $\text{HN}_2$  obtained by theory has been supported by

the recent experimental work of Selgren et al. [8], who estimate the ground state lifetime of  $\text{HN}_2$  to be less than  $5 \times 10^{-7}$  sec. Thus, both theory and experiment suggest a short lifetime for  $\text{HN}_2$ , which limits its role in combustion processes. This is in contrast to combustion models [9] which require lifetimes at least several orders of magnitude longer than current estimates.

Previous theoretical studies of the lifetime of the  $\text{HN}_2$  species were based on a one-dimensional estimate of tunneling. In order to obtain a more accurate estimate of quantum mechanical effects for this reaction a global potential energy surface is required. Computations directed toward that goal are reported herein. The computational method is discussed in Section II, the results are presented in Section III, and the conclusions are given in Section IV.

## II. Computational Details.

The calculations used the CASSCF/CCI method [10,11] with a selected reference list. The details of these calculations are given in I. Two basis sets were used. The first basis set was the same as that given in I except for two changes in the H basis set. The original H basis used as contraction coefficients the natural orbitals from a CI calculation on  $\text{H}_2$ , as described by Almlöf and Taylor [12], however using only three contracted s type functions leads to an  $\approx 1$  kcal/mol error in the H atom energy, thus we replace the first contracted s type function with the SCF orbital for the H atom. In addition, the d function on H was omitted since it was found to have only a very small contribution to the energy. The first basis set is  $[4s3p2d1f/3s^*2p]$  and is referred to as basis set 1, where  $3s^*$  indicates the modified contraction of the H s functions. The second basis set, which is  $[5s4p3d2f/4s^*3p2d]$  and is referred to as basis set 2, is that given by Almlöf and Taylor except for the modified contraction of the H s functions.

The relative positions of the atoms for these calculations are specified in terms of

the NN distance ( $r_{NN}$ ), the H to center of mass of  $N_2$  distance ( $r_{H-NN}$ ), and the angle ( $\theta$ ) between a line connecting H to the center of mass of  $N_2$  and a normal to the NN bond at the bond midpoint ( $\theta$  is  $0^\circ$  for T-shaped  $H-N_2$  and  $90^\circ$  for collinear  $H-N_2$ ).

Most of the calculations were carried out in  $C_s$  symmetry. As discussed below, some of the calculations for  $\theta = 0^\circ$  and  $90^\circ$  used  $C_{2v}$  symmetry.  $\theta$  was varied from  $0^\circ$  through  $90^\circ$  in  $10^\circ$  increments. For each  $\theta$  value both  $r_{H-NN}$  and  $r_{NN}$  were varied to obtain minimum energy cuts at fixed  $\theta$  values.

The calculations were carried out on the NASA Ames Cray Y-MP/832. These calculations used the MOLECULE[13]-SWEDEN[14] system of programs.

### III. Results and Discussion

The computed energies are given in Table AI of the appendix. In order to aid in visualizing the surface, the energy was evaluated along fixed  $\theta$  minimum energy cuts. For each  $\theta$  and  $r_{H-NN}$ ,  $r_{NN}$  was varied and the energy at the minimum and the optimal  $r_{NN}$  are given in Table I. These minimum energy cuts are shown graphically in Figs. 1 and 2.

From Fig. 1 it is evident that for large  $r_{H-NN}$  a T-shaped  $H-N_2$  geometry is favored. This geometrical arrangement minimizes non-bonded H-N repulsions in the long-range repulsive region of the potential. As discussed in ref. 6, at shorter  $r_{H-NN}$  an NH bond is formed leading to a chemically bonded bent  $HN_2$  species. This structure has an  $\angle HNN$  of  $\approx 120^\circ$  ( $\theta \approx 50^\circ$ ). At  $r_{H-NN} \approx 3.5 a_0$ , the bent HNN structure drops below the T-shaped structure leading to a sharp curvature in the reaction path. Formation of  $HN_2$  involves breaking an NN  $\pi$  bond as the HN bond forms with a resultant barrier. As is evident from Fig. 1, the barrier occurs at approximately the same  $r_{H-NN}$  as the sharp change in  $\theta$ . This reflects a crossing between the T-shaped structure, which is lowest in the repulsive part of the surface,

and the bent  $\text{HN}_2$  structure, which is more stable in the chemically bonded region of the surface.

It should be noted here that the PES obtained in I did not show the sharp curvature in  $\theta$  which is evident in the present PES. This difference appears to be a basis set effect. The basis set used in I placed the T-shaped structure too high with respect to the bent  $\text{HN}_2$  structure and thus the bent structure remains lowest at larger  $r_{H-NN}$ . From Fig. 2 it is evident that the surface is quite flat with respect to variations in  $\theta$  for  $r_{H-NN}$  larger than the  $\approx 4.0 a_0$ . Thus, the sharp curvature in  $\theta$  observed in the present work may not be especially significant in the dynamics of  $\text{H} + \text{N}_2$  collisions.

In order to define an approximate MEP, polynomial fits ( six-term quadratic in  $r_{NN}$  and  $\theta$ ) were obtained at each  $r_{H-NN}$  distance using the three  $\theta$  values nearest the minimum and three values of  $r_{NN}$  (9 points). At the  $\text{HN}_2$  minimum and entrance channel saddle point ten-term quadratic polynomials in all three coordinates were obtained to define the stationary points. It should be noted that this procedure defines the stationary points rigorously (within the accuracy of the polynomial fit), but the MEP connecting the stationary points is only obtained approximately as defined above. The primary problem with the approximate procedure used here to define the MEP is that the reaction coordinate is taken as  $r_{H-NN}$  and therefore variations of the energy along this coordinate are not allowed. In order to indicate that this constraint has been imposed we designate the approximate MEP obtained here as a constrained energy minimum path (CEM). The CEM is given in Table II. Additional calculations were carried out along the CEM using the [5s4p3d2f/4s\*3p2d] basis set. These results are also given in Table II. In Fig. 3, the energy along the CEM with both basis sets is compared with the energy along the CEM of ref. 6 (using the basis set of ref. 6). From Fig. 3 it is seen that the present calculations give

a narrower barrier and smaller barrier height to  $\text{HN}_2$  dissociation. Both of these changes result from the improved contraction of the H s basis set which stabilizes  $\text{H} + \text{N}_2$  with respect to  $\text{HN}_2$ .

Table III shows the geometrical parameters of the stationary points on the  $\text{HN}_2$  surface. For the  $\text{HN}_2$  minimum and H- $\text{N}_2$  entrance channel saddle point the geometries are compared to the results obtained in I. Here it is seen that at the  $\text{HN}_2$  minimum the bond lengths are within  $0.01 a_0$  and the bond angle is within  $1^\circ$  of the values obtained in I. These differences are probably within the precision of the fits used to derive the geometrical parameters. For the H- $\text{N}_2$  minimum, on the other hand, the differences are larger. This difference reflects the changes in the large  $r_{\text{H}-\text{NN}}$  portion of the surface as discussed above. The relative energies are also given in Table III. Here it is seen that the best estimate ( $[5s4p3d2f/4s^*3p2d]$  basis set energies at the geometry obtained with the  $[4s3p2d1f/3s^*2p]$  basis) is that the bottom of the  $\text{HN}_2$  well is 3.9 kcal/mol above the bottom of the  $\text{H} + \text{N}_2$  well as compared to 3.0 kcal/mol from I. The barrier to dissociation at the same level of calculation is 11.3 kcal/mol as compared to 12.2 kcal/mol from I.

Fig. 4 and Fig. 5 compare the variation of  $\theta$  and  $r_{\text{NN}}$  along the CEM as a function of  $r_{\text{H}-\text{NN}}$  for the present work and the calculations in I. From Fig. 4 it is seen that the  $\theta$  variation is quite different in the present work, with  $\theta$  rising sharply from  $0^\circ$  at  $r_{\text{H}-\text{NN}}$  about  $3.75 a_0$ , but for smaller  $r_{\text{H}-\text{NN}}$   $\theta$  is similar. On the other hand, from Fig. 5 it is seen that the variation in  $r_{\text{NN}}$  is quite similar for the present work and ref. I. These results are consistent with the observations made above.

Figs. 1 and 2 also shows higher energy regions of the surface corresponding to  $\theta$  values near  $0^\circ$  and  $90^\circ$ . Here it is evident that there are saddle points for H atom exchange (i.e. motion of an H atom between symmetry equivalent minima on the potential energy surface) along cuts with  $\theta = 0^\circ$  and  $90^\circ$ . For these two choices of  $\theta$

the actual symmetry is  $C_{2v}$  and the barrier (maximum on the surface) prior to the saddle point corresponds to a curve crossing ( ${}^2A_1 \rightarrow {}^2B_2$  for  $\theta = 0^\circ$  and  ${}^2\Sigma^+ \rightarrow {}^2\Pi$  for  $\theta = 90^\circ$ ). To clarify these regions of the surface, we report energies for both electronic states involved in the curve crossing. For  $\theta = 90^\circ$  the calculations for both states were carried out in  $C_{2v}$  symmetry leading to an actual curve crossing which is evident in Fig. 1 and Table I. For  $\theta = 90^\circ$ , the  ${}^2B_2$  symmetry points were computed in  $C_{2v}$  symmetry, while the  ${}^2A_1$  symmetry points were computed in  $C_s$  symmetry. While this region of the surface should also exhibit a curve crossing, this region of the surface is plotted in Fig. 1 as if there were an avoided crossing. Since this region of the surface is  $\approx 60$  kcal/mol above  $H + N_2$ , this inconsistency should not be important. Table III also shows the saddle point geometries and barriers for the two exchange saddle points. Both of these saddle points are above the barrier height for dissociation of  $HN_2$  to  $H + N_2$ .

#### IV. Conclusions.

Previous studies [6] of the  $H + N_2$  surface have been extended by the use of improved basis sets and consideration of larger regions of the surface, with the goal of mapping out a global potential energy surface suitable for use in dynamical studies.

Most of the surface has been characterized with a  $[4s3p2d1f/3s^*2p]$  basis set which differs from the basis set used in ref. 6 only in the contraction of the H s basis. This basis provides a more balanced description of free H atom and bonded H (as in  $HN_2$ ).

In the large  $r_{H-NN}$  region, the CEM for H atom addition to  $N_2$  obtained with the new basis set is different from that obtained in ref. 6. The new CEM shows a sharp curvature in the vicinity of the saddle point for H atom addition, with  $\theta$  decreasing sharply to  $0^\circ$  (T-shaped  $HN_2$  structure) for  $r_{H-NN}$  greater than  $3.5 a_0$ . In the region

of the  $\text{HN}_2$  minimum the new surface and that of ref. 6 appear to be similar as evidenced by essentially identical  $\text{HN}_2$  equilibrium geometries. Calculations using a [5s4p3d2f/4s\*3p2d] basis set along the CEM defined with the [4s3p2d1f/3s\*2p] basis set place  $\text{HN}_2$  3.9 kcal/mol above  $\text{H} + \text{N}_2$  and predict a barrier to dissociation of 11.3 kcal/mol (before correction for zero-point energy). These energetics are within 1 kcal/mol of those predicted in ref. 6.

The barrier height for dissociation of  $\text{HN}_2$  to  $\text{H} + \text{N}_2$  is slightly smaller and the barrier is slightly narrower than in the calculations of ref. 6. Within a one-dimensional tunneling model, this result suggests an even shorter lifetime for  $\text{HN}_2$  than had been predicted in ref. 6.

It should be noted here that one reaction which has not been previously considered is:



Recent studies of the potential energy surface for this reaction [15] indicate no barrier for H abstraction. Thus, though the lifetime of  $\text{HN}_2$  is short, it is very reactive toward H atom, and if formed could effectively scavenge H atoms formed in Eq. (3). This could account for the failure to observe H atoms even if both Eq. (3) and Eq. (4) are important product channels.

Saddle points have also been characterized for H atom exchange via T-shaped and collinear  $\text{HN}_2$  complexes. The barrier heights with the [4s3p2d1f/3s\*2p] basis set are 46.0 and 29.8 kcal/mol for these two processes, respectively.

#### ACKNOWLEDGMENTS

S.P. Walch was supported by a NASA grant(NCC2-478).

## References

1. J.A. Miller, M.C. Branch, and R.J. Kee, *Combust. Flame*, **43**, 81(1981).
2. R.K. Lyon, Sandia Laboratories Report No. SAND70-8635, 1970.
3. R.K. Lyon, U.S. Patent 3,900,544, August 1975.
4. R.K. Lyon, *Int. J. Chem. Kinet.*, **8**, 315(1976).
5. see ref. 6 and references therein.
6. S.P. Walch, R.J. Duchovic, and C.M. Rohlfig, *J. Chem. Phys.*, **90**, 3230(1989).
7. L.A. Curtiss, D.L. Drapcho, and J.A. Pople, *Chem. Phys. Lett.*, **103**, 437(1984).
8. S.F. Selgren, P.W. McLoughlin, and G.I. Gellene, *J. Chem. Phys.*, **90**, 1624(1989).
9. J.A. Miller, private communication.
10. P.E.M. Siegbahn, A. Heiberg, B. Roos, and B. Levy, *Phys. Scr.* **21**, 323(1980).
11. P.E.M. Siegbahn, *Int. J. Quantum Chem.* **23**, 1869(1983).
12. J. Almlöf and P.R. Taylor, *J. Chem. Phys.* **86**, 4070(1987).
13. J. Almlöf, MOLECULE, a vectorized Gaussian integral program.
14. SWEDEN is a vectorized SCF-MCSCF-direct CI- conventional CI-CPF-MCPF program written by P.E.M. Siegbahn, C.W. Bauschlicher, Jr., B. Roos, P.R. Taylor, A. Heiberg, J. Almlöf, S.R. Langhoff, and D.P. Chong.
15. S.P. Walch, *J. Chem. Phys.*, **91**, 389(1989).

Table I. H + N<sub>2</sub> energy along fixed  $\theta$  cuts<sup>a</sup>.

$r_{H-NN}$	$\theta$	$r_{NN}$	Energy <sup>b</sup>	$\delta E(\text{kcal/mol})^c$
5.0	0.0	2.1	-0.88024	1.19
4.5	0.0	2.1	-0.87748	2.92
4.0	0.0	2.1	-0.87145	6.70
3.75	0.0	2.1	-0.86629	9.94
3.5	0.0	2.098	-0.85890	14.58
3.25	0.0	2.099	-0.84837	21.18
3.0	0.0	2.102	-0.83334	30.62
2.75	0.0	2.106	-0.81194	44.04
2.25	0.0	2.356	-0.79226	56.39 <sup>d</sup>
2.0	0.0	2.369	-0.80010	51.47 <sup>d</sup>
1.75	0.0	2.435	-0.79515	54.58 <sup>d</sup>
5.0	10.0	2.1	-0.88017	1.23
4.5	10.0	2.1	-0.87734	3.01
4.0	10.0	2.1	-0.87127	6.81
3.75	10.0	2.1	-0.86615	10.03
3.5	10.0	2.099	-0.85893	14.56
3.25	10.0	2.102	-0.84885	20.88
3.0	10.0	2.109	-0.83509	29.52
2.75	10.0	2.126	-0.81729	40.69
2.5	10.0	2.264	-0.80302	49.64
2.25	10.0	2.322	-0.81092	44.68
2.0	10.0	2.351	-0.81407	42.71
1.75	10.0	2.385	-0.80219	50.16
5.0	20.0	2.1	-0.87994	1.37
4.5	20.0	2.1	-0.87693	3.26
4.0	20.0	2.1	-0.87073	7.15

3.75	20.0	2.1	-0.86573	10.29
3.5	20.0	2.103	-0.85903	14.50
3.25	20.0	2.111	-0.85043	19.89
3.0	20.0	2.128	-0.84046	26.15
2.75	20.0	2.183	-0.83181	31.58
2.5	20.0	2.260	-0.83275	30.99
2.25	20.0	2.306	-0.83593	28.99
2.0	20.0	2.331	-0.82961	32.96
1.75	20.0	2.374	-0.80068	51.11
5.0	30.0	2.1	-0.87950	1.65
4.5	30.0	2.1	-0.87612	3.77
4.0	30.0	2.1	-0.86962	7.85
3.5	30.0	2.109	-0.85898	14.53
3.25	30.0	2.126	-0.85298	18.29
3.0	30.0	2.162	-0.84863	21.02
2.75	30.0	2.226	-0.85129	19.35
2.5	30.0	2.268	-0.85609	16.34
2.25	30.0	2.297	-0.85048	17.23
2.0	30.0	2.314	-0.83173	31.63
1.75	30.0	2.360	-0.77193	69.15
5.0	40.0	2.1	-0.87876	2.11
4.5	40.0	2.1	-0.87474	4.64
4.0	40.0	2.1	-0.86761	9.11
3.5	40.0	2.119	-0.85846	14.85
3.25	40.0	2.143	-0.85564	16.62
3.0	40.0	2.204	-0.85913	14.43
2.75	40.0	2.224	-0.86698	9.51
2.5	40.0	2.281	-0.87015	7.52
2.25	40.0	2.259	-0.85459	17.28
2.0	40.0	2.263	-0.79989	51.61

5.0	50.0	2.1	-0.87767	2.80
4.5	50.0	2.1	-0.87264	5.96
4.0	50.0	2.1	-0.86425	11.22
3.5	50.0	2.131	-0.85652	16.07
3.25	50.0	2.177	-0.85758	15.41
3.0	50.0	2.229	-0.86608	10.07
2.75	50.0	2.248	-0.87320	5.60
2.5	50.0	2.237	-0.86772	9.04
2.25	50.0	2.208	-0.82346	36.82
2.0	50.0	2.157	-0.71216	106.66
5.0	60.0	2.1	-0.87627	3.68
4.5	60.0	2.1	-0.86980	7.74
4.0	60.0	2.1	-0.85911	14.45
3.5	60.0	2.141	-0.85060	19.78
3.25	60.0	2.206	-0.85444	17.38
3.0	60.0	2.241	-0.86436	11.15
2.75	60.0	2.242	-0.86608	10.07
2.5	60.0	2.190	-0.84011	26.37
2.25	60.0	2.116	-0.75716	78.42
5.0	70.0	2.1	-0.87477	4.62
4.5	70.0	2.1	-0.86655	9.78
4.0	70.0	2.1	-0.85207	18.86
3.5	70.0	2.147	-0.83766	27.91
3.25	70.0	2.234	-0.84331	24.36
3.0	70.0	2.248	-0.85270	18.47
2.75	70.0	2.209	-0.84521	23.17
2.5	70.0	2.130	-0.79685	53.51
5.0	80.0	2.1	-0.87357	5.37

4.5	80.0	2.1	-0.86376	11.53
4.0	80.0	2.1	-0.84485	23.39
3.5	80.0	2.135	-0.81577	41.64
3.25	80.0	2.279	-0.82676	34.75
3.0	80.0	2.250	-0.83652	28.62
2.75	80.0	2.184	-0.82043	38.72
2.5	80.0	2.088	-0.75359	80.66
10.0	90.0	2.1	-0.88213	0.00
6.05	90.0	2.1	-0.88057	0.98
5.05	90.0	2.1	-0.87371	5.28
4.55	90.0	2.1	-0.86392	11.43
4.05	90.0	2.1	-0.84428	23.75
3.75	90.0	2.1	-0.82357	36.75
3.5	90.0	2.060	-0.79957	51.8 <sup>e</sup>
3.5	90.0	2.332	-0.79301	55.9 <sup>f</sup>
3.25	90.0	2.295	-0.81616	41.40
3.0	90.0	2.241	-0.82552	35.52
2.75	90.0	2.169	-0.80590	47.84

<sup>a</sup> Unless otherwise noted energies are in  $E_H$ , bond lengths are in  $a_0$ , and angles are in degrees.

<sup>b</sup> The energy includes a multireference Davidson's correction (See Ref. I) and is relative to  $-109.00000 E_H$ .

<sup>c</sup> Energy relative to the  $H + N_2$  asymptote.

<sup>d</sup> These points are for the  ${}^2B_2$  state and are computed with  $C_{2v}$  symmetry.

<sup>e</sup> This point and preceding points for  $\theta = 90^\circ$  are for the  ${}^2\Sigma^+$  state and are computed with  $C_{2v}$  symmetry.

<sup>f</sup> This point and preceding points for  $\theta = 90^\circ$  are for the  ${}^2\Sigma^+$  state and are computed with  $C_{2v}$  symmetry.

Table II. Computed Energies for  $\text{HN}_2$  Along the CEM<sup>a</sup>.

$r_{H-NN}$	$r_{NN}$	$\theta$	Energy(bs 1 <sup>b</sup> )	Energy(bs 2 <sup>c</sup> )
20.5	2.095	32.5	(-.88213)	0.0
10.0	2.1	0.0		-109.87596(-.89360) 0.0
5.0	2.1	0.0	(-.88024)	1.2 -109.87402(-.89190) 1.07
4.5	2.1	0.0	(-.87748)	2.9 -109.87118(-.88929) 2.70
4.0	2.1	0.0	(-.87145)	6.7 -109.86501(-.88354) 6.31
3.75	2.1	0.0	(-.86629)	9.9 -109.85974(-.87860) 9.41
3.5	2.11	28.4	(-.85905)	14.5 -109.85125(-.87170) 13.74
3.35	2.17	48.5	(-.85698)	15.8 -109.84416(-.86936) 15.21
3.25	2.17	48.9	(-.85766)	15.3 -109.84520(-.87102) 14.17
3.00	2.23	52.9	(-.86636)	9.9 -109.85240(-.88010) 8.47
2.75	2.24	49.6	(-.87307)	5.7 -109.86002(-.88713) 4.06
2.69	2.25	47.3	(-.87321)	5.6 -109.86037(-.88732) 3.94
2.5	2.26	43.1	(-.87075)	7.1 -109.85655(-.88656) 4.42

<sup>a</sup> Unless otherwise noted energies are in  $E_H$ , bond lengths are in  $a_0$ , and angles are in degrees.

<sup>b</sup> [4s3p2d1f/3s\*2p] ANO basis set. Selected reference ( $C_i > 0.05$ ) CASSCF/CCI calculations correlating eleven electrons. The values in parenthesis include a multi-reference Davidson's correction (See Ref. 1) and are relative to  $-109.00000 E_H$ . The second column of numbers are relative energies in kcal/mol.

<sup>c</sup> [5s4p3d2f/4s3p2d] ANO basis set. Selected reference ( $C_i > 0.05$ ) CASSCF/CCI calculations correlating eleven electrons. The first column gives the CCI and CCI + Davidson's correction total energies (in  $E_H$ ), while the second column gives relative energies in kcal/mol.

Table III. Stationary Points on the H + N<sub>2</sub> Surface<sup>a</sup>.

	H-N <sub>2</sub>	HN <sub>2</sub>	H-N <sub>2</sub> ( $\theta=0^\circ$ )	H-N <sub>2</sub> ( $\theta=90^\circ$ )
$r_{NN}$	2.173	2.253	2.390	2.240
$r_{H-NN}$	3.355	2.695	1.955	3.052
$\theta$	48.5	47.3	0.0	90.0
$r_{NH}$	2.641	2.017		
$\theta'^b$	122.7	115.0		
E(bs 1)	15.8	5.6	51.6	35.4
E(bs 2)	15.2	3.9		
$r_{NN}^b$	2.146	2.262		
$r_{NH}^b$	2.753	2.007		
$\theta'^b$	118.6	116.3		
E <sup>c</sup>	15.2	3.0		

<sup>a</sup> Bond lengths are in a<sub>0</sub>, angles are in degrees, and energies are in kcal/mol relative to the H + N<sub>2</sub> asymptote.

<sup>b</sup>  $\angle$  HNN.

<sup>c</sup> values from ref. 6.

### Figure Captions.

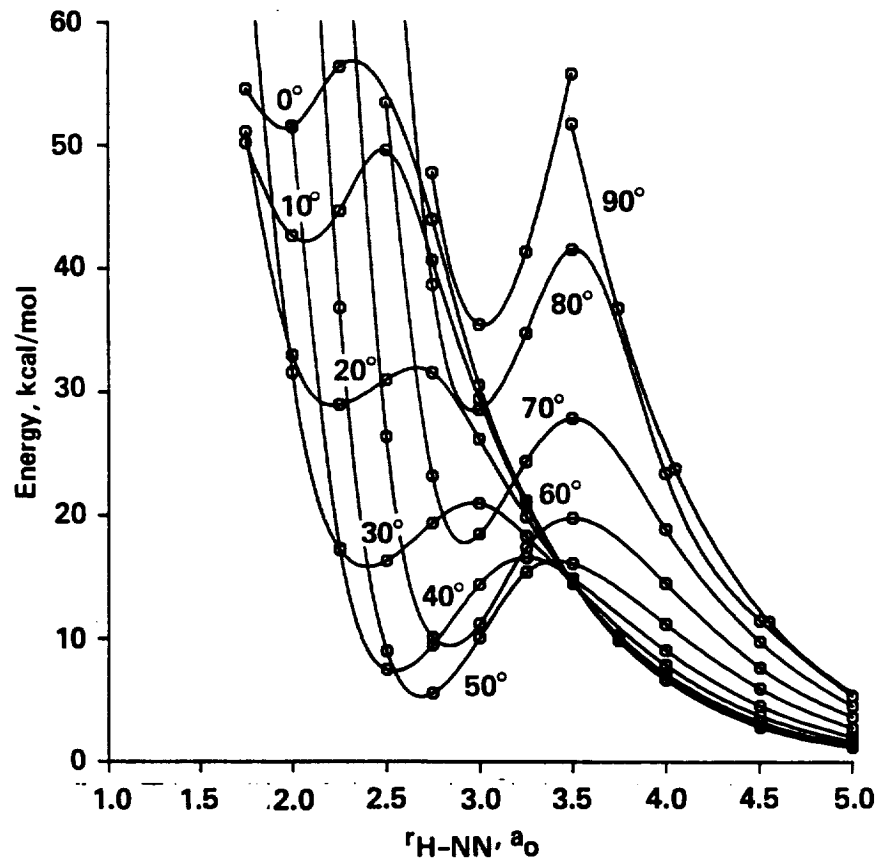
Fig. 1. Potential surface for  $\text{H} + \text{N}_2$ . The figure shows ten fixed  $\theta$  minimum energy cuts. For each  $r_{\text{H}-\text{NN}}$ ,  $r_{\text{NN}}$  was varied and the minimum energy is shown in the figure.

Fig. 2. Potential surface for  $\text{H} + \text{N}_2$ . The figure shows the same information as in Fig. 1 in the format of a perspective plot.

Fig. 3. Comparison of energy as a function of  $r_{\text{H}-\text{NN}}$  along the CEM from I and the present calculations. For the present calculations results are shown with both basis sets.

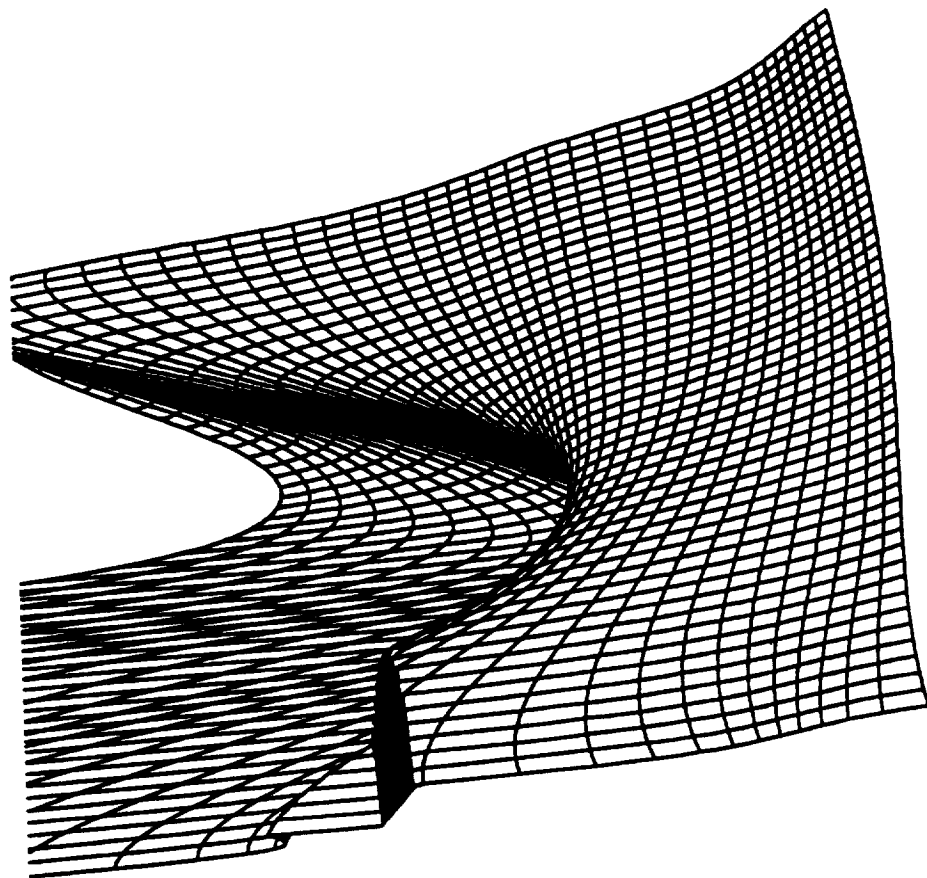
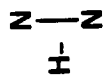
Fig. 4. Comparison of  $\theta$  as a function of  $r_{\text{H}-\text{NN}}$  for the CEM from I and the present work.

Fig. 5. Comparison of  $r_{\text{NN}}$  as a function of  $r_{\text{H}-\text{NN}}$  for the CEM from I and the present work.



Walch-1

# THE H + N<sub>2</sub> SURFACE

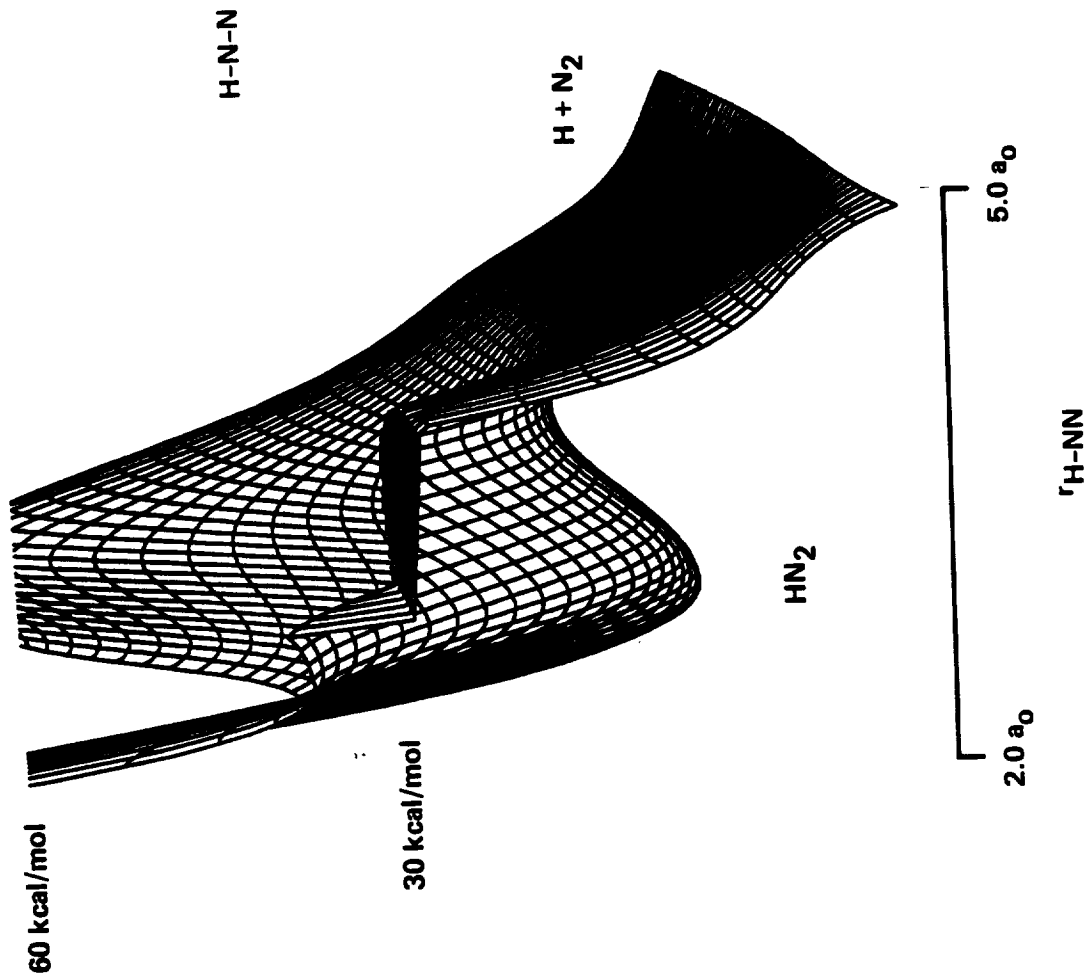


90°

$\theta$

0°

Wair



60 kcal/mol

30 kcal/mol

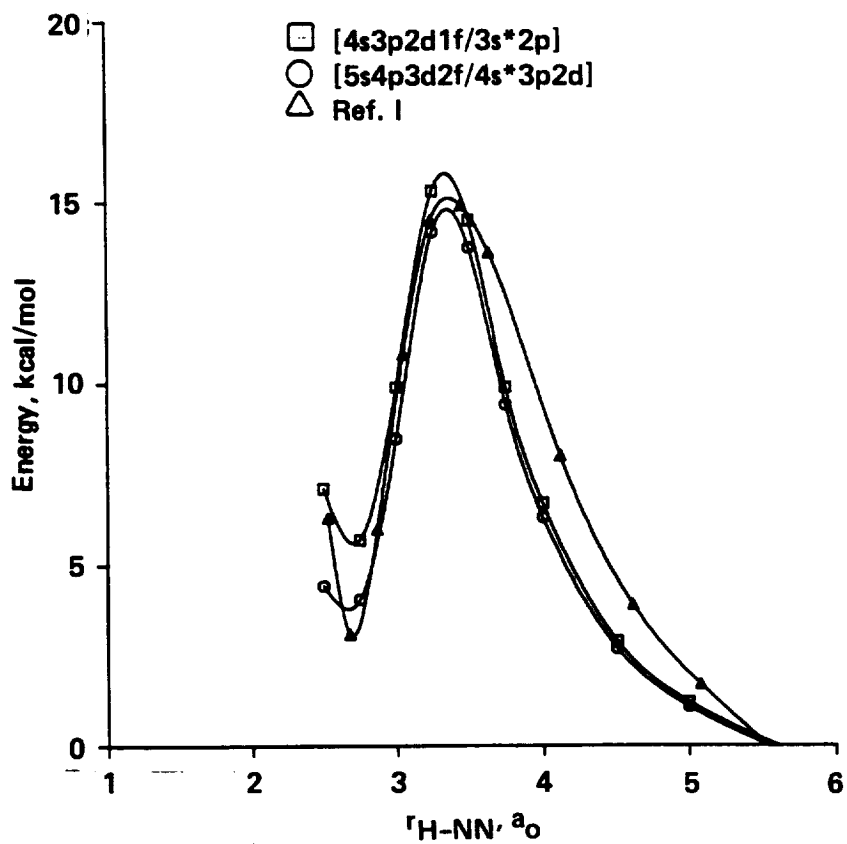
H + N<sub>2</sub>

HN<sub>2</sub>

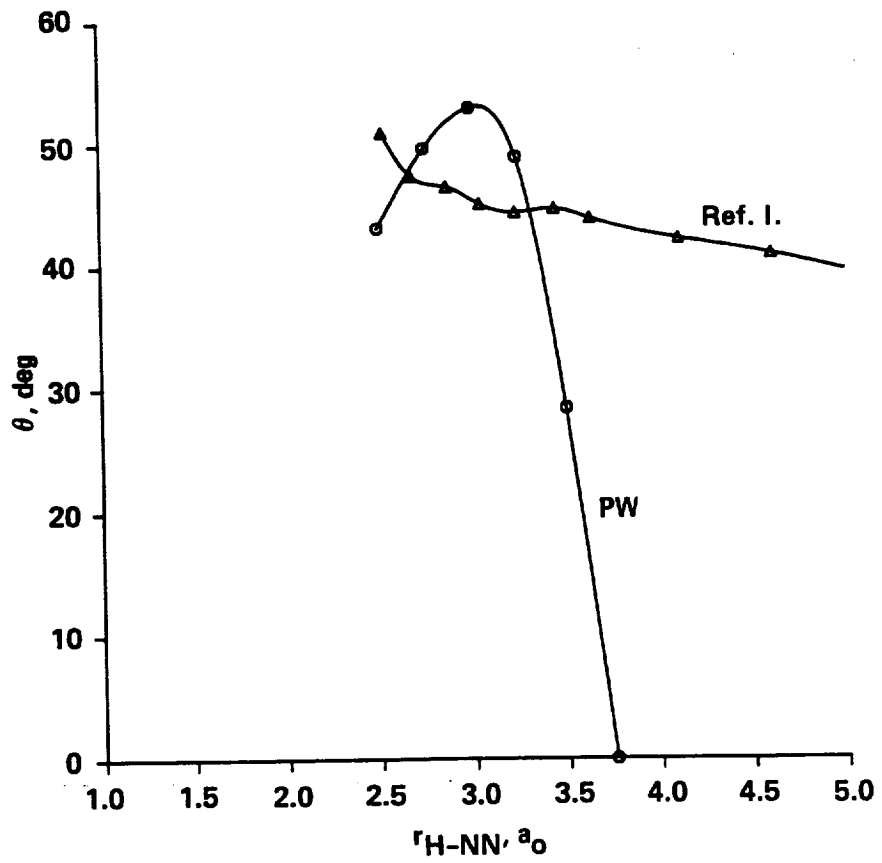
5.0 a<sub>0</sub>

2.0 a<sub>0</sub>

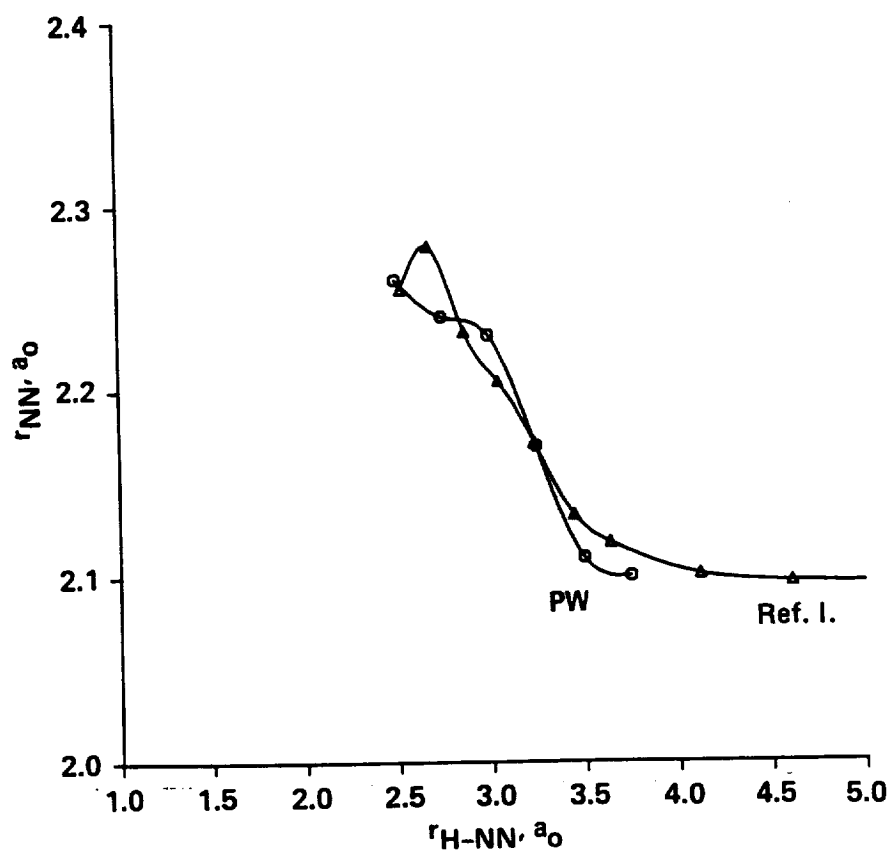
r<sub>H-NN</sub>



Walch-3



Waich-4



Walch-5

Appendix. The appendix contains a table of all the computed CASSCF/CCI energies. The energies are in the form CCI(CCI + Q). Note that for the CCI + Q energies -109. is not repeated. Thus, for the first point the CCI energy is -109.86500 and the CCI+Q energy is -109.88213. Distances are in  $a_0$ , angles are in degrees, and energies are in  $E_H$ .

Table AI. Computed Energies for  $\text{HN}_2$  ( $C_s$  symmetry) <sup>a</sup>.

$r_{H-NN}$	$\theta$	$r_{NN}$	Energy
20.544	32.53	2.095	-109.86500(-.88213)
6.587	37.92	2.095	-109.86490(-.88207)
5.598	39.33	2.095	-109.86378(-.88106)
5.088	39.20	2.096	-109.86190(-.87934)
4.608	40.92	2.097	-109.85794(-.87573)
4.119	42.24	2.101	-109.85037(-.86903)
3.636	43.93	2.118	-109.83871(-.85970)
3.446	44.71	2.133	-109.83452(-.85710)
3.241	44.37	2.172	-109.83273(-.85705)
3.052	45.12	2.205	-109.83597(-.86164)
2.872	46.53	2.232	-109.84263(-.86896)
2.683	47.38	2.278	-109.84633(-.87277)
2.528	50.88	2.255	-109.83772(-.86807)
5.00	0.0	2.1	-109.86286(-.88024)
4.50	0.0	2.1	-109.85989(-.87748)
4.00	0.0	2.1	-109.85347(-.87145)
3.75	0.0	2.1	-109.84800(-.86629)
3.5	0.0	2.0	-109.83458(-.85234)
3.5	0.0	2.1	-109.84019(-.85890)
3.5	0.0	2.2	-109.83189(-.85168)
3.25	0.0	2.0	-109.82335(-.84159)
3.25	0.0	2.1	-109.82911(-.84837)
3.25	0.0	2.2	-109.82098(-.84139)

3.0	0.0	2.0	-109.80740(-.82622)
3.0	0.0	2.1	-109.81342(-.83334)
3.0	0.0	2.2	-109.80556(-.82675)
2.75	0.0	2.0	-109.78478(-.80428)
2.75	0.0	2.1	-109.79121(-.81192)
2.75	0.0	2.2	-109.78378(-.80589)
2.25	0.0	2.2	-109.76161(-.78499) <sup>b</sup>
2.25	0.0	2.4	-109.76708(-.79170) <sup>b</sup>
2.25	0.0	2.6	-109.74818(-.77464) <sup>b</sup>
2.0	0.0	2.2	-109.76928(-.79222) <sup>b</sup>
2.0	0.0	2.4	-109.77533(-.79983) <sup>b</sup>
2.0	0.0	2.6	-109.75578(-.78536) <sup>b</sup>
1.75	0.0	2.2	-109.75963(-.78234) <sup>b</sup>
1.75	0.0	2.4	-109.76739(-.79486) <sup>b</sup>
1.75	0.0	2.6	-109.74839(-.78885) <sup>b</sup>
5.00	10.0	2.1	-109.86278(-.88017)
4.5	10.0	2.1	-109.85974(-.87734)
4.00	10.0	2.1	-109.85325(-.87127)
3.75	10.0	2.1	-109.84779(-.86615)
3.5	10.0	2.0	-109.83438(-.85223)
3.5	10.0	2.1	-109.84011(-.85893)
3.5	10.0	2.2	-109.83199(-.85191)
3.5	10.0	2.3	-109.81467(-.83586)
3.25	10.0	2.0	-109.82340(-.84176)
3.25	10.0	2.1	-109.82945(-.84885)

3.25	10.0	2.2	-109.82172(-.84232)
3.0	10.0	2.0	-109.80818(-.82717)
3.0	10.0	2.1	-109.81491(-.83504)
3.0	10.0	2.2	-109.80809(-.82951)
2.75	10.0	2.0	-109.78755(-.80728)
2.75	10.0	2.1	-109.79593(-.81686)
2.75	10.0	2.2	-109.79162(-.81383)
2.5	10.0	2.2	-109.77858(-.80208)
2.5	10.0	2.3	-109.77631(-.80272)
2.5	10.0	2.4	-109.76975(-.79875)
2.25	10.0	2.2	-109.77911(-.80543)
2.25	10.0	2.3	-109.78303(-.81074)
2.25	10.0	2.4	-109.77951(-.80866)
2.0	10.0	2.2	-109.77873(-.80542)
2.0	10.0	2.3	-109.78458(-.81308)
2.0	10.0	2.4	-109.78201(-.81316)
1.75	10.0	2.2	-109.76126(-.78976)
1.75	10.0	2.3	-109.76931(-.80008)
1.75	10.0	2.4	-109.76984(-.80213)
1.75	10.0	2.5	-109.76474(-.79837)
5.00	20.0	2.1	-109.86253(-.87994)
4.5	20.0	2.1	-109.85926(-.87693)
4.00	20.0	2.1	-109.85255(-.87073)
3.75	20.0	2.1	-109.84714(-.86573)

3.5	20.0	2.0	-109.83374(-.85187)
3.5	20.0	2.1	-109.83985(-.85902)
3.5	20.0	2.2	-109.83224(-.85260)
3.5	20.0	2.3	-109.81564(-.83737)
3.25	20.0	2.0	-109.82351(-.84229)
3.25	20.0	2.1	-109.83044(-.85035)
3.25	20.0	2.2	-109.82393(-.84513)
3.0	20.0	2.0	-109.81042(-.82999)
3.0	20.0	2.1	-109.81917(-.83995)
3.0	20.0	2.2	-109.81514(-.83721)
2.75	20.0	2.1	-109.80775(-.82938)
2.75	20.0	2.2	-109.80864(-.83171)
2.75	20.0	2.3	-109.80209(-.82702)
2.5	20.0	2.2	-109.80710(-.83164)
2.5	20.0	2.3	-109.80611(-.83227)
2.5	20.0	2.4	-109.79911(-.82681)
2.25	20.0	2.2	-109.80679(-.83203)
2.25	20.0	2.3	-109.80918(-.83592)
2.25	20.0	2.4	-109.80413(-.83292)
2.0	20.0	2.2	-109.79636(-.82300)
2.0	20.0	2.3	-109.80084(-.82925)
2.0	20.0	2.4	-109.79820(-.82774)
1.75	20.0	2.2	-109.76285(-.78997)
1.75	20.0	2.3	-109.77098(-.79920)
1.75	20.0	2.4	-109.77114(-.80050)

1.75	20.0	2.5	-109.76594(-.79644)
5.00	30.0	2.1	-109.86204(-.87950)
4.5	30.0	2.1	-109.85834(-.87612)
4.00	30.0	2.1	-109.85117(-.86962)
3.5	30.0	2.0	-109.83235(-.85102)
3.5	30.0	2.1	-109.83908(-.85892)
3.5	30.0	2.2	-109.83236(-.85353)
3.5	30.0	2.3	-109.81702(-.83968)
3.25	30.0	2.0	-109.82331(-.84290)
3.25	30.0	2.1	-109.83170(-.85256)
3.25	30.0	2.2	-109.82721(-.84944)
3.0	30.0	2.0	-109.81354(-.83419)
3.0	30.0	2.1	-109.82529(-.84720)
3.0	30.0	2.2	-109.82482(-.84811)
3.0	30.0	2.3	-109.81668(-.84163)
2.75	30.0	2.1	-109.82182(-.84478)
2.75	30.0	2.2	-109.82660(-.85101)
2.75	30.0	2.3	-109.82314(-.84909)
2.5	30.0	2.1	-109.82036(-.84411)
2.5	30.0	2.2	-109.82973(-.85465)
2.5	30.0	2.3	-109.82964(-.85577)
2.5	30.0	2.4	-109.82283(-.85065)
2.25	30.0	2.1	-109.81328(-.83738)
2.25	30.0	2.2	-109.82531(-.85102)
2.25	30.0	2.3	-109.82651(-.85468)

2.25	30.0	2.4	-109.82141(-.85048)
2.0	30.0	2.2	-109.80028(-.82697)
2.0	30.0	2.3	-109.80442(-.83166)
2.0	30.0	2.4	-109.80087(-.82900)
1.75	30.0	2.2	-109.73752(-.76349)
1.75	30.0	2.3	-109.74431(-.77111)
1.75	30.0	2.4	-109.74390(-.77155)
1.75	30.0	2.5	-109.73880(-.76737)
5.00	40.0	2.1	-109.86124(-.87876)
4.5	40.0	2.1	-109.85682(-.87474)
4.00	40.0	2.1	-109.84875(-.86761)
3.5	40.0	2.0	-109.82968(-.84927)
3.5	40.0	2.1	-109.83725(-.85822)
3.5	40.0	2.2	-109.83178(-.85427)
3.25	40.0	2.1	-109.83258(-.85497)
3.25	40.0	2.2	-109.83056(-.85441)
3.25	40.0	2.3	-109.82094(-.84638)
3.0	40.0	2.1	-109.83138(-.85494)
3.0	40.0	2.2	-109.83417(-.85912)
3.0	40.0	2.3	-109.82908(-.85555)
2.75	40.0	2.1	-109.83349(-.85775)
2.75	40.0	2.2	-109.84071(-.86613)
2.75	40.0	2.3	-109.83901(-.86556)
2.5	40.0	2.1	-109.83269(-.85699)

2.5	40.0	2.2	-109.84250(-.86782)
2.5	40.0	2.3	-109.84138(-.87003)
2.5	40.0	2.4	-109.83351(-.86516)
2.25	40.0	2.2	-109.82436(-.85343)
2.25	40.0	2.3	-109.82640(-.85402)
2.25	40.0	2.4	-109.81962(-.84787)
2.0	40.0	2.2	-109.77239(-.79853)
2.0	40.0	2.3	-109.77264(-.79941)
2.0	40.0	2.4	-109.76594(-.79338)
5.00	50.0	2.1	-109.86009(-.87767)
4.5	50.0	2.1	-109.85456(-.87264)
4.00	50.0	2.1	-109.84489(-.86425)
3.5	50.0	2.0	-109.82496(-.84585)
3.5	50.0	2.1	-109.83333(-.85592)
3.5	50.0	2.2	-109.82917(-.85355)
3.25	50.0	2.1	-109.83116(-.85542)
3.25	50.0	2.2	-109.83160(-.85738)
3.25	50.0	2.3	-109.82463(-.85200)
3.0	50.0	2.1	-109.83408(-.85913)
3.0	50.0	2.2	-109.83941(-.86573)
3.0	50.0	2.3	-109.83636(-.86395)
2.75	50.0	2.1	-109.83797(-.86292)
2.75	50.0	2.2	-109.84619(-.87212)
2.75	50.0	2.3	-109.84466(-.87193)

2.5	50.0	2.1	-109.83092(-.85516)
2.5	50.0	2.2	-109.83659(-.86682)
2.5	50.0	2.3	-109.83547(-.86502)
2.5	50.0	2.4	-109.82699(-.85629)
2.25	50.0	2.1	-109.79041(-.81729)
2.25	50.0	2.2	-109.79623(-.82343)
2.25	50.0	2.3	-109.79127(-.81891)
2.0	50.0	2.1	-109.68516(-.71048)
2.0	50.0	2.2	-109.68518(-.71118)
2.0	50.0	2.3	-109.67480(-.70143)
5.00	60.0	2.1	-109.85864(-.87627)
4.5	60.0	2.1	-109.85160(-.86980)
4.00	60.0	2.1	-109.83931(-.85911)
3.5	60.0	2.0	-109.81672(-.83878)
3.5	60.0	2.1	-109.82542(-.84960)
3.5	60.0	2.2	-109.82221(-.84852)
3.25	60.0	2.1	-109.82448(-.85027)
3.25	60.0	2.2	-109.82713(-.85443)
3.25	60.0	2.3	-109.82238(-.85119)
3.0	60.0	2.1	-109.82960(-.85539)
3.0	60.0	2.2	-109.83666(-.86359)
3.0	60.0	2.3	-109.83453(-.86281)
2.75	60.0	2.1	-109.83116(-.85612)
2.75	60.0	2.2	-109.83850(-.86520)
2.75	60.0	2.3	-109.83475(-.86445)

2.5	60.0	2.1	-109.80891(-.83542)
2.5	60.0	2.2	-109.81218(-.84005)
2.5	60.0	2.3	-109.80424(-.83298)
2.25	60.0	2.0	-109.72073(-.74571)
2.25	60.0	2.1	-109.73104(-.75694)
2.25	60.0	2.2	-109.72431(-.75113)
5.00	70.0	2.1	-109.85713(-.87477)
4.5	70.0	2.1	-109.84835(-.86655)
4.00	70.0	2.1	-109.83233(-.85207)
3.5	70.0	2.0	-109.80363(-.82589)
3.5	70.0	2.1	-109.81150(-.83647)
3.5	70.0	2.2	-109.80836(-.83609)
3.25	70.0	2.0	-109.79430(-.81919)
3.25	70.0	2.1	-109.80968(-.83641)
3.25	70.0	2.2	-109.81468(-.84286)
3.25	70.0	2.3	-109.81215(-.84167)
3.0	70.0	2.1	-109.81609(-.84207)
3.0	70.0	2.2	-109.82445(-.85158)
3.0	70.0	2.3	-109.82245(-.85139)
2.75	70.0	2.1	-109.81248(-.83784)
2.75	70.0	2.2	-109.81754(-.84516)
2.75	70.0	2.3	-109.81082(-.84016)
2.5	70.0	2.0	-109.75691(-.78129)
2.5	70.0	2.1	-109.76982(-.79601)

2.5	70.0	2.2	-109.76491(-.79239)
5.00	80.0	2.1	-109.85594(-.87357)
4.50	80.0	2.1	-109.84566(-.86376)
4.00	80.0	2.1	-109.82574(-.84485)
3.5	80.0	2.0	-109.78759(-.80793)
3.5	80.0	2.1	-109.79197(-.81525)
3.5	80.0	2.2	-109.78617(-.81393)
3.25	80.0	2.1	-109.78609(-.81359)
3.25	80.0	2.2	-109.79567(-.82460)
3.25	80.0	2.3	-109.79648(-.82661)
3.25	80.0	2.4	-109.79009(-.82167)
3.0	80.0	2.1	-109.79720(-.82374)
3.0	80.0	2.2	-109.80728(-.83511)
3.0	80.0	2.3	-109.80537(-.83508)
2.75	80.0	2.1	-109.78944(-.81562)
2.75	80.0	2.2	-109.79227(-.82025)
2.75	80.0	2.3	-109.78164(-.81123)
2.5	80.0	2.0	-109.72087(-.74564)
2.5	80.0	2.1	-109.72725(-.75344)
2.5	80.0	2.2	-109.71316(-.74068)
21.05	90.0	2.1	-109.86483(-.88199) <sup>b</sup>
6.05	90.0	2.1	-109.86330(-.88057) <sup>b</sup>
5.05	90.0	2.1	-109.85613(-.87371) <sup>b</sup>

4.55	90.0	2.1	-109.84596(-.86392) <sup>b</sup>
4.05	90.0	2.1	-109.82564(-.84428) <sup>b</sup>
3.75	90.0	2.1	-109.80529(-.82357) <sup>b</sup>
3.5	90.0	2.0	-109.77937(-.79711) <sup>b</sup>
3.5	90.0	2.1	-109.77977(-.79847) <sup>b</sup>
3.5	90.0	2.2	-109.76629(-.78616) <sup>b,c</sup>
3.5	90.0	2.2	-109.75722(-.78543) <sup>b,d</sup>
3.5	90.0	2.3	-109.76266(-.79256) <sup>b</sup>
3.5	90.0	2.4	-109.76010(-.79101) <sup>b</sup>
3.25	90.0	2.1	-109.76888(-.79522) <sup>b</sup>
3.25	90.0	2.2	-109.78418(-.81206) <sup>b</sup>
3.25	90.0	2.3	-109.78787(-.81615) <sup>b</sup>
3.25	90.0	2.4	-109.78359(-.81114) <sup>b</sup>
3.0	90.0	2.1	-109.78695(-.81289) <sup>b</sup>
3.0	90.0	2.2	-109.79886(-.82445) <sup>b</sup>
3.0	90.0	2.3	-109.79832(-.82330) <sup>b</sup>
2.75	90.0	2.1	-109.77936(-.80255) <sup>b</sup>
2.75	90.0	2.2	-109.78223(-.80519) <sup>b</sup>
2.75	90.0	2.3	-109.77041(-.79357) <sup>b</sup>

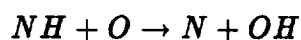
<sup>a</sup> [4s3p2d1f/3s\*2p] ANO basis set. Selected reference ( $C_i > 0.05$ ) CASSCF/CCI calculations correlating eleven electrons.

<sup>b</sup> Points computed in  $C_{2v}$  symmetry.

<sup>c</sup> This point and preceding points with  $\theta = 90^\circ$  are  ${}^2\Sigma^+$  symmetry.

<sup>d</sup> This point and following points with  $\theta = 90^\circ$  are  $^2\Pi$  symmetry.

**Theoretical Characterization of the  
 $^5\Pi$  and  $^3\Pi$  Potential Energy Surfaces for**



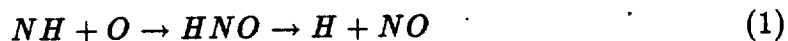
Stephen P. Walch<sup>a</sup>  
ELORET Institute  
Sunnyvale, Ca. 94087

Abstract. The reactant, product, and saddle point regions of the  $^5\Pi$  and  $^3\Pi$  potential energy surfaces for the reaction  $NH + O \rightarrow N + OH$  have been characterized using complete active space self consistent field / externally contracted configuration interaction (CASSCF/CCI) calculations with large atomic natural orbital (ANO) basis sets. The computed barrier heights are 5.6 and 11.7 kcal/mol on the  $^5\Pi$  and  $^3\Pi$  surfaces, respectively. Transition state theory with an Eckart tunneling correction is used to estimate the rate constant on the  $^5\Pi$  surface.

<sup>a</sup>Mailing Address: NASA Ames Research Center, Moffett Field, CA 94035.

## I. Introduction

The lowest three potential energy surfaces (PES's) of  $^1A'$ ,  $^3A''$ , and  $^1A''$  symmetry for  $H + NO \rightarrow HNO/HON$  have been discussed elsewhere [1]. In Ref. 1 the barriers for H atom addition to NO to give HNO and the regions of the PES's around the HNO/HON equilibrium geometries were characterized and a schematic of the PES's for HNO/HON was constructed based on ab initio quantum chemical calculations [1-4] and qualitative arguments. That schematic of the PES's for HNO/HON is reproduced here as Fig. 1. In this paper, we focus on the PES's for the reaction of  $NH + O$ . From Fig. 1 it is seen that the reactants  $NH + O$  correlate with the  $^1A'$ ,  $^3A''$ , and  $^1A''$  surfaces of HNO leading to  $H + NO$  as one product.



Reaction (1) has been studied by Melius et al. [4] using Møller-Plesset perturbation theory and bond additivity corrections. These authors were mainly interested in more complex reactions, which are important in the thermal De- $NO_x$  process [5-7], but did comment that reaction (1) could proceed with no activation energy on the singlet or triplet HNO surfaces.

From Fig. 1 it is seen that an alternative reaction pathway is the production of  $N + OH$ .



Reaction (2) is believed to be important in the combustion of nitramines [8], which are of interest as rocket propellants. Benson et al. [9] have recommended the expression

$$K = 6.3E + 11T^{0.5} \exp(-8000/RT) \text{cm}^3 \text{mol}^{-1} \text{sec}^{-1} \quad (3)$$

for the rate constant of reaction (2). However, this expression is only an estimate of the rate constant and is not based on experimental data. Melius et al. [4] predicted a small activation energy for reaction (2) on the quintet surface, where H abstraction is the dominant process. In this paper, that abstraction pathway is studied in more detail.

As discussed in section II, reactants and products of reaction (2) may be connected by surfaces of  $^5\Pi$  and  $^3\Pi$  symmetry. Of these only the  $^3A''$  component of the  $^3\Pi$  surface correlates with the low-lying states of HNO/HON, which have been discussed elsewhere [1]. Thus, for bent geometries, the  $^5A'$  and  $^5A''$  components of the  $^5\Pi$  surface and the  $^3A'$  component of the  $^3\Pi$  surface do not interact with HNO/HON. In addition, for the  $^3A''$  component of  $^3\Pi$ , the collinear geometry corresponds to a saddle point. Thus, the  $^5\Pi$  and  $^3\Pi$  surfaces are expected to dominate reaction (2), and these surfaces are studied here.

Qualitative features of the PES's are discussed in section II, the computational method is discussed in Section III, the results are presented in Section IV, and the conclusions are given in Section V.

## II. Qualitative Features.

The ground state of NH is  $^3\Sigma^-$  and the ground state of O is  $^3P$ . From this it follows that the ground state reactants give rise to PES's of  $^{1,3,5}A'$  and  $^{1,3,5}A''$  symmetry. The ground state of OH is  $^2\Pi$  and the ground state of N is  $^4S$ . Thus, the ground state products give rise to PES's of  $^{3,5}A'$  and  $^{3,5}A''$  symmetry. From the preceding discussion, it is seen that PES's of  $^{3,5}A'$  and  $^{3,5}A''$  symmetry connect the reactants and products of reaction (2). For collinear geometries these surfaces

correspond to the  $^3,^5\Pi$  surfaces considered in this paper.

The low-lying electronic states of HNO/HON are of  $^1A'$ ,  $^1A''$ , and  $^3A''$  symmetry. Thus, only the  $^3A''$  surface of HNO/HON is of the same symmetry as the PES's for reaction (2). As discussed later, the  $^3A''$  component of  $^3\Pi$  is stabilized for highly bent geometries ( $\angle$  NHO less than  $135^\circ$ ), but the collinear geometry corresponds to a saddle point. From Fig. 1 it is expected that any reactants which "leak" into this channel will lead to  $H + NO$ , since the barriers to isomerization of HNO to HON are larger than the HN bond energy.

As discussed above,  $NH + O$  can also lead to surfaces of  $^1A'$  and  $^1A''$  symmetry. These surfaces were not studied in this paper, since they can not correlate with the products of reaction (2). This channel is expected to lead to  $H + NO$  product via HNO/HON, as for the  $^3A''$  surface.

### III. Computational Details.

The calculations are complete active space self consistent field /externally contracted configuration interaction (CASSCF/CCI) and are basically the same as in ref. 1. Two basis sets were used. The smaller basis set is a  $[4s3p2d1f/3s2p1d]$  atomic natural orbital (ANO) basis set as developed by Almlöf and Taylor [10]. This basis set is denoted as b.s. 1. and is the same basis set as was used in ref. 1. As discussed elsewhere [11-12] b.s. 1 leads to an error of  $\approx 1$  kcal/mol in the free H atom energy and an improved contraction of the H s orbitals has been developed [11]. However, for reaction (2) this defect in the basis is not expected to lead to significant errors, since free H atom is not involved. As a further check on the accuracy of the results, additional calculations were carried out with a larger  $[5s4p3d2f/4s3p2d]$  ANO basis set, denoted as b.s. 2.

Most of the calculations were carried out in  $C_{2v}$  symmetry. In the CASSCF calculation 10 electrons were correlated (all but the O1s, N1s, and O2s electrons,

which leads to a  $4\sigma 2\pi$  active space. In the subsequent CCI calculations 12 electrons were correlated (all but the O1s and N1s electrons). The CAS for eight electrons in  $3\sigma 2\pi$  active orbitals was used as a reference space.

The saddle points on the  $^5\Pi$  and  $^3\Pi$  surfaces were obtained from a fit to a six-term quadratic polynomial in  $r_{OH}$  and  $r_{NH}$ . Bending potentials were obtained for both surfaces with  $r_{OH}$  and  $r_{NH}$  fixed at the saddle point values. The wavefunctions in  $C_s$  symmetry were equivalent to those for the  $C_{2v}$  symmetry calculations, except in the case of the  $^3\Pi$  surface only ten electrons were correlated (due to memory limitations).

The calculations were carried out on the NASA Ames Cray Y-MP/832. These calculations used the MOLECULE[13]-SWEDEN[14] system of programs.

#### IV. Results and Discussion.

The computed energies for the  $^5\Pi$  and  $^3\Pi$  states are given in Tables I and II, respectively. Table III shows the stationary point geometries and energies. In the case of the two saddle points the geometry was obtained by fitting to a six-term polynomial, while for the reactants and products the geometry was obtained from a parabolic fit.

The computed exoergicity for reaction (2) is 22.9 kcal/mol with b.s 1. Using the  $D_0$  value of 3.37 eV for NH recommended by Bauschlicher et al. [15] in conjunction with the experimental [16]  $D_0$  for OH and experimental [16]  $\omega_e$  values for NH and OH, leads to 24.2 kcal/mol as the best estimate of this energy difference. The error of 1.3 kcal/mole is twice the error estimate in ref. 15 of  $\pm 0.7$  kcal/mol for the  $D_0$  of NH. Calculations with b.s. 2 lead to an exoergicity of 23.1 kcal/mol and reduce the error to 1.1 kcal/mol. This basis set differs from that used in ref. 15 in that it did not have a g function. This basis set difference and contraction error due to the contracted CI must account for the remainder of the difference between the two

calculations. The computed NH and OH bond lengths are  $\approx 0.01 a_0$  longer than experiment.

The computed barrier heights are 5.6 and 11.7 kcal/mol for the  ${}^5\Pi$  and  ${}^3\Pi$  surfaces, respectively, with b.s. 1. The barrier height on the  ${}^5\Pi$  surface is reduced by only 0.07 kcal/mol with b.s. 2.

Table I also gives energies for bent N-H-O on the  ${}^5A'$  and  ${}^5A''$  surfaces. Table IV gives energies for bent N-H-O on the  ${}^3A'$  and  ${}^3A''$  surfaces. In both cases only  $\angle NHO$  was varied, with  $r_{NH}$  and  $r_{OH}$  fixed at the saddle point values. In the case of the  ${}^3A'$  and  ${}^3A''$  surfaces, only ten electrons were correlated (due to memory restrictions). This approximation is justified based on the HNO calculations in ref. 1, where it was found that the results with 10 and 12 correlated electrons are very similar. The bending potentials are also shown in Fig. 2. Here it is seen that the  ${}^5A'$  and  ${}^5A''$  bending potentials are quite similar. (Note that there is a residual splitting for the collinear geometry due to symmetry breaking.) However, the bending potentials for the  ${}^3A'$  and  ${}^3A''$  PES's (See Fig. 3.) differ considerably for highly bent geometries, with the  ${}^3A''$  curve dropping for  $\angle NHO$  smaller than  $140^\circ$ . As discussed earlier, this result is expected, since the  ${}^3A''$  state correlates with HNO/HON for bent geometries. The flat  ${}^3A''$  bending potential suggests that this component of the  ${}^3\Pi$  surface would lead to H + NO product via HNO\*/HON\*.

Table III also gives harmonic frequencies obtained for the saddle point on the  ${}^5A'$  and  ${}^5A''$  surface. These frequencies are based on the polynomial fits discussed above and were obtained with the program SURVIB [17]. In order to correct for the slight symmetry breaking evident in Fig. 2, the energy at the predicted collinear saddle point was computed in  $C_{2v}$  symmetry and the bending curves for the two components of the  ${}^5\Pi$  surface were shifted by the difference between the  $C_{2v}$  and  $C_s$  symmetry calculations. In spite of this correction, there is still a slight ( $< 4 \text{ cm}^{-1}$ )

difference in the frequencies of the in-plane vibrational modes, which arises from different quality least squares fits of the  ${}^5A'$  and  ${}^5A''$  energies.

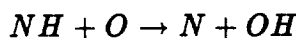
Transition state theory (TST) calculations were carried out using rigid rotor and harmonic oscillator partition functions [18] and an estimate of tunneling through an Eckart barrier based on the formalism of Miller [19]. The 5.52 kcal/mol barrier obtained with b.s. 2 was used without adjustment. In these calculations the reactants NH and O had electronic degeneracy of 3 and spatial degeneracy of 1 and 3, respectively, while the saddle point N-H-O species had a spin degeneracy of 5 (quintet surface) and a spatial degeneracy of 1 for each component ( ${}^5A'$  and  ${}^5A''$ ) of the  ${}^5\Pi$  state. The TST theory calculations were carried out separately for each component of the  ${}^5\Pi$  surface and the rate constants for the two components are summed to give the overall rate constant for reaction (2) on the  ${}^5\Pi$  surface. There is also a  ${}^5\Sigma$  surface, but this surface correlates with an excited state of OH and does not contribute to the rate for reaction (2). The results of the TST calculations are given in Table V. The value of  $\kappa$ , a multiplicative constant which gives the effect of tunneling, is also given in Table V. As expected, tunneling is only important at lower temperatures: the effect is less than a factor of two for  $T < 500\text{K}$ . It is expected that the  ${}^5\Pi$  surface will dominate the rate for reaction (2) since the barrier for the  ${}^3\Pi$  surface is twice as large.

The TST rate constants for the  ${}^5\Pi$  surface and the rate constant recommended by Benson [9] (eqn (3) ) are also plotted as a function of temperature in Fig. 3. From Fig. 3 it is seen that Eqn. 3 is a factor of  $\approx 2.0$  below the computed rate constant in the high temperature region but is more than two orders of magnitude below the computed rate constant at low temperatures. Based on previous work [20-21] for similar systems with moderate barriers, the TST theory rate constant is expected to be within a factor of 2 of experiment. Because TST does not take into

account barrier recrossing effects and because variational effects are not included in the present calculation, the TST rate constant should be larger than experiment, possibly by as much as the factor of 2 difference between the computed rate constant and Eqn. 3 seen at high temperature. However, it is clear that the rate constant at low temperature is much larger than predicted by Eqn. 3, and it is believed that the TST rate constant is much more reliable and should replace Eqn. 3 as the best estimate of the rate constant for reaction (2).

## V. Conclusions.

The computed barrier heights for the  $^5\Pi$  and  $^3\Pi$  surfaces for



are 5.6 and 11.7 kcal/mol, respectively. Thus, the  $^5\Pi$  surface is expected to dominate the kinetics for this reaction. Transition state theory calculations plus an estimate of tunneling based on an Eckart barrier give a rate constant on the  $^5\Pi$  surface which is a factor of  $\approx 2.0$  greater at high temperatures and more than two orders of magnitude greater at low temperatures than a rate constant expression recommended by Benson (not based on experimental data). While transition state theory may slightly overestimate rates ( up to a factor of 2) due to neglect of recrossing effects, it is clear that the computed rate constant is far more reliable than the previous recommendation, and should replace it.

The  $^3\Pi$  surface has also been characterized. The  $^3A''$  component of this surface is of the same symmetry as the lower lying HNO/HON surface. This leads to a complex bending curve for this component of the  $^3\Pi$  surface and the possibility that part of the flux may bleed off into the H + NO product channel.

## ACKNOWLEDGMENTS

S.P. Walch was supported by a NASA grant(NCC2-478). Helpful discussions

with Drs. R.L. Jaffee, R.J. Duchovic, C.M. Rohlfing, and C.F. Melius are gratefully acknowledged.

## References

1. S.P. Walch and C.M. Rohlifing, *J. Chem. Phys.*, **91**, 2939(1989).
2. G.F.Adams and G.D. Bent, Technical Report BRL-TR-2737, U.S. Army Ballistic Research Laboratory, Aberdeen Proving Ground, Maryland, June, 1986.
- 3a. P.J. Bruna, *Chem. Phys.* **49**, 39(1980).
- 3b. P.J. Bruna and C.M. Marian, *Chem. Phys. Lett.* **67**, 109(1979).
4. C.F. Melius and J.S. Binkley, in "The Chemistry of Combustion Processes", ACS Symposium Series, **249**, 71(1984).
5. R.K. Lyon, Sandia Laboratories Report No. SAND70-8635, 1970.
6. R.K. Lyon, U.S. Patent 3,900,544, August 1975.
7. R.K. Lyon, *Int. J. Chem. Kinet.*, **8**, 315(1976).
8. C.F. Melius, Proc. of the 25<sup>th</sup> JANNAF Combustion Meeting, October 1988.
9. S.W. Benson, Environmental Protection Agency, Washington, D.C. Report No. EPA-600-2-75-019(1975).
10. J. Almlöf and P.R. Taylor, *J. Chem. Phys.* **86**, 4070(1987).
11. S.P. Walch and C.M. Rohlifing, *J. Chem. Phys.*, **91**, 2373(1989)
12. S.P. Walch, *J. Chem. Phys.*, in press
13. J. Almlöf, MOLECULE, a vectorized Gaussian integral program.
14. SWEDEN is a vectorized SCF-MCSCF-direct CI- conventional CI-CPF-MCPF program written by P.E.M. Siegbahn, C.W. Bauschlicher, Jr., B. Roos, P.R. Taylor, A. Heiberg, J. Almlöf, S.R. Langhoff, and D.P. Chong.
15. C.W. Bauschlicher, Jr. and S.R. Langhoff, *Chem. Phys. Lett.*, **135**, 67(1987).
16. K.P. Huber and G. Herzberg, *Molecular Spectra and Molecular Structure*, Vol.4, Constants of Diatomic Molecules (Van Nostrand Reinhold, New York,

- 1979).
17. L.B. Harding and W.C. Ermler, SURVIB, a normal mode analysis program for polyatomic molecules.
  18. J.F. Lee, F.W. Sears, and D.L. Turcotte, "Statistical Thermodynamics", Addison-Wesley Publishing, Reading, Massachusetts (1963).
  19. W.H. Miller, J. Amer. Chem. Soc., **101**, 6810(1979).
  20. S.P. Walch, A.F. Wagner, T.H. Dunning, Jr., and G.C. Schatz, J. Chem. Phys., **72**, 2894(1980).
  21. G.C. Schatz and S.P. Walch, J. Chem. Phys., **72**, 776(1980).

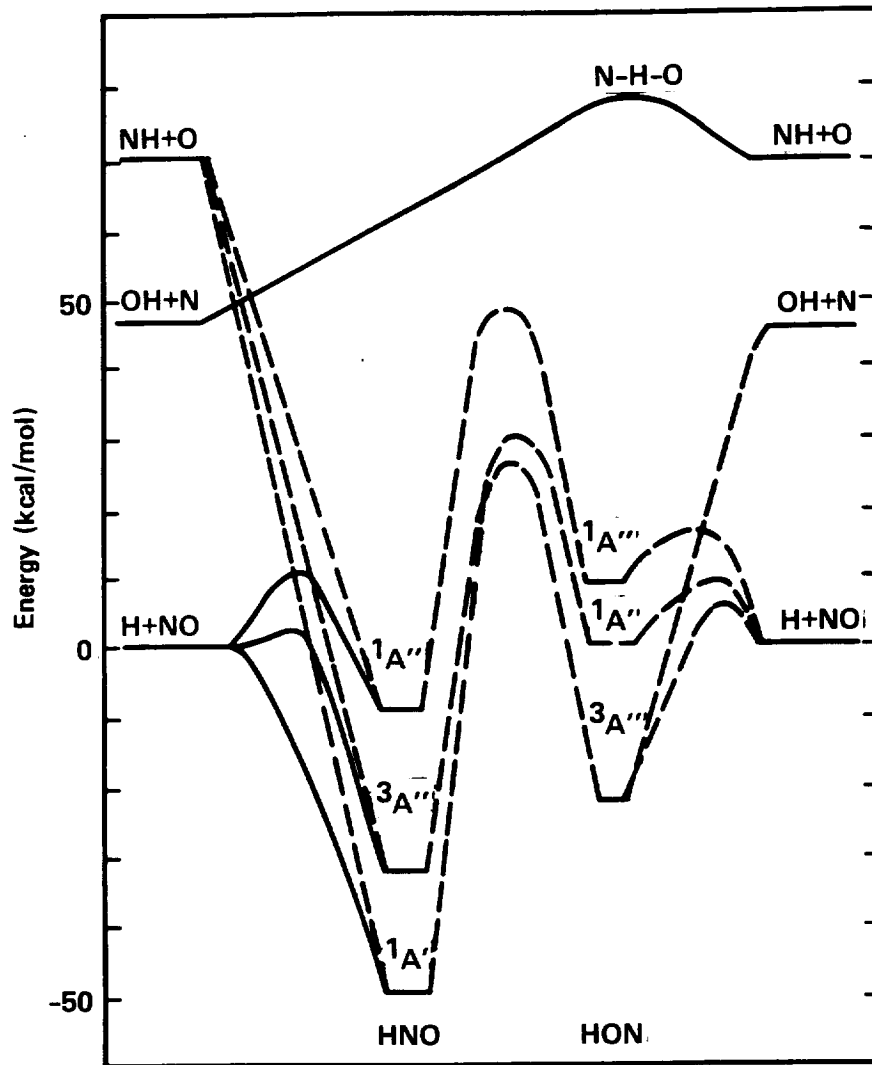
### Figure Captions.

Fig. 1. Schematic of the potential surfaces of HNO/HON (See Ref. 1). Two product channels are shown for the reaction of  $\text{NH} + \text{O}$ .  $\text{H} + \text{NO}$  products arise from the  $^1\text{A}'$ ,  $^3\text{A}''$ , and  $^1\text{A}''$  surfaces of HNO, while  $\text{OH} + \text{N}$  products arise via an H abstraction process predominately on a quintet surface (See the text).

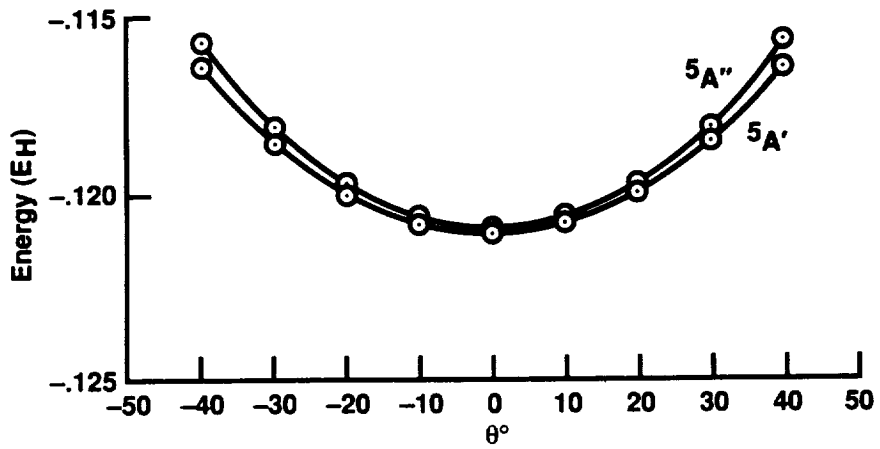
Fig. 2. Bending potentials for the  $^5\text{A}'$  and  $^5\text{A}''$  states of N-H-O.

Fig. 3. Bending potentials for the  $^3\text{A}'$  and  $^3\text{A}''$  states of N-H-O.

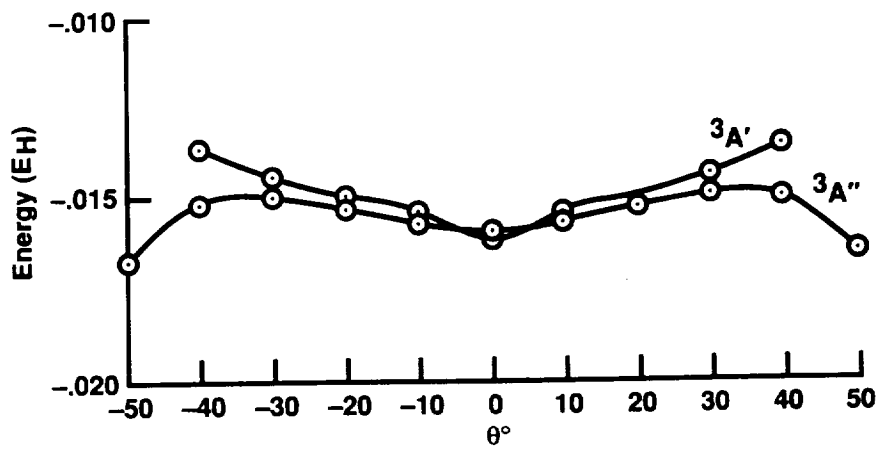
Fig. 4. Computed rate constant for reaction (2) on the  $^5\Pi$  surface. The rate constant is computed separately for the  $^5\text{A}'$  and  $^5\text{A}''$  components of the  $^5\Pi$  surface and the total rate constant is the sum of the separate rate constants. The rate expression estimated by Benson is also shown for comparison.



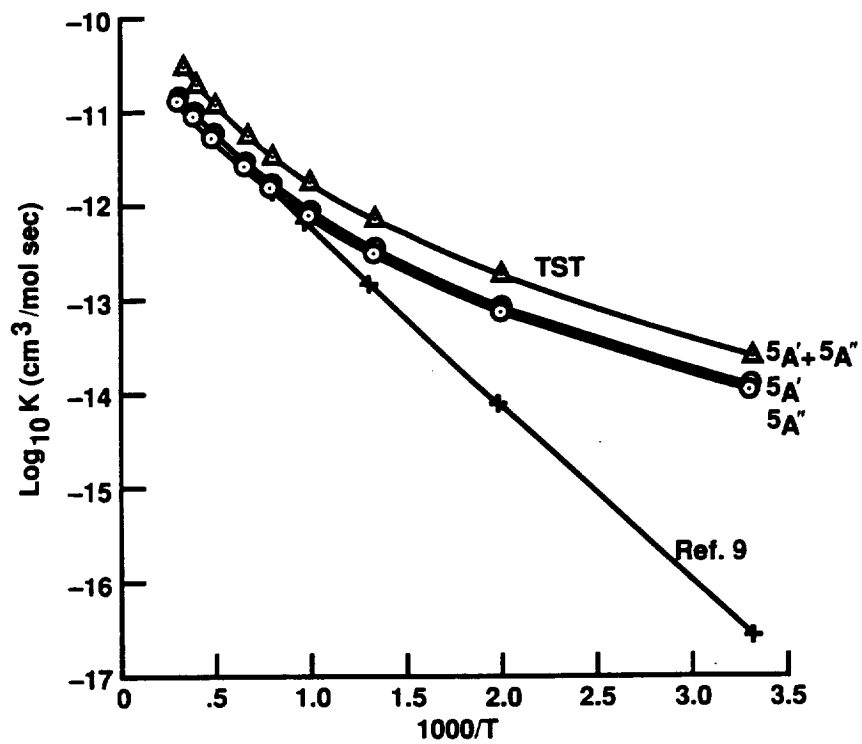
WALCH - 1



Walch -2



Walch -3



Walch-4

Table I. Computed Energies for N-H-O ( $^5\Pi$  state) <sup>a</sup>.

$r_{NH}$	$r_{OH}$	$\theta$	Energy
1.9	20.0	180.	-130.10584(-.12822)
1.994	20.0	180.	-130.10669(-.12914)
2.1	20.0	180.	-130.10403(-.12653)
1.9	2.4	180.	-130.08127(-.10763)
1.9	2.6	180.	-130.08721(-.11266)
1.9	2.8	180.	-130.09191(-.11639)
1.9	3.0	180.	-130.09566(-.11935)
2.0	2.4	180.	-130.08881(-.11537)
2.0	2.6	180.	-130.09219(-.11795)
2.0	2.8	180.	-130.09520(-.11999)
2.0	3.0	180.	-130.09792(-.12187)
2.1	2.2	180.	-130.09172(-.11853)
2.1	2.4	180.	-130.09335(-.12002)
2.1	2.6	180.	-130.09413(-.12016)
2.1	2.8	180.	-130.09532(-.12042)
2.1	3.0	180.	-130.09692(-.12113)
2.2	2.0	180.	-130.09485(-.12106)
2.2	2.2	180.	-130.09745(-.12411)
2.2	2.4	180.	-130.09592(-.12263)
2.2	2.6	180.	-130.09409(-.12034)
2.2	2.8	180.	-130.09338(-.11876)
2.3	2.0	180.	-130.10232(-.12820)

2.3	2.2	180.	-130.10174(-.12818)
2.3	2.4	180.	-130.09729(-.12393)
2.3	2.6	180.	-130.09290(-.11926)
2.3	2.8	180.	-130.09018(-.11580)
2.5	2.0	180.	-130.11344(-.13864)
2.098	2.732	180. <sup>b</sup>	-130.09475(-.12097)
2.098	2.732	170.	-130.09451(-.12069)
2.098	2.732	160.	-130.09374(-.11984)
2.098	2.732	150.	-130.09243(-.11846)
2.098	2.732	140.	-130.09029(-.11639)
2.098	2.732	180. <sup>c</sup>	-130.09470(-.12082)
2.098	2.732	170.	-130.09442(-.12051)
2.098	2.732	160.	-130.09358(-.11961)
2.098	2.732	150.	-130.09211(-.11806)
2.098	2.732	140.	-130.08977(-.11570)
20.0	1.7	180.	-130.13727(-.15959)
20.0	1.75	180.	-130.14087(-.16327)
20.0	1.837	180.	-130.14317(-.16572)
20.0	1.9	180.	-130.14238(-.16503)

<sup>a</sup> [4s3p2d1f/3s2p1d] ANO basis set. Second order CASSCF/CCI calculations correlating twelve electrons.

<sup>b</sup> Calculation in C<sub>s</sub> symmetry( <sup>5</sup>A' state).

<sup>c</sup> Calculation in C<sub>s</sub> symmetry( <sup>5</sup>A'' state).

Table II. Computed Energies for N-H-O ( $^3\Pi$  state) <sup>a</sup>.

$r_{NH}$	$r_{OH}$	$\theta$	Energy
1.9	2.4	180.	-130.07188(-.09930)
1.9	2.6	180.	-130.07911(-.10506)
1.9	2.8	180.	-130.08576(-.11034)
2.0	2.2	180.	-130.07420(-.10199)
2.0	2.4	180.	-130.07816(-.10581)
2.0	2.6	180.	-130.08280(-.10923)
2.0	2.8	180.	-130.08799(-.11298)
2.1	2.2	180.	-130.08147(-.10898)
2.1	2.4	180.	-130.08178(-.10948)
2.1	2.6	180.	-130.08349(-.11039)
2.1	2.8	180.	-130.08700(-.11242)
2.2	2.0	180.	-130.08757(-.11438)
2.2	2.2	180.	-130.08708(-.11431)
2.2	2.4	180.	-130.08386(-.11135)
2.2	2.6	180.	-130.08240(-.10966)
2.2	2.8	180.	-130.08389(-.10979)
2.3	1.8	180.	-130.08807(-.11367)
2.3	2.0	180.	-130.09522(-.12150)
2.3	2.2	180.	-130.09167(-.11856)
2.3	2.4	180.	-130.08518(-.11240)
2.3	2.6	180.	-130.08045(-.10783)
2.3	2.8	180.	-130.07953(-.10591)

<sup>a</sup> [4s3p2d1f/3s2p1d] ANO basis set. Second order CASSCF/CCI calculations correlating twelve electrons.

Table III. Computed Stationary Point Properties for the  $^5\Pi$  and  $^3\Pi$  surfaces of NH + O.

	$r_{NH}$	$r_{OH}$	$\delta E$		frequencies
			b.s. 1	b.s. 2	
NH + O	1.975	20.0	0.0	0.0	3110
N-H-O( $^5\Pi$ )					
$^5A'$	2.098	2.732	5.59	5.52	855.,600.(2),-1175.
$^5A''$	2.098	2.732	5.59	5.52	853.,620.(2),-1179.
N-H-O( $^3\Pi$ )					
	2.152	2.571	11.72		
N + OH	20.0	1.847	-22.9	-23.1	

Table IV. Computed Energies for N-H-O ( $^3\Pi$  state) Bent Geometries <sup>a</sup>.

$r_{NH}$	$r_{OH}$	$\theta$	Energy
2.152	2.571	180.	-129.99839(-.01616) <sup>b</sup>
2.152	2.571	170.	-129.99807(-.01536)
2.152	2.571	160.	-129.99772(-.01495)
2.152	2.571	150.	-129.99712(-.01437)
2.152	2.571	140.	-129.99626(-.01360)
2.152	2.571	180.	-129.99835(-.01590) <sup>c</sup>
2.152	2.571	170.	-129.99817(-.01566)
2.152	2.571	160.	-129.99780(-.01528)
2.152	2.571	150.	-129.99735(-.01496)
2.152	2.571	140.	-129.99712(-.01508)
2.152	2.571	130.	-129.99790(-.01663)

<sup>a</sup> [4s3p2d1f/3s2p1d] ANO basis set. Second order CASSCF/CCI calculations correlating ten electrons.

<sup>b</sup>  $^3A'$  state.

<sup>b</sup>  $^3A''$  state.

Table V. Computed Transition State Theory Rate Constant for Reaction (1) on the  $^5\Pi$  Surface.

T	$\kappa$ $^5A'$	rate	$\kappa$ $^5A''$	rate	total
300.00	3.5326	0.1265E-13	3.5778	0.1165E-13	0.2430E-13
500.00	1.5864	0.9191E-13	1.5927	0.8566E-13	0.1776E-12
750.00	1.2364	0.3675E-12	1.2385	0.3440E-12	0.7115E-12
1000.00	1.1313	0.9007E-12	1.1324	0.8442E-12	0.1745E-11
1250.00	1.0848	0.1728E-11	1.0855	0.1620E-11	0.3348E-11
1500.00	1.0596	0.2862E-11	1.0600	0.2685E-11	0.5547E-11
2000.00	1.0344	0.6050E-11	1.0347	0.5676E-11	0.1173E-10
2500.00	1.0242	0.1042E-10	1.0245	0.9774E-11	0.2019E-10
3000.00	1.0153	0.1581E-10	1.0153	0.1483E-10	0.3064E-10

Draft date June 26, 1990  
To be submitted to J. Chem. Phys

**A Potential Energy Surface For  $H_2+H_2O$ :  
*ab initio* calculations and analytical representation.**

David W. Schwenke,  
NASA Ames Research Center, MS 230-3, Moffett Field, CA, 94035

Stephen P. Walch\* and Peter R. Taylor\*  
ELORET Institute, Palo Alto, CA 94303

**Abstract:**

We have performed extensive *ab initio* calculations on the ground state potential energy surface of  $H_2+H_2O$ , using a large contracted Gaussian basis set and a high level of correlation treatment. An analytical representation was then obtained which represents the calculated energies with an overall root-mean-square error which is  $0.64 mE_h$ . All nine internal degrees of freedom are explicitly included in the fit. The analytical representation is also well behaved as the  $H_2$  bond dissociates; it thus can be used to study collision-induced dissociation or recombination of  $H_2$ . The strategy used to minimize the number of energy calculations is discussed as well as other advantages of the present method for determining the analytical representation.

---

\* Mailing address: NASA Ames Research Center, MS 230-3, Moffett Field, CA, 94035

## I. Introduction

An important series of reactions for modeling combustion are the three-body recombination processes



where A and B are either atoms or small molecules and M is the third body. For hydrogen combustion, a wide variety of components have been studied experimentally,<sup>1</sup> and a very interesting result is that for A=H, B=OH, most nonreactive third bodies give similar rates, with the exception of M=H<sub>2</sub>O, which appears to cause a much higher rate of recombination. Because of the experimental uncertainties involved, it is important to verify this observation with theoretical studies, and to explain the cause of the differences. A study of this type by necessity requires comparison to other third bodies and recombining molecules, and the results of extensive calculations for A=B=H, M=H and H<sub>2</sub> have recently been reported.<sup>2</sup> The next logical system to consider is A=B=H, M=H<sub>2</sub>O, and in this paper we report the first step in these calculations, namely the determination of an analytical representation of the potential energy of the collision partners.

The potential energy surface (PES) can be obtained from empirical models, from fits to various types of experimental information, from *ab initio* electronic structure calculations, or combinations of these methods. However, for processes that sample a large amount of the PES the only practical method is to use *ab initio* data. In the dynamics techniques we are planning to use for the H<sub>2</sub>+H<sub>2</sub>O system, we will include highly excited H<sub>2</sub> molecules and collision energies corresponding to several thousand degrees Kelvin,<sup>2</sup> thus we are primarily interested in relatively high energy portions of surface. Points in arbitrary regions of the PES will be required in the dynamics calculations, thus it is necessary to construct an interpolating function so that the number of *ab initio* electronic structure calculations can be kept to a minimum. The construction of a faithful interpolating function can be an arduous task if an inappropriate strategy is used.

In this paper we report a successful extension to a nonreactive diatom-polyatomic system of a method for constructing interpolating functions originally applied to a nonreactive atom-diatom system.<sup>3</sup> This method has also been modified for use for a diatom-diatom system.<sup>4</sup> The basic strategy used in the present work is to introduce a simple trial function which has many of the global properties of

the pentatomic system, and then make corrections to this function to make up for its local inadequacies. It is expected that this procedure will reduce the complexity of the function which is being represented, resulting in a reduction of the number of points required and an increase in the accuracy of the result. The analytical representation used in the present work has other attractive features: most of the numerical parameters are linear, which makes their optimization straightforward, and also the function is designed for efficient computer evaluation. Many of the techniques introduced in this paper concerning polyatomics are more general than the present application and are thus expected to be valuable in other attempts to produce analytical representations of potential energy surfaces involving polyatomics.

In Sec. II we discuss our electronic structure calculations, then in Sec. III we give the interpolating function. Our final discussions and conclusions are contained in Sec. IV. All quantities are quoted in Hartree atomic units unless otherwise noted, thus the unit of energy is  $E_h = 2625.500$  kJ/mol, the unit of length is  $a_0 = 0.5291771 \times 10^{-10}$  m, and the unit of mass is  $m_e = 9.109534 \times 10^{-31}$  kg.

## II. Electronic Structure Calculations.

For a one-electron basis we used a (13s8p6d4f/8s6p4d) Gaussian primitive basis set, derived from the van Duijneveldt<sup>5</sup> (13s8p/8s) set by adding polarization functions as described in Ref. 6. These functions were then contracted using the ANO scheme<sup>6</sup> to yield a [4s3p2d1f/3s2p1d] basis set. Finally in order to improve the description of the outermost regions of the charge density, the most diffuse s and p primitive functions on O and the most diffuse primitive s function on H were uncontracted,<sup>7,8</sup> giving rise to our final basis, denoted [4+1s 3+1p 2d 1f/3+1s 2p 1d], which was used in all calculations of the supermolecule. This basis will give more accurate multipole moments than the [4s3p2d1f/3s2p1d] basis, and thus can be expected to lead to an improved description of the long-range interactions.

The energy calculations were designed to give an accurate description of the process  $H + H + H_2O \rightarrow H_2 + H_2O$  with the  $H_2O$  geometry always near its equilibrium configuration. The most important nondynamical electron correlation effects were taken into account by means of CASSCF calculations, and the dynamical correlation effects were estimated using the size-extensive ACPF<sup>9</sup> method. The

CASSCF configurations correspond to a single configuration description of H<sub>2</sub>O and a two-electron two active orbital description of H<sub>2</sub>, and the ACPF calculations used the same reference space. All calculations were carried out using the MOLECULE-SWEDEN<sup>10</sup> program system on either the NAS CRAY Y-MP/832 or the Ames ACF CRAY Y-MP/832.

The computed H<sub>2</sub>O fragment properties obtained using these methods are given in Table I, where they are also compared to experimental measurements<sup>11-15</sup>. Calculations are carried out for four H<sub>2</sub>O geometries. These correspond to the equilibrium (denoted EQ),<sup>16</sup> an approximate turning point for the symmetric stretch normal mode (denoted SS), the asymmetric stretch normal mode (denoted AS), and the bending normal mode (denoted B). The normal mode analysis was performed using the H<sub>2</sub>O potential of Ref. 17 which is a slight modification of the fit of Ref. 18 to the *ab initio* electronic structure calculations of Ref. 19. The modification is to adjust the expansion coefficient  $a_{002}$  to reproduce experimental bending vibrational energy levels in a variational basis set calculation. This function represents well the results from the present calculation — the function given in Ref. 17 predicts energy differences between the equilibrium and distorted geometries given in this table to be uniformly 0.1 mE<sub>h</sub> lower than our *ab initio* calculations.

Also in Table I, we compare to experimental values for the dipole moment, the quadrupole moment, and the mean polarizability defined as

$$\bar{\alpha} = \frac{1}{3} (\alpha_{xx} + \alpha_{yy} + \alpha_{zz}). \quad (2)$$

The quadrupole and dipole moments are computed as expectation values, while the polarizability is computed as an energy derivative, as in Ref. 8. For the quadrupole moment and mean polarizability, the experimental measurements are of vibrationally-thermally-averaged results whereas the theoretical results are for a specific geometry. Nonetheless, the agreement is quite satisfactory, with differences on the order of a few per cent. For the dipole moment, it is possible to estimate values for particular geometries from experiment. To do so we follow Ref. 13 and write (note that we use different axis labels and directions than from those in Ref. 13)

$$\mu_z = \mu_z^0 + \mu_z^1 q_1 + \mu_z^2 q_2 + \mu_z^{22} q_2^2, \quad (3)$$

and

$$\mu_x = \mu_x^1 q_3, \quad (4)$$

where  $q_i$  is a dimensionless normal mode coordinate. These coordinates were computed from

$$q_i = \left( \frac{\lambda_i}{\hbar^2} \right)^{1/4} \sum_j m_j^{1/2} l_{ji} \Delta x_j, \quad (5)$$

where  $\lambda_i$  is an eigenvalue of the mass-weighted Cartesian Hessian matrix, the sum over  $j$  is over all coordinates and atoms in  $\text{H}_2\text{O}$ ,  $m_j$  is the mass of the atom associated with index  $j$ ,  $\Delta x_j$  is the displacement from equilibrium for the atom/coordinate associated with index  $j$ , and  $l_{ji}$  is the  $j^{\text{th}}$  component of the  $i^{\text{th}}$  normalized eigenvector of the mass-weighted Cartesian Hessian matrix. The eigenvectors were phased to be consistent with Ref. 13. For the AS geometry, it is necessary to rotate the coordinates before applying Eq. (5) in order to properly separate vibration and rotation. This is done as described in Ref. 20, and the rotation angle is  $-5.363^\circ$ . The dipole moment components given by Eqs. (3) and (4) are then rotated by  $5.363^\circ$  to make the comparisons in Table I. We take  $\mu_z^0$  from Ref. 11,  $\mu_z^1$ ,  $\mu_z^3$  and  $\mu_z^{22}$  from Ref. 12, and  $\mu_z^2$  from Ref. 13. Again the agreement is satisfactory, with differences of a few per cent or less. Of particular note is the fact that the accuracy for the different geometries is about the same.

In Table II we summarize the energies of the noninteracting fragments. We will need energies for  $\text{H}_2$  bond lengths close to, but not exactly equal to points in Table II, and these were generated by interpolation. The six points in Table II with  $\text{H}_2\text{O}$  at the EQ geometry and  $\text{H}_2$  bond length ( $r_{\text{H}_2}$ ) varying from 1.2 to 2.2 were fit to a five term expansion in  $1/r_{\text{H}_2}$ , and energies were determined at the bond lengths 1.201, 1.601, 1.801 and 2.001  $a_0$ . The difference between using the five term expansion and a six term expansion is no larger than 0.01  $\text{mE}_h$ .

Four sets of calculations for the interacting system were carried out. The first consisted of the calculation of  $\text{H}+\text{H}_2\text{O}$  interactions at two relative orientations with the  $\text{H}_2\text{O}$  geometry fixed at the equilibrium geometry. This geometry has OH bond lengths equal to 1.8111  $a_0$ , and an HOH angle equal to  $104.45^\circ$ . These results are given in Table III. The second set is made up of 9 different relative orientations of  $\text{H}_2$  and  $\text{H}_2\text{O}$ , with the  $\text{H}_2$  at its equilibrium separation of 1.401  $a_0$  and the  $\text{H}_2\text{O}$  at the experimental equilibrium geometry. The results of these calculations are given in Table IV. The third set relaxes the restriction that  $\text{H}_2$  be at equilibrium, and the results for these calculations are given in Table V. The final set relaxes the  $\text{H}_2\text{O}$  equilibrium geometry restrictions, and the results are given in Table VI. Since the

interpolating function obtained using the data of Tables I-V represents the data in Table VI well, we computed no other points. In all, a total of 181 points were computed. It should be noted that although we quote only five decimal digits for the energy in the tables, when fitting the points, eight digits were used. Since the errors in the fit are larger than  $0.01mE_h$ , the difference between using eight and five digits should not be significant.

The relative orientations of  $H_2$  and  $H_2O$  are given by a code of the form  $a \pm bc$  where  $a$  is  $z$  or  $x$ , and  $b$  and  $c$  are  $x$ ,  $y$ , or  $z$ . This code will uniquely specify the orientations in the Cartesian coordinate system which has the O at the origin and the  $H_2$  center of mass on the positive  $z$  axis. The first part of the code gives the axis the  $H_2$  bond is parallel to, and the last two elements of the four part code give the plane the  $H_2O$  lies in. Furthermore, the bisector of the HOH angle is the  $b$  axis, and the sign on  $b$  indicates the sign of the  $b$  axis components of the coordinates of the H atoms in  $H_2O$ . For example,  $z - zx$  indicates that the  $H_2$  is on the  $z$  axis and the  $H_2O$  lies in the  $zx$  plane with the H atoms having coordinates  $(\pm 1.431545, 0, -1.109420)$ .

### III. Interpolating function

The basic idea of Ref. 3 is that although a pairwise-additive potential is not quantitatively accurate, it is always physically reasonable for a nonreactive system, thus it can be productive to start out with a pairwise additive potential and then make corrections to it. In particular, the pairwise additive potential was shifted by a small amount to make it always positive, then was multiplied by a function which never differs greatly from unity.

In the extension to a diatom-diatom system,<sup>4</sup> the main modification was to explicitly consider the long-range forces and to include the complications arising when atom exchange can occur. In the present application we will ignore the possibility of atom exchange between the  $H_2$  and  $H_2O$  and write the potential energy as

$$V = V^{int} + V^{H_2} + V^{H_2O}, \quad (6)$$

where  $V^{H_2}$  is the asymptotic  $H_2$  fragment potential,  $V^{H_2O}$  is the asymptotic  $H_2O$  fragment potential, and  $V^{int}$  is the interaction potential. This last term is given by

$$V^{int} = s \left[ f^{SV} (V^0 + \epsilon) - \epsilon + V^{LR} \right] + (1 - s)V^0, \quad (7)$$

where  $f^{SV}$  is the multiplicative correction function for small vibrational displacements,  $s$  is a switching function,  $V^0$  is a sum of pairwise potentials,  $\epsilon$  is a constant which ensures that  $f^{SV}$  will remain close to unity even if  $V^0$  is small and  $V^{int}$  is large, or vice versa, and  $V^{LR}$  is the long-range part of the potential. We now discuss each of the functions that go into  $V$  in detail.

The function  $V^{H_2}$  is taken from Ref. 4, and is an accurate representation of the best ground state  $H_2$  potential curve. It includes radiative, relativistic and adiabatic corrections to the very accurate Born-Oppenheimer calculations of Ref. 21, although of course these corrections are considerably smaller than our overall uncertainties. For the function  $V^{H_2O}$ , we take the expression from Ref. 17, which is a slight modification of the fit of Ref. 18 to the *ab initio* electronic structure calculations of Ref. 19. The choice of the fragment potentials is not important for the determination of the interaction potential and other choices may be more suitable for a particular application. For example  $V^{H_2} \rightarrow \infty$  as  $r_{H_2} \rightarrow 0$  for the function of Ref. 4 and  $V^{H_2O}$  has spurious deep wells for some geometries highly distorted from equilibrium for the function of Ref. 17, and these features may cause difficulty. Thus we encourage users of this potential to substitute these fragment potentials with other choices if required.

The zeroth-order potential  $V^0$  is written as the sum of the two  $H+H_2O$  interactions, and each “ $H_3O$ ” potential is written as

$$V^{H_3O} = V^{HH}(R_{HH_a}) + V^{HH}(R_{HH_b}) + V^{HO}(R_{HO}), \quad (8)$$

where  $V^{HA}$  is a non-bonding pair potential between the lone H and atom A,  $R_{HA}$  is the distance between the lone H and atom A, and the hydrogens in  $H_2O$  are labeled  $a$  and  $b$ . The pair potentials are represented as

$$V^{HA} = b^{HA} \exp(-c^{HA} R_{HA}), \quad (9)$$

with  $b^{HA}$  and  $c^{HA}$  constants. The constants in Eqs. (8)–(9) were determined by fitting the data in Table III using nonlinear least squares. For these calculations, we take the zero of energy to be  $-77.34187E_h$ , which is the value in Table III with the  $H_2$  bond length equal to  $10 a_0$ . In the least squares procedure, all points with interaction energies less than  $40 mE_h$  were equally weighted, while the other points were given a weight of zero. Thus 17 points were used to determine the

four parameters. This fit has a root-mean-square (rms) error of  $0.40 \text{ mE}_h$  and the parameters are given in Table VII and the fit is compared graphically to the data in Fig. 1.

The points with interaction energies greater than  $40 \text{ mE}_h$  were not included in the fitting procedure because a plot of the energies in Table III for the geometry  $z - zx$  reveals an avoided crossing for an OH distance  $\approx 2.0 a_0$ . This feature corresponds to an interaction with the  $1^2A_1$  state of  $\text{H}_3\text{O}$ , which may be thought<sup>22</sup> of as a 3s Rydberg state arising from  $\text{H}_3\text{O}^+$ . Since this feature occurs for energies greater than  $40 \text{ mE}_h$ , it is not expected to be important in the energy range over which the present potential is expected to be accurate. We therefore do not attempt to reproduce this feature of the potential, and neglect these higher energy points.

To proceed further, we must define our coordinates in more detail. Two kinds of coordinates are used in the analytical representation of the  $\text{H}_2 + \text{H}_2\text{O}$  potential. The first consists of distances between points, such as atoms or centers of mass. The second is more suitable for scattering calculations and consists of angles as well as distances. We will assume that the input to the calculation of the analytical representation will consist of Cartesian coordinates of the atoms in some arbitrary laboratory-fixed coordinate system. From these coordinates, the calculation of distances between points is straightforward, while the determination of the second set of coordinates is more complicated.

The second set of coordinates will consist of  $\Phi, \Delta, \Gamma, r, r_{\text{H}_2}, \theta, r_{\text{OH}_a}, r_{\text{OH}_b}, \Theta, \alpha, \beta,$  and  $\gamma$ . The Euler angles  $\Phi, \Delta,$  and  $\Gamma$  specify the relative orientation between the laboratory-fixed coordinate system and the body-fixed coordinate system,  $r$  is the distance between the centers of mass of  $\text{H}_2$  and  $\text{H}_2\text{O}$ ,  $r_{\text{H}_2}$  is the  $\text{H}_2$  bond length,  $\theta$  specifies the  $\text{H}_2$  orientation in the body-fixed coordinate system,  $r_{\text{OH}_a}, r_{\text{OH}_b},$  and  $\Theta$  specify the  $\text{H}_2\text{O}$  geometry, and the Euler angles  $\alpha, \beta$  and  $\gamma$  specify the orientation of the water molecule in the body-fixed coordinate system.

We determine these coordinates from the laboratory-fixed Cartesian coordinates of the atoms via the following procedure. We first shift the origin of the laboratory-fixed coordinates to the center of mass of the  $\text{H}_2\text{O}$  molecule, and then construct the rotation matrix  $\mathbf{R}^{\text{Body}}$  which rotates these laboratory-fixed coordinates to the body-fixed coordinates. That is, we find the matrix which satisfies

$$x_i^{\text{BodyA}} = \sum_j R_{ij}^{\text{Body}} x_j^{\text{LabA}} \quad (10)$$

and

$$x_i^{LabA} = \sum_j R_{ji}^{Body} x_j^{BodyA}, \quad (11)$$

where  $x_i^{BodyA}$  is the  $i^{th}$  component of the Cartesian coordinates of point A in the body-fixed coordinate system and  $x_j^{LabA}$  is the  $j^{th}$  component of the coordinates of point A in the laboratory-fixed coordinate system. Now we choose our body-fixed  $z$  axis to go from the origin to the center of mass of the  $H_2$ , and the body-fixed  $xz$  plane to contain  $H_2$ . It is then a simple matter to construct orthogonal unit vectors along the body-fixed  $z$  and  $x$  axes with components expressed the laboratory-fixed coordinate system. To get the unit vector along the body-fixed  $y$  axis, we simply take the cross product of these two unit vectors ( $\vec{y} = \vec{z} \times \vec{x}$ ). Then since the  $x_j^{BodyA}$  in Eq. (11) are just columns of the unit matrix, we can identify the elements of the rotation matrix  $\mathbf{R}^{Body}$  with the elements of the unit vectors expressed in the laboratory-fixed coordinate system. This rotation matrix determines the Euler angles  $\Phi, \Delta, \Gamma$ , but we never explicitly need to know these angles — it is the rotation matrix which is of use. Once  $\mathbf{R}^{Body}$  has been determined, we can rotate the atomic coordinates to the body-fixed coordinate system.

The lengths  $r$  and  $r_{H_2}$  are easily determined from the body-fixed coordinates of the  $H_2$ , and the angle  $\theta$  is the angle which rotates the  $H_2$  about its center of mass to lie on the  $z$  axis. However as in the case with the angles  $\Phi, \Delta$ , and  $\Gamma$ , it is not necessary to explicitly determine  $\theta$ , but rather just the rotation matrix  $\mathbf{R}^{H_2}$  which rotates the  $H_2$  coordinates so that only the  $z$  components are nonzero. The nonzero entries of this rotation matrix can be found by simple arithmetic operations from the Cartesian coordinates and  $r_{H_2}$ .

The internal  $H_2O$  coordinates are  $r_{OH_a}$ , the distance from the O to hydrogen atom  $a$ ,  $r_{OH_b}$ , the distance from the O to hydrogen atom  $b$ , and  $\Theta$ , the HOH angle. These coordinates are easily determined from the Cartesian coordinates of the atoms and are chosen because they are used for the  $H_2O$  fragment potential of Ref. 17. In order to specify the Euler angles  $\alpha, \beta, \gamma$ , we define a standard  $H_2O$  orientation.<sup>23</sup> This consists of the O atom lying on the positive  $z$  axis, the center of mass at the origin, the H atoms in the  $xz$  plane, and  $H_b$  having  $x$  positive. Then the Euler angles are those angles which rotate the particular body frame  $H_2O$  coordinates to the standard orientation. As before, it is only necessary to know the rotation matrix  $\mathbf{R}^{H_2O}$  which rotates the particular  $H_2O$  coordinates to the standard

orientation. This can be determined in the same manner as  $\mathbf{R}^{Body}$ , described above, without the explicit determination of the Euler angles.

We now turn to the long-range part of the potential. We will include the dipole-quadrupole and quadrupole-quadrupole electrostatic interactions, the dipole-induced dipole interaction, and the leading dispersion contribution. These consist of terms which decay as  $r^{-4}$  through  $r^{-6}$ . To compute these interactions, we took the  $\text{H}_2\text{O}$  properties from Table I, the  $\text{H}_2$  quadrupole moment from Ref. 24 and polarizability from Ref. 25, and the dispersion coefficients from Ref. 26. These were then used in damped versions of the appropriate formulas from Ref. 27.

Specifically, for the dipole-quadrupole interaction, we begin with the expressions

$$V^{\mu\Theta} = -\frac{1}{3} \sum_{ijk} \tilde{\mu}_{1,i} \tilde{\Theta}_{2,jk} T_{2,ijk}, \quad (12)$$

$$T_{2,ijk} = -3 \left[ 5r_i r_j r_k - r^2 (r_i \delta_{jk} + r_j \delta_{ik} + r_k \delta_{ij}) \right] r^{-7}, \quad (13)$$

where  $i, j, k$  refer to  $x, y$  or  $z$  components of the various tensors,  $\tilde{\mu}_{1,i}$  is an element of the dipole moment tensor for  $\text{H}_2\text{O}$ ,  $\tilde{\Theta}_{2,jk}$  is an element of the quadrupole moment tensor for  $\text{H}_2$ , and  $r_i$  is a component of the vector from the center of mass of the  $\text{H}_2\text{O}$  to the center of mass of the  $\text{H}_2$ . It should be noted that the multipole moments and  $r_i$  must all have been calculated using parallel coordinate systems for these equations to be valid. We will evaluate Eqs. (12) and (13) in the body-fixed coordinate system. In this case the only nonzero contribution from the  $r_i$  comes from  $i = 3$ , (*i.e.* the  $z$  component) thus Eq. (13) becomes

$$T_{2,ijk} = -3 [5\delta_{i3}\delta_{j3}\delta_{k3} - \delta_{i3}\delta_{jk} - \delta_{j3}\delta_{ik} - \delta_{k3}\delta_{ij}] r^{-4}. \quad (14)$$

We now modify Eq. (14) to remove the singularity at  $r = 0$  by changing  $r^{-4}$  to  $(r^4 + d^4)^{-1}$ , with  $d$  a positive damping parameter. Finally, before we can apply Eq. (12), it is necessary to obtain the components of the dipole moment and quadrupole moment tensors with respect to the body-fixed coordinates. We do this by rotating the laboratory-fixed coordinates using the rotation matrices determined when calculating the body-fixed coordinates. That is, in Eq. (12), we use the moments

$$\tilde{\mu}_{1,i} = \sum_j R_{ji}^{\text{H}_2\text{O}} \mu_j, \quad (15)$$

and

$$\tilde{\Theta}_{2,ij} = \sum_{kl} R_{ki}^{\text{H}_2} R_{lj}^{\text{H}_2} \Theta_{kl}^{\text{H}_2}, \quad (16)$$

where  $\mu_j$  is from Table I, and

$$\Theta_{kl}^{\text{H}_2} = -\delta_{kl}(-1)^{\delta_{k3}}(1 + \delta_{k3})Q/4, \quad (17)$$

with  $Q$  the quadrupole moment from Ref. 24. Now because  $\Theta_{kl}^{\text{H}_2}$  is diagonal and  $\mathbf{R}^{\text{H}_2}$  only rotates about the  $y$  axis, several terms in Eq. (12) vanish, and the so the dipole-quadrupole interaction simplifies to

$$V^{\mu\ominus} = -\left[2\tilde{\mu}_{1,1}\tilde{\Theta}_{2,13} - 3\tilde{\mu}_{1,3}\tilde{\Theta}_{2,33}\right]/(r^4 + d^4). \quad (18)$$

For the quadrupole-quadrupole interaction, we proceed in the same manner, starting with

$$V^{\ominus\ominus} = \frac{1}{9} \sum_{ijkl} \tilde{\Theta}_{1,ij} \tilde{\Theta}_{2,kl} T_{2,ijkl}, \quad (19)$$

$$\begin{aligned} T_{2,ijkl} = & 3 \left[ 35r_i r_j r_k r_l - 5r^2 (r_i r_l \delta_{jk} + r_j r_l \delta_{ik} \right. \\ & + r_k r_l \delta_{ij} + r_j r_k \delta_{il} + r_i r_k \delta_{jl} + r_i r_j \delta_{kl}) \\ & \left. + r^4 (\delta_{il} \delta_{jk} + \delta_{lj} \delta_{ik} + \delta_{kl} \delta_{ij}) \right] r^{-9}. \end{aligned} \quad (20)$$

After including damping and taking advantage of the fact that we evaluate this expression in the body frame and that certain elements of the  $\text{H}_2$  quadrupole are always zero, the quadrupole-quadrupole interaction simplifies to

$$\begin{aligned} V^{\ominus\ominus} = & \frac{1}{3(r^5 + d^5)} \left[ \tilde{\Theta}_{2,11}(2\tilde{\Theta}_{1,11} - 5\tilde{\Theta}_{1,33}) + \tilde{\Theta}_{2,22}(2\tilde{\Theta}_{1,22} - 5\tilde{\Theta}_{1,33}) \right. \\ & \left. + 12\tilde{\Theta}_{2,33}\tilde{\Theta}_{1,33} - 16\tilde{\Theta}_{2,13}\tilde{\Theta}_{1,13} \right], \end{aligned} \quad (21)$$

where  $\tilde{\Theta}_{2,ij}$  is defined by Eq. (16) and

$$\tilde{\Theta}_{1,ij} = \sum_{kl} R_{ki}^{\text{H}_2\text{O}} R_{lj}^{\text{H}_2\text{O}} \Theta_{kl}^{\text{H}_2\text{O}}, \quad (22)$$

with  $\Theta_{kl}^{\text{H}_2\text{O}}$  from Table I.

For the dipole-induced dipole interaction we begin with the expression

$$V^{\text{ind}} = -\frac{1}{2} \sum_{ij} \tilde{\alpha}_{2,ij} F_{2,i}^{\text{H}_2\text{O}} F_{2,j}^{\text{H}_2\text{O}}, \quad (23)$$

$$F_{2,i}^{\text{H}_2\text{O}} = \sum_k T_{2,ik} \tilde{\mu}_{2,k}, \quad (24)$$

where

$$T_{2,ik} = (3r_i r_k - \delta_{ik} r^2) / r^{-5} \quad (25)$$

and  $\tilde{\alpha}_{2,ij}$  is given by

$$\tilde{\alpha}_{2,ij} = \sum_{kl} D_{ki}^{\text{H}_2} D_{lj}^{\text{H}_2} \alpha_{kl}^{\text{H}_2}, \quad (26)$$

where  $\alpha_{kl}^{\text{H}_2}$  is an element of the  $\text{H}_2$  polarizability tensor. In terms of the  $\parallel$  and  $\perp$  components of the polarizability, we have  $\alpha_{11}^{\text{H}_2} = \alpha_{22}^{\text{H}_2} = \alpha_{\perp}^{\text{H}_2}$  and  $\alpha_{33}^{\text{H}_2} = \alpha_{\parallel}^{\text{H}_2}$ . The other components are zero. Simplifying and damping as before, we obtain

$$V^{\text{ind}} = -\frac{1}{2}(\tilde{\alpha}_{2,11} \tilde{\mu}_{1,1}^2 + \tilde{\alpha}_{2,22} \tilde{\mu}_{1,2}^2 + 4\tilde{\alpha}_{2,33} \tilde{\mu}_{1,3}^2 - 4\tilde{\alpha}_{2,1,3} \tilde{\mu}_{1,1} \tilde{\mu}_{1,3}) / (r^6 + d^6). \quad (27)$$

Finally, for the dispersion interaction we use

$$V^{\text{disp}} = -c_6 / (r^6 + d^6). \quad (28)$$

Then the long-range potential is given by

$$V^{\text{LR}} = V^{\mu\ominus} + V^{\ominus\ominus} + V^{\text{ind}} + V^{\text{disp}}. \quad (29)$$

To represent the dependence of the multipole moments, polarizabilities, and dispersion coefficients on the vibrational coordinates, we proceeded as follows. For the  $\text{H}_2$  quadrupole moment, we used the expression from Ref. 4 for  $Q$ . This function was determined by fitting the accurate results of Ref. 24.

For the  $\text{H}_2$  polarizability, we fit the data of Ref. 25 to the form

$$\alpha_c = (g_{0c} + g_{1c}X + g_{2c}X^2) / (1 + X^2), \quad (30)$$

where the subscript  $c$  refers to  $\parallel$  or  $\perp$ ,  $g_{ic}$  is a parameter, and

$$X = \exp[h_c(r_{\text{H}_2} - r_c)]. \quad (31)$$

The parameters  $g_{ic}$ ,  $h_c$  and  $r_c$  were determined by nonlinear least squares, with the exception that  $g_{2c}$  was constrained to be nine so that the asymptotic value of  $\alpha_c$  is accurately obtained. The points were unequally weighted in the fit, with most points having a weight of one. The five points near the equilibrium bond length

had larger weights, and a point near the maximum and a point past the maximum were also more heavily weighted. The weighted rms error for  $\alpha_{\parallel}$  is  $5.7 \times 10^{-2} a_0^3$  and the weighted rms error for  $\alpha_{\perp}$  is  $4.4 \times 10^{-2} a_0^3$ . A comparison of these fits and the data points is given in Fig. 2, and the values of the parameters are given in Table VIII.

For the dependence of the dispersion coefficient on the H<sub>2</sub> bond length, we used the procedure of Ref. 4, *i.e.* we assume

$$c_6 = r_{\text{H}_2}^{m_6^0} (\bar{a}_6^0 + \bar{b}_6^0 r_{\text{H}_2}) \exp[-(d_Q r_{\text{H}_2})^2] \bar{c}_6, \quad (32)$$

with the parameters  $m_6^0$ ,  $\bar{a}_6^0$ ,  $\bar{b}_6^0$ , and  $d_Q$  taken from Ref. 4. The parameters for Eq.(32) are given in Table VIII.

For the multipole moments and mean polarizability of H<sub>2</sub>O, we make the approximation

$$M(r_{\text{OH}_a}, r_{\text{OH}_b}, \Theta) = M^{000} + M^{100} r_{\text{OH}_a} + M^{010} r_{\text{OH}_b} + M^{110} r_{\text{OH}_a} r_{\text{OH}_b} + M^{001} \Theta, \quad (33)$$

where  $M$  is a component of either the dipole moment, the quadrupole moment, or the mean polarizability. The parameters in Eq.(33) are determined by fitting the data from Table I and are given in Table IX.

To determine the dependence of the dispersion coefficient on the H<sub>2</sub>O geometry, we invoke the Slater-Kirkwood approximation<sup>28</sup> and the geometric mean rule. The Slater-Kirkwood approximation gives the H<sub>2</sub>O-H<sub>2</sub>O dispersion coefficient as a constant times  $\bar{\alpha}^{3/2}$ , while the geometric mean rule gives the H<sub>2</sub>O-H<sub>2</sub> dispersion coefficient as the geometric mean between the H<sub>2</sub>O-H<sub>2</sub>O and H<sub>2</sub>-H<sub>2</sub> coefficients. Thus we take the dispersion coefficient to be proportional to  $\bar{\alpha}^{3/4}$  and multiply the expression of Eq. (32) by the ratio of the 3/4 power of the mean polarizability computed from Eq. (33) and the equilibrium value of  $9.35 a_0^3$ .

We now turn to the remaining ingredients of  $f^{SV}$ . Before we proceed we need to specify the switching function  $s$  in Eq.(7). This function is designed to correct for deficiencies in the potential when the H<sub>2</sub> bond is greatly stretched. Thus we write

$$s = \bar{s}/(1 + \bar{s}), \quad (34)$$

with

$$\bar{s} = \exp[-a^s(r_{\text{H}_2} - r^s)]. \quad (35)$$

Our procedure to determine  $f^{SV}$  will be to guess values for the nonlinear parameters  $\epsilon$ ,  $d$ ,  $a^s$ , and  $r^s$ , and then invert Eq. (7) and solve for the multiplicative correction function. This function is then fitted, and then the four nonlinear parameters defining the numerically determined  $f^{SV}$  are adjusted until a satisfactory fit is obtained.

We will expand the multiplicative correction function as follows:

$$f^{SV} = \sum_{pqmm'} \nu_{pqmm'}^{SV}(r, r_{H_2}, r_{OH_a}, r_{OH_b}, \Theta) A_{pqmm'}(\theta, \alpha, \beta, \gamma), \quad (36)$$

where  $\nu_{pqmm'}^{SV}$  is a yet to be determined function and  $A_{pqmm'}$  is an angular function. The prototype angular function is<sup>29</sup>

$$\tilde{A}_{pqmm'} = Y_{p-m}(\theta, 0) \mathcal{D}_{mm'}^{(q)}(\alpha, \beta, \gamma), \quad (37)$$

where  $Y_{pm}$  is a spherical harmonic, and  $\mathcal{D}_{mm'}^{(q)}$  is a Wigner rotation matrix element.<sup>30</sup> These angular functions are orthogonal, but are complex. This implies relations between the expansion coefficients, as  $f^{SV}$  is real. Since it can be easily shown that

$$\tilde{A}_{pqmm'}^* = (-1)^{m'} \tilde{A}_{pq-m-m'}, \quad (38)$$

we can restrict the sum in Eq. (36) to  $m > 0$ ,  $m'$  unrestricted, or  $m = 0$ ,  $m' \geq 0$ , and take the real part of the angular functions. Of the real angular functions with  $p, q \leq 2$ , we have chosen to use the nine angular functions given in Table X. It should be noted that for convenience, the normalization factors for these functions have been omitted.

An important simplification is that since we are assuming as input Cartesian coordinates the angular functions can be evaluated without trigonometric functions. This is because these functions are contained in the rotation matrices. In particular,

$$\cos \beta = R_{33}^{H_2O}, \quad (39)$$

$$\sin^2 \beta \cos(2\gamma) = (R_{13}^{H_2O})^2 - (R_{23}^{H_2O})^2, \quad (40)$$

$$\cos^4(\beta/2) \cos 2(\alpha + \gamma) = \left( \frac{R_{11}^{H_2} + R_{22}^{H_2}}{2} \right)^2 - \left( \frac{R_{21}^{H_2} - R_{12}^{H_2}}{2} \right)^2, \quad (41)$$

and

$$\sin^4(\beta/2) \cos 2(\alpha - \gamma) = \left( \frac{R_{11}^{\text{H}_2} - R_{22}^{\text{H}_2}}{2} \right)^2 - \left( \frac{R_{21}^{\text{H}_2} + R_{12}^{\text{H}_2}}{2} \right)^2. \quad (42)$$

We now turn to the functions  $\nu_{pqmm'}^{SV}$ . We will first fit the data of Table IV, *i.e.* those points with both the H<sub>2</sub> and H<sub>2</sub>O at their equilibrium geometry. For this fit, the  $\nu_{pqmm'}^{SV}$  are dependent only on the variable  $r$ , and we expand them as

$$\nu_{pqmm'}^{SV} = \delta_{p0} \delta_{q0} \delta_{m0} \delta_{m'0} + \sum_{i=1,3} v_{pqmm'i}^{SV} \exp \left[ -\alpha^{SR} (r - r^{SR} + id^{SR})^2 \right]. \quad (43)$$

Following the principles of Hamilton and Light,<sup>31</sup> we set the exponential parameter  $\alpha^{SR}$  equal to  $(1/d^{SR})^2$ . In the fitting procedure, for a fixed combination of the six nonlinear parameters,  $r^{SR}$ ,  $d^{SR}$ ,  $d$ ,  $\epsilon$ ,  $a^s$ , and  $r^s$ , we determine the linear parameters  $v_{pqmm'i}^{SV}$  that minimize the rms error of the multiplicative correction function  $f^{SV}$ . The points in this fit are weighted by the inverse of the number of points for a given relative orientation, *e.g.* for geometry  $z - zx$  the weight was 1/9 and for geometry  $z + zx$ , the weight was 1/8. Then the nonlinear parameters are adjusted to minimize the rms errors in the fit to the potential subject to the constraint that  $r^{SR} \geq 0$ . After several trials it was determined that the damping parameter  $d$  would not be large enough to provide adequate damping if it was allowed to vary freely, so it was constrained to be always greater than four. This became apparent when H<sub>2</sub> was allowed to be distorted away from equilibrium. The switching parameters in Eq. (35) are also adjusted, considering data with the H<sub>2</sub> bond stretched. The resulting parameters are given in Table XI. The weighted rms error in the fit to the  $f^{SV}$  is  $7.2 \times 10^{-5}$ , and the unweighted rms error in  $V^{int}$  is only 0.13 mE<sub>h</sub>. A total of 78 points are included in this fit. The largest relative errors occur in attractive regions of the potential, but since the magnitude of the potential is very small there and we plan to use this potential for dynamics calculations at high temperatures, we made no attempt to improve the fit to these features by weighting the points differently.

We next consider fitting the data in Table V, which includes several values of the H<sub>2</sub> bond length. Here we will proceed in a multi-step process. First of all, we proceed in a similar manner as described above for the data of Table IV, and determine functions  $\nu_{pqmm'}^{SV}(r_{\text{H}_2})$  and coefficients  $v_{pqmm'i}^{SV}(r_{\text{H}_2})$ . The current procedure differs from that used above in that the nonlinear parameters are fixed at the values determined above, and the data of Table V is not used directly. Since

slightly different values of  $H_2$  bond lengths were used for the different geometries, we synthesize a consistent set of data by taking all points in Tables IV and V which differ only in the value of the  $H_2$  bond length, and interpolate to a common group of bond lengths. These lengths are 1.2, 1.401, and 1.6  $a_0$ , and the interpolation was carried out by fitting the points to a polynomial in  $1/r_{H_2}$  which exactly reproduced the input data. This was only carried out for geometries and values of  $r$  where there were at least three different values of the  $H_2$  bond length. This yields 35 data points per  $r_{H_2}$  which were used to determine the 27 parameters  $v_{pqmm'i}^{SV}(r_{H_2})$ . These fits to  $f^{SV}$  gave rms errors in  $V^{int}$  from  $22\mu E_h$  to  $62\mu E_h$ . Then the resulting parameters were fit to the form

$$v_{pqmm'i}^{SV}(r_{H_2}) = \sum_{j=0}^2 \tilde{v}_{pqmm'ij}^{SV}(r_{H_2} - 1.401a_0)^j. \quad (44)$$

This gives a trial set of expansion coefficients, however it does not exactly reproduce the fit to the data of Table IV, since only 35 rather than 78 points are used for the 1.401  $a_0$  data. We correct this by replacing  $\tilde{v}_{pqmm'i0}^{SV}$  with the  $v_{pqmm'i}^{SV}$  of Table XI. This is akin to separately fitting the function and its derivatives.<sup>32</sup> The parameters for Eq. (44) are given in Table XII. The overall rms error for the 156 data points in Tables IV and V with  $H_2$  bond length less than 3  $a_0$  using these parameters is only 0.64  $mE_h$ .

So far we have not discussed the inclusion of the switching function in Eq. (7). The need for such a function can be seen from considering orientations with the  $H_2$  on the  $z$  axis, such as the  $z + yx$  orientation shown in Fig. 3. The *ab initio* calculations predict that as  $r_{H_2}$  and  $r$  increase with the H to O distance fixed,  $V^{int}$  decreases approximately linearly. However, this can not continue indefinitely because eventually the further H will no longer interact with the fixed  $H_3O$  fragment and the interaction energy will become constant. This is exactly what the sum of pairwise potentials,  $V^0$ , predicts, while  $f^{SV}$  will continue to predict a decrease. Thus we switch to the  $V^0$  potential for  $r_{H_2}$  greater than about 2.5  $a_0$ .

We now turn to the data of Table VI, which has the  $H_2$  at its equilibrium bond length and the  $H_2O$  at distorted geometries. In principle, one could continue the procedure used to fit the data in Table V and expand the coefficients  $\tilde{v}_{pqmm'ij}^{SV}$  in terms of the  $H_2O$  internal coordinates, however this would require a vast increase in the number of *ab initio* energies. We thus proceed in the following manner: the

potential as it stands has a dependence on the  $\text{H}_2\text{O}$  internal coordinates through  $V^0$  and  $V^{LR}$ , and we ask how well this reproduces the *ab initio* calculations. Thus we performed a series of test calculations with displaced  $\text{H}_2\text{O}$  geometries and compared to the predictions of the fit. The results of the test calculations are given in Table VI, and the comparison between the *ab initio* and predicted values for  $V^{int}$  are given in Table XIII. Of the twelve entries in this table, eight have differences less than  $1 \text{ mE}_h$  (often much less), three have differences between 1 and  $2 \text{ mE}_h$ , and the final point, which is high-energy, has a difference of  $8 \text{ mE}_h$ , which is only 6% of the interaction energy. Thus although the fit to this data is not as good as the fit to the data in Tables IV and V, the degree of agreement is fair, and thus we conclude that the analytical representation is satisfactory as it stands for describing small  $\text{H}_2\text{O}$  distortions with  $\text{H}_2$  at equilibrium.

We also have not yet considered points where both the  $\text{H}_2$  and  $\text{H}_2\text{O}$  are displaced from equilibrium, however, since the analytical representation does a good job when either molecule is at its equilibrium geometry, and furthermore no parameters are explicitly required to represent the  $\text{H}_2\text{O}$  distortions, we will assume that the present analytical representation will describe these points accurately as well. Therefore we propose that the analytical representation as it stands will provide a realistic representation of the  $\text{H}_2+\text{H}_2\text{O}$  interaction potential.

#### IV. Discussion and Conclusions

We have produced an analytical representation of the  $\text{H}_2+\text{H}_2\text{O}$  potential energy surface suitable for dynamics calculations. All nine internal degrees of freedom are included, and the overall rms error between the 156 *ab initio* points in Tables IV and V and the function is only  $0.64 \text{ mE}_h$ . This is obtained with a function containing a total of 139 parameters, of which 87 are obtained from the 156 points and 52 which are obtained from other data.

We have computed the minimum energy for the  $\text{H}_2+\text{H}_2\text{O}$  van der Waals complex predicted using this potential. The depth of the minimum is quite small,  $0.43 \text{ kcal/mol}$ , which is on the same order of the overall rms error in the fit,  $0.40 \text{ kcal/mol}$ , so the reliability of the prediction can be questioned. However, the rms error for attractive points is only  $0.08 \text{ kcal/mol}$ , so it is likely that the prediction of the van der Waals complex is reasonable. The geometry of the minimum is asymmetric, but very close to a  $C_{2v}$  symmetry structure, with the  $\text{H}_2$  pointing toward the  $\text{H}_2\text{O}$

center of mass. The angle between the  $H_2$  bond and the  $H_2O$  plane is about  $151^\circ$ , with the H atoms pointing away from each other. The value of  $r$  at the minimum is  $5.81 a_0$  and the geometries of the  $H_2$  and  $H_2O$  are close to their equilibrium values.

The analytical representation of the  $H_2+H_2O$  potential energy surface proposed here has several desirable features. It represents the *ab initio* interaction energies well, and does so with relatively few parameters. In addition it is well behaved as  $H_2$  dissociates, so it can be used to study three-body recombination. From a practical point of view, it is useful to observe that most of the least squares parameters are linear parameters, so it is easy to determine them. Of the remaining parameters, the analytical representation is not a sensitive function of their exact values, so it is not difficult to obtain reasonable values for them. From a computational point of view, the potential should be reasonably efficient to evaluate, for a minimum number of special functions are required. In particular, the only trigonometric function used is arc cosine, to determine the HOH angle for the  $H_2O$  fragment potential. From a conceptual point of view, a major advantage of the present analytical representation is that it was not necessary to explicitly include parameters describing small distortions of the  $H_2O$  molecule. This greatly reduces the number of *ab initio* calculations required to determine the interpolating function.

## VI. Acknowledgements

SPW is supported by NASA grant no. NCC2-478 and PRT is supported by NASA grant no. NCC2-371. The calculations on the NAS CRAY Y-MP/832 were made possible with a grant of computer time from the NAS facility.

## References.

1. D. L. Baulch, D. D. Drysdale, D. G. Horne, and A. C. Lloyd, *Evaluated Kinetic Data For High Temperature Reactions*, C.R.C. Press, Cleveland, Ohio, 1972.
2. D. W. Schwenke, *J. Chem. Phys.*, in press.
3. F. B. Brown, D. W. Schwenke, and D. G. Truhlar, *Theor. Chim. Acta* **68**, 23 (1985).
4. D. W. Schwenke, *J. Chem. Phys.* **89**, 2076 (1988).
5. F. B. van Duijneveldt, IBM Research Report RJ 945 (IBM, San Jose, 1971).
6. J. Almlöf and P. R. Taylor, *J. Chem. Phys.* **86**, 4070 (1987).
7. C. W. Bauschlicher, *Chem. Phys. Lett.* **142**, 71 (1987).
8. J. Almlöf and P. R. Taylor, *J. Chem. Phys.* **92**, 551 (1990).
9. R. J. Gdanitz and R. Ahlrichs, *Chem. Phys. Lett.* **143**, 413 (1988).
10. MOLECULE-SWEDEN is an electronic structure program system written by J. Almlöf, C. W. Bauschlicher, M. R. A. Blomberg, D. P. Chong, A. Heiberg, S. R. Langhoff, P.-Å. Malmqvist, A. P. Rendell, B. O. Roos, P. E. M. Siegbahn, and P. R. Taylor.
11. S. A. Clough, Y. Beers, G. P. Klein, and L. S. Rothman, *J. Chem. Phys.* **59**, 2254 (1973).
12. J. M. Flaud and C. Camy-Peyret, *J. Mol. Spectrosc.* **55**, 278 (1975).
13. C. Camy-Peyret and J.-M. Flaud, *Mol. Phys.* **32**, 523 (1976).
14. J. Verhoeven and A. Dymanus, *J. Chem. Phys.* **52**, 3222 (1970).
15. G. D. Zeiss and W. J. Meath, *Mol. Phys.* **33**, 1155 (1977).
16. JANAF Thermochemical Tables, 2nd ed., edited by D. R. Stull and H. Prophet, *Natl. Stand. Ref. Data Ser. 37* (National Bureau of Standards, Washington, D.C., 1971).
17. J. M. Bowman, A. Wierzbicki and J. Zúñiga, *Chem. Phys. Lett.* **150**, 269 (1988).
18. W. C. Ermler (unpublished).
19. R. J. Bartlett, S. J. Cole, G. D. Purvis, W. C. Ermler, H. C. Hsieh, and I. Shavitt, *J. Chem. Phys.* **87**, 6579 (1987).
20. E. B. Wilson, J. C. Decius, and P. C. Cross, *Molecular Vibrations*, Dover, New York, 1980, p. 13.
21. W. Kolos, K. Szalewicz, and H. J. Monkhorst, *J. Chem. Phys.* **84**, 3278 (1986).
22. D. Talbi and R.P. Saxon, *J. Chem. Phys.* **91**, 2376(1989)
23. C. F. Curtiss, J. O. Hirschfelder, and F. T. Alder, *J. Chem. Phys.* **18**, 1638 (1950).

24. W. Kołos and L. Wolniewicz, *J. Chem. Phys.* **43**, 2429 (1965).
25. W. Kołos and L. Wolniewicz, *J. Chem. Phys.* **46**, 1426 (1967).
26. W. Rijks and P. E. S. Wormer, *J. Chem. Phys.* **90**, 6507 (1989).
27. A. D. Buckingham, *Adv. Chem. Phys.* **12**, 107 (1967).
28. J. C. Slater and J. G. Kirkwood, *Phys. Rev.* **37**, 682 (1931).
29. L. W. Hunter and C. F. Curtiss, *J. Chem. Phys.* **58**, 3884 (1973).
30. A. R. Edmonds, *Angular momentum in quantum mechanics*, Princeton University Press, Princeton, 1960.
31. I. P. Hamilton and J. C. Light, *J. Chem. Phys.* **84**, 306 (1986).
32. D. W. Schwenke and D. G. Truhlar, *J. Chem. Phys.* **88**, 4800 (1988).

Table I. Properties of H<sub>2</sub>O fragment. For H<sub>2</sub>O, the O is at the origin and the H atoms lie in the  $xz$  plane. All values quoted are in atomic units. The numbers in parenthesis are experimental results.

H <sub>2</sub> O geometry				
	EQ	B	SS	AS
$\pm x_H$	1.431545	1.561	1.515	1.418
$z_{H_a}$	-1.10942	-1.013	-1.233	-0.9053
$z_{H_b}$	-1.10942	-1.013	-1.233	-1.315
$E^{ACPF}$	-76.34202	-76.33813	-76.33309	-76.33295
$\mu_z$	-0.7504	-0.6974	-0.7762	-0.7502
	(-0.7268 <sup>a</sup> )	(-0.6719 <sup>b</sup> )	(-0.7529 <sup>b</sup> )	(-0.7258 <sup>b</sup> )
$\mu_x$	0.	0.	0.	0.0300
	0.	0.	0.	(0.0304 <sup>b</sup> )
$\Theta_{zz}^c$	1.874	2.382	1.927	1.827
	(1.96 <sup>d</sup> )			
$\Theta_{yy}^c$	-1.757	-1.875	-1.922	-1.759
	(-1.86 <sup>d</sup> )			
$\Theta_{xx}^c$	0.	0.	0.	0.3904
$\bar{\alpha}^e$	9.35	9.79	10.39	9.36
	(9.642 <sup>f</sup> )			

<sup>a</sup> From Ref. 11.

<sup>b</sup> Computed using the data from Refs. 11 – 13. See text for details.

<sup>c</sup> Calculated with the origin at the center of mass.  $\Theta_{zz}$  is computed by requiring that the quadrupole moment tensor be traceless.

<sup>d</sup> From Ref. 14.

<sup>e</sup> Mean polarizability computed using the [4+1s 3+1p 2+1d/3+1s 2+1p] basis set and methods of Ref. 8.

<sup>f</sup> From Ref. 15.

Table II. Energies for noninteracting  $\text{H}_2 + \text{H}_2\text{O} + 77 E_h$ . The shortest atom-atom distance between the fragments is at least  $20 a_0$ .

$r_{\text{H}_2}^a$	$\text{H}_2\text{O}^b$	$E^{ACPF}$	$r_{\text{H}_2}^a$	$\text{H}_2\text{O}^b$	$E^{ACPF}$
1.401	B	-0.51168	1.6	EQ	-0.50982
1.401	SS	-0.50670	1.8	EQ	-0.49633
1.401	AS	-0.50648	2.0	EQ	-0.47935
1.2	EQ	-0.50556	2.2	EQ	-0.46128
1.401	EQ	-0.51555	10.0	EQ	-0.34187

<sup>a</sup>  $\text{H}_2$  bond length.

<sup>b</sup>  $\text{H}_2\text{O}$  geometry.

Table III. Energies for  $\text{H}+\text{H}+\text{H}_2\text{O} + 77 E_h$ . All energies and distances are in atomic units.

$R_{\text{OH}}^a$	$E^{ACPF}$	$R_{\text{OH}}$	$E^{ACPF}$
geometry	$z - zx^b$	geometry	$z + zx$
1.50	-0.23800	2.7000	-0.27793
1.75	-0.28452	3.2000	-0.31222
2.00	-0.29341	3.7188	-0.32870
2.25	-0.29812	3.9688	-0.33305
2.50	-0.30628	4.2188	-0.33605
3.00	-0.32296	4.4688	-0.33810
3.50	-0.33308	4.7188	-0.33950
4.00	-0.33816	5.2188	-0.34105
5.00	-0.34149	5.7188	-0.34168
10.00	-0.34187	6.2188	-0.34190
		7.2188	-0.34196

<sup>a</sup> Distance of closest H to O in  $\text{H}_2\text{O}$ . The other H is  $20 a_0$  from the O.

<sup>b</sup> See text for geometry code.

Table IV. Energies for  $\text{H}_2+\text{H}_2\text{O} +77 E_h$  with  $\text{H}_2$  and  $\text{H}_2\text{O}$  at their equilibrium geometries. All energies and distances are in atomic units.

$R_{\text{OX}}^a$	$E^{\text{ACPF}}$	$R_{\text{OX}}$	$E^{\text{ACPF}}$
geometry	$z - zx$	geometry	$z + zx$
2.00	-0.39854	2.5	-0.40682
2.25	-0.44006	3.0	-0.46738
2.50	-0.46767	3.5	-0.49552
2.75	-0.48595	4.0	-0.50775
3.00	-0.49787	5.0	-0.51467
3.50	-0.51022	6.0	-0.51555
4.00	-0.51479	7.0	-0.51558
5.00	-0.51650	20.0	-0.51554
10.00	-0.51564		
geometry	$z + yx$	geometry	$z - zx$
2.2	-0.42505	2.5	-0.36057
2.4	-0.45114	3.0	-0.44664
2.6	-0.47025	3.5	-0.48662
2.8	-0.48412	4.0	-0.50384
3.0	-0.49410	5.0	-0.51378
3.2	-0.50119	6.0	-0.51527
3.5	-0.50807	7.0	-0.51547
4.0	-0.51361	20.0	-0.51554
5.0	-0.51616		
10.0	-0.51561		
geometry	$x - zy$	geometry	$x + zx$
2.5	-0.36970	2.5	-0.22643
3.0	-0.45060	3.0	-0.38570
3.5	-0.48848	3.5	-0.45984
4.0	-0.50480	4.0	-0.49283
5.0	-0.51408	5.0	-0.51267
6.0	-0.51539	5.5	-0.51486

7.0            -0.51552  
 20.0           -0.51555

6.0            -0.51561  
 6.5            -0.51582  
 7.0            -0.51583  
 20.0           -0.51555

	geometry	$x + zy$
2.5		-0.28418
3.0		-0.40844
3.5		-0.46952
4.0		-0.49730
5.0		-0.51388
5.5		-0.51556
6.0		-0.51604
7.0		-0.51601
20.0		-0.51555

	geometry	$x + yx$
2.5		-0.34296
3.0		-0.43577
3.5		-0.48047
4.0		-0.50060
5.0		-0.51307
6.0		-0.51521
7.0		-0.51552
20.0		-0.51555

	geometry	$x + xy$
2.75		-0.40140
3.00		-0.43867
3.25		-0.46443
3.50		-0.48190

	geometry	$x + xy$
4.00		-0.50137
4.50		-0.50980
5.00		-0.51334
10.00		-0.51555

---

<sup>a</sup> Distance between O and nearest H if the H<sub>2</sub> bond points to the O, otherwise the distance between O and the H<sub>2</sub> center of mass.

Table V. Energies for  $\text{H}_2 + \text{H}_2\text{O} + 77 E_h$  with  $\text{H}_2\text{O}$  at its equilibrium geometry and  $\text{H}_2$  displaced from equilibrium. All energies and distances are in atomic units.

$R_{\text{OX}}^a$	$r_{\text{H}_2}$	$E^{\text{ACPF}}$	$R_{\text{OX}}^a$	$r_{\text{H}_2}$	$E^{\text{ACPF}}$
geometry		$z - zx$	geometry		$x + xy$
2.00	1.6	-0.41306	2.75	1.601	-0.39807
2.00	1.8	-0.41768	2.75	1.201	-0.39044
2.00	2.0	-0.41642	3.00	1.601	-0.43342
2.00	2.2	-0.41173	3.00	1.201	-0.42923
2.25	1.6	-0.44747	3.25	1.601	-0.45831
2.25	1.8	-0.44575	3.25	1.201	-0.45554
2.50	1.2	-0.44861	3.50	1.601	-0.47547
2.50	1.6	-0.47019	3.50	1.201	-0.47310
2.50	1.8	-0.46416	4.00	1.601	-0.49496
3.00	1.2	-0.48445	4.00	1.201	-0.49229
3.00	1.6	-0.49532			
geometry		$z + zx$	geometry		$x - zx$
2.5	1.8	-0.40498	2.5	1.6	-0.35863
3.0	1.2	-0.45385	2.5	1.2	-0.34837
3.0	1.6	-0.46488	3.0	1.2	-0.43792
3.5	1.2	-0.48448	3.0	1.6	-0.44049
3.5	1.6	-0.49079	3.5	1.2	-0.47799
			3.5	1.6	-0.47989
geometry		$x - zy$	geometry		$x + zx$
2.5	1.2	-0.35527	2.5	1.6	-0.22158
2.5	1.6	-0.37009	2.5	1.2	-0.21865
3.0	1.6	-0.44546	3.0	1.6	-0.37847
3.0	1.2	-0.44091	3.0	1.2	-0.37893
3.5	1.2	-0.47941	3.5	1.2	-0.45227
3.5	1.6	-0.48221	3.5	1.6	-0.45243
geometry		$x + zy$	geometry		$x + yx$
2.5	1.6	-0.29103	3.0	1.6	-0.42983

2.5	1.8	-0.29236	3.0	1.2	-0.42693
2.5	2.0	-0.29171	2.5	1.2	-0.32995
2.5	2.2	-0.29083	2.5	1.6	-0.34194
3.0	1.2	-0.39687	2.5	1.8	-0.33464
3.0	1.6	-0.40586	3.5	1.6	-0.47373
3.5	1.2	-0.45984	3.5	1.2	-0.47190
3.5	1.6	-0.46419			
<b>geometry</b>		<b><math>z + yx</math></b>	<b>geometry</b>		<b><math>z + yx</math></b>
2.2	1.601	-0.43573	2.8	1.601	-0.48406
2.2	1.801	-0.43687	3.0	1.201	-0.48000
2.2	2.201	-0.43270	3.0	1.601	-0.49231
2.4	1.601	-0.45703	3.2	1.201	-0.48839
2.4	1.801	-0.45402	3.2	1.601	-0.49820
2.6	1.601	-0.47265	3.5	1.201	-0.49648
2.6	1.801	-0.46658	3.5	1.601	-0.50394
2.8	1.201	-0.46814	4.0	1.201	-0.50299
			4.0	1.601	-0.50855

---

<sup>a</sup> Distance between O and nearest H if the H<sub>2</sub> bond points to the O, otherwise the distance between O and the H<sub>2</sub> center of mass.

Table VI. Energies for  $\text{H}_2+\text{H}_2\text{O} + 77 E_h$  with  $\text{H}_2$  at its equilibrium geometry and  $\text{H}_2\text{O}$  displaced from equilibrium. All energies and distances are in atomic units.

$R_{\text{OX}}^a$	$E^{ACPF}$		$R_{\text{OX}}^a$	$E^{ACPF}$	
geometry	$z + zx,$	AS	geometry	$z - zx,$	AS
3.	-0.37285		3.	-0.43794	
4.	-0.48282		4.	-0.49483	
geometry	$z + zx,$	SS	geometry	$z - zx,$	SS
3.	-0.36676		3.	-0.44101	
4.	-0.48045		4.	-0.49566	
geometry	$z + zx,$	B	geometry	$z - zx,$	B
4.	-0.48928		3.	-0.44223	
3.	-0.38958		4.	-0.49963	

<sup>a</sup> Distance between O and nearest H.

Table VII. Parameters for non-bonding pair potentials in atomic units.

A	$b^{\text{HA}}$	$c^{\text{HA}}$
H	1.618	2.085
O	1.113	1.384

Table VIII. Coefficients for bond-length dependence of  $H_2$  long-range potential parameters in atomic units.

$c$	$g_{0c}$	$g_{1c}$	$g_{2c}$	$h_c$	$r_c$
	-1.26998	26.9001	9	0.882033	2.85570
⊥	-0.176017	3.69209	9	0.715359	1.8981
$m_6^0$	$a_6^0$	$b_6^0$	$d_Q$	$\bar{c}_6$	
1	1.17467	1.72657	0.449685	7.26091	

Table IX. Parameters for the vibrational dependence of the H<sub>2</sub>O electrostatic properties. See Eq. (33).

$M$	$M^{000}$	$M^{100}$	$M^{010}$	$M^{110}$	$M^{001}$
$\mu_z$	-1.034	-0.1463	-0.1463	0.05971	0.3387
$\mu_x$	0.000	0.1194	-0.1194	0.000	0.000
$\Theta_{zz}^a$	6.246	-5.581	-5.581	3.307	2.741
$\Theta_{yy}^a$	2.085	-1.151	-1.151	0.2764	-0.3180
$\Theta_{zz}^a$	0.000	1.552	-1.552	0.000	0.000
$\bar{\alpha}$	-11.97	7.545	7.545	-2.033	0.3624

<sup>a</sup> calculated with the origin at the center of mass of the H<sub>2</sub>O.

Table X. Angular expansion functions.

no.	$p$	$q$	$m$	$m'$	$A_{pqmm'}$
1	0	0	0	0	1
2	0	1	0	0	$\cos \beta$
3	0	2	0	0	$3 \cos^2 \beta - 1$
4	2	0	0	0	$3 \cos^2 \theta - 1$
5	2	1	0	0	$\cos \beta (3 \cos^2 \theta - 1)$
6	2	2	0	0	$(3 \cos^2 \beta - 1)(3 \cos^2 \theta - 1)$
7	0	2	0	2	$\sin^2 \beta \cos(2\gamma)$
8	2	2	2	2	$\sin^2 \theta \cos^4(\beta/2) \cos 2(\alpha + \gamma)$
9	2	2	2	-2	$\sin^2 \theta \sin^4(\beta/2) \cos 2(\alpha - \gamma)$

Table XI. Parameters for the fit of Eq.(43) in atomic units.

$p$	$q$	$m$	$m'$	$v_{pqmm'1}^{SV}$	$v_{pqmm'2}^{SV}$	$v_{pqmm'3}^{SV}$
0	0	0	0	8.0288800E-01	4.9208551E-02	-1.9085039E-03
0	1	0	0	3.1244004E-01	-9.0318002E-03	-3.9700638E-04
0	2	0	0	-3.2853972E-02	1.7373376E-03	-4.6648941E-04
2	0	0	0	-1.2802147E-01	-7.8669031E-03	-1.4491438E-03
2	1	0	0	-1.0989261E-02	1.8603093E-03	1.5477987E-05
2	2	0	0	1.3347056E-02	-2.8587331E-04	-6.2784176E-05
0	2	0	2	-1.7133020E-02	5.8373975E-04	2.0297984E-04
2	2	2	2	6.0174056E-02	2.5171433E-04	-6.3496729E-05
2	2	2	-2	-1.4148450E-01	1.5470255E-02	-3.9044009E-04
$r^{SR}$	$d^{SR}$	$d$	$\epsilon$	$a^s$	$r^s$	
0.	1.72	4.0	0.562	2.5	3.0	

Table XII. Parameters for the fit of Eq.(44) in atomic units.

$p$	$q$	$m$	$m'$	$\tilde{v}_{pqmm'1j}^{SV}$	$\tilde{v}_{pqmm'2j}^{SV}$	$\tilde{v}_{pqmm'3j}^{SV}$
$j = 1$						
0	0	0	0	-7.8409154E-01	5.7772398E-02	-5.2699265E-03
0	1	0	0	-2.8981900E-02	-6.4440092E-03	1.8197968E-04
0	2	0	0	-2.7464954E-02	5.4274961E-03	7.8214372E-05
2	0	0	0	-1.7779328E-01	-2.2780539E-02	-2.5086883E-04
2	1	0	0	-3.3807402E-02	1.3647800E-03	-4.6390793E-04
2	2	0	0	2.2092459E-02	-8.8503368E-04	4.5817703E-04
0	2	0	2	2.6905372E-02	-8.4002092E-03	2.6707433E-03
2	2	2	2	8.2026964E-02	1.2664571E-04	2.8665551E-05
2	2	2	-2	-2.3292928E-01	2.3490078E-02	-2.2725534E-03
$j = 2$						
0	0	0	0	-2.6892232E-01	-3.7369693E-02	2.9057342E-03
0	1	0	0	1.7217490E-01	-1.5812969E-02	1.5763320E-03
0	2	0	0	1.1942930E-01	-1.2523267E-02	2.4867362E-03
2	0	0	0	-2.0629499E-01	-1.1532656E-02	-5.2182780E-04
2	1	0	0	1.8435082E-01	-2.7919859E-02	4.9524319E-03
2	2	0	0	1.0729963E-01	-6.8764652E-03	1.2178887E-03
0	2	0	2	-4.1360738E-02	3.7667774E-03	-7.1684775E-04
2	2	2	2	1.4759330E-02	1.0189559E-03	-9.5442150E-05
2	2	2	-2	-3.7665040E-02	-2.4012130E-03	1.2519036E-03

Table XIII. Comparison of analytical representation to the *ab initio* data of Table VI. All energies are in  $mE_h$ .

$r (a_0)$	$H_2O^b$	geometry	$V^{int}$	
			<i>ab initio</i>	fit
3.	B	$x + zx$	122.1	114.1
3.	SS	$x + zx$	139.9	139.2
3.	AS	$x + zx$	133.6	134.4
4.	B	$x + zx$	22.41	21.08
4.	SS	$x + zx$	26.25	24.36
4.	AS	$x + zx$	23.66	23.61
3.	B	$x - zx$	69.45	70.10
3.	SS	$x - zx$	65.69	67.25
3.	AS	$x - zx$	68.54	68.88
4.	B	$x - zx$	12.05	11.99
4.	SS	$x - zx$	11.04	11.20
4.	AS	$x - zx$	11.66	11.61

<sup>b</sup>  $H_2O$  geometry.

Figure captions:

Fig. 1: Comparison of  $V^0$  to the *ab initio* data of Table III. Both have  $0.01 E_h$  added to them. The solid line and  $\circ$  are for the  $z + zx$  orientation and the dashed line and  $\square$  are for the  $z - zx$  configuration.

Fig. 2: Comparison of the fit to the  $H_2$  polarizability to the *ab initio* data from Ref. 25. The solid line and  $\circ$  are for the  $\parallel$  component and dashed line and  $\square$  are for the  $\perp$  component.

Fig. 3: Comparison of  $V^{int}$  to data for  $z + yx$  orientation. The variable  $r$  changes with  $r_{H_2}$  to maintain a fixed  $R_{OH}$  distance. The curves are for  $R_{OH}=2.2, 2.4, 2.6, 2.8, 3.0, 3.2, 3.5,$  and  $4.0 a_0$ .

H<sub>3</sub>O potential + 0.01E<sub>h</sub>

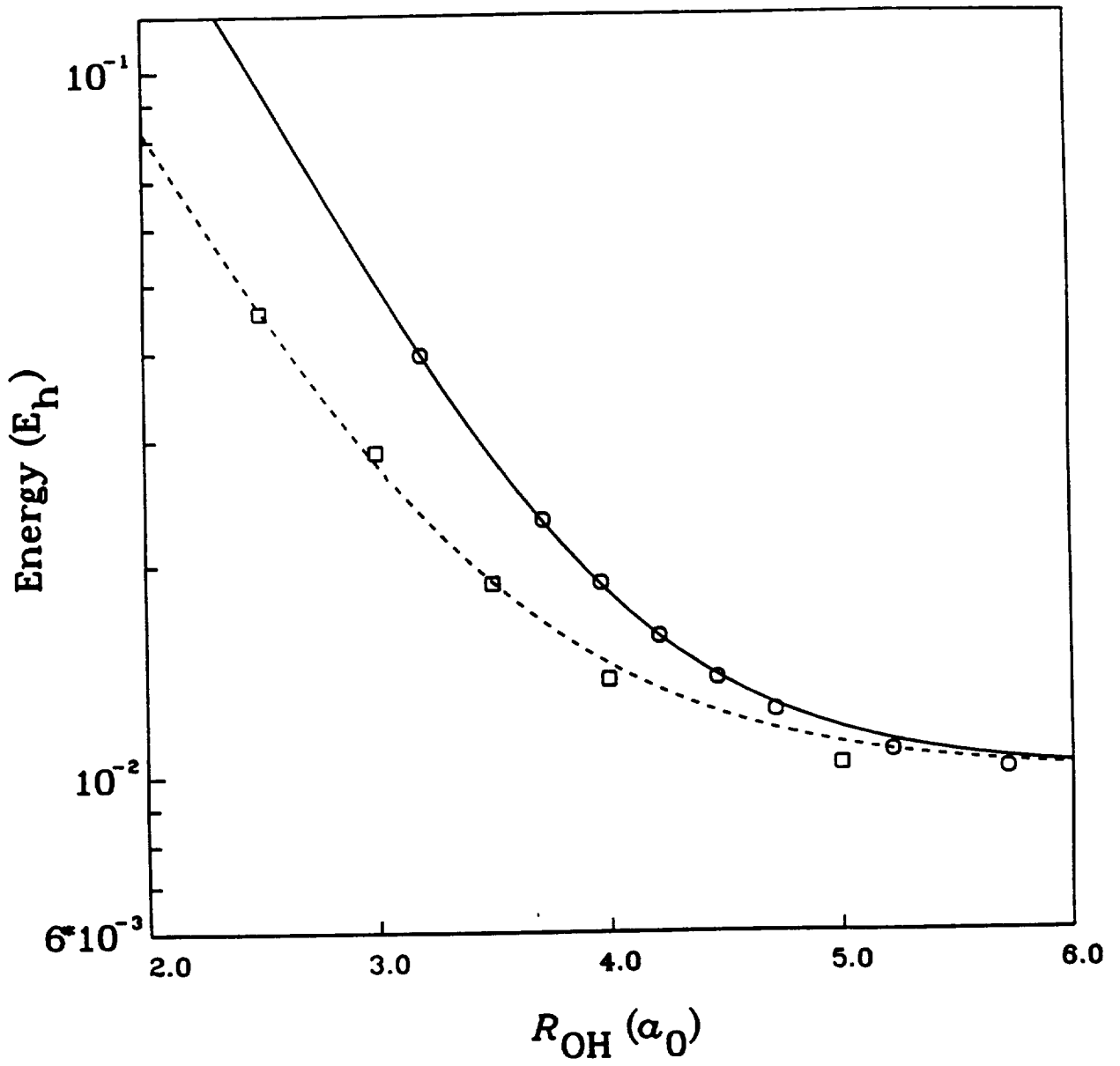


fig. 1

# H<sub>2</sub> polarizability

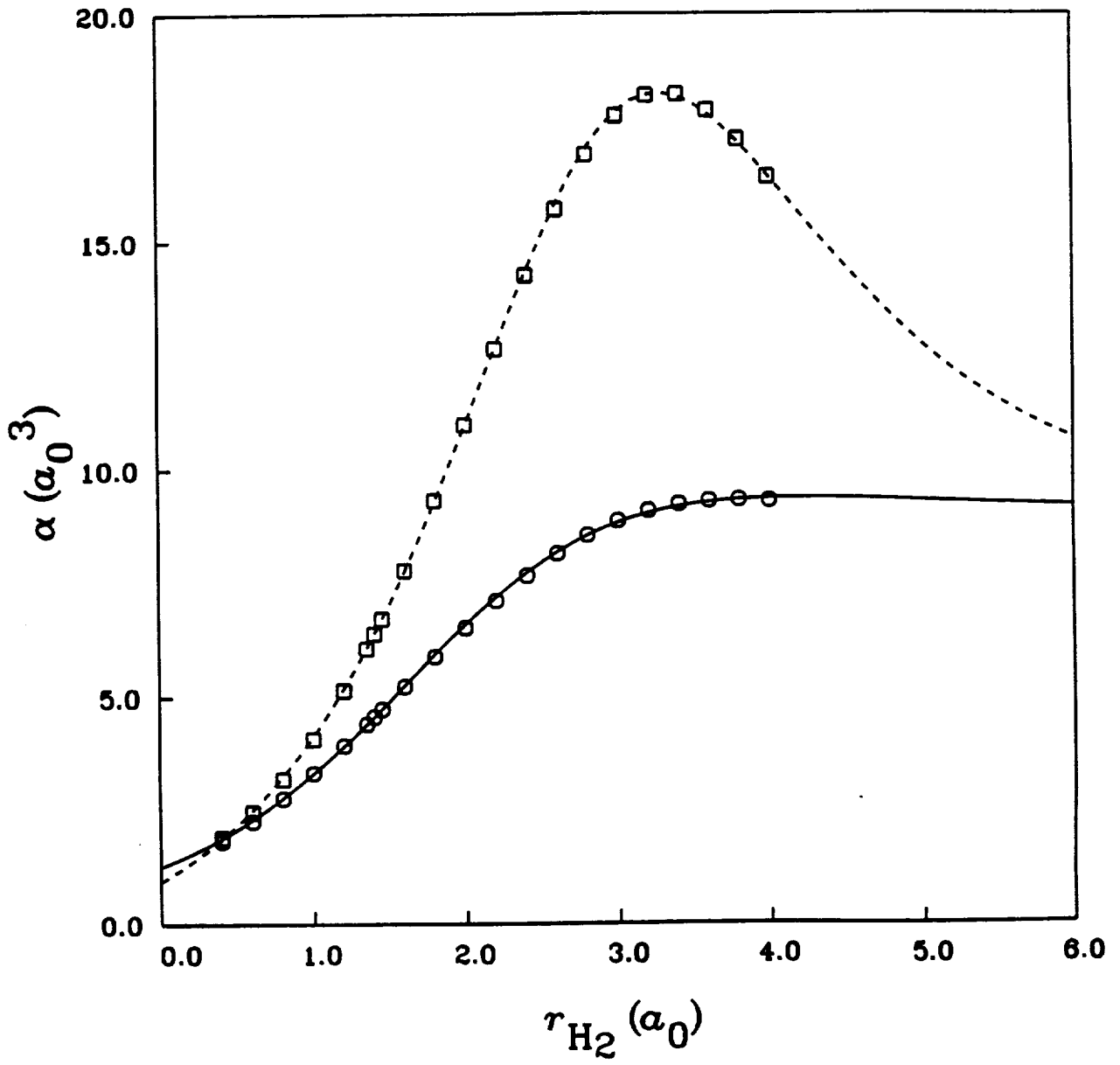


fig. 2

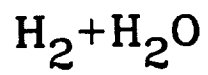
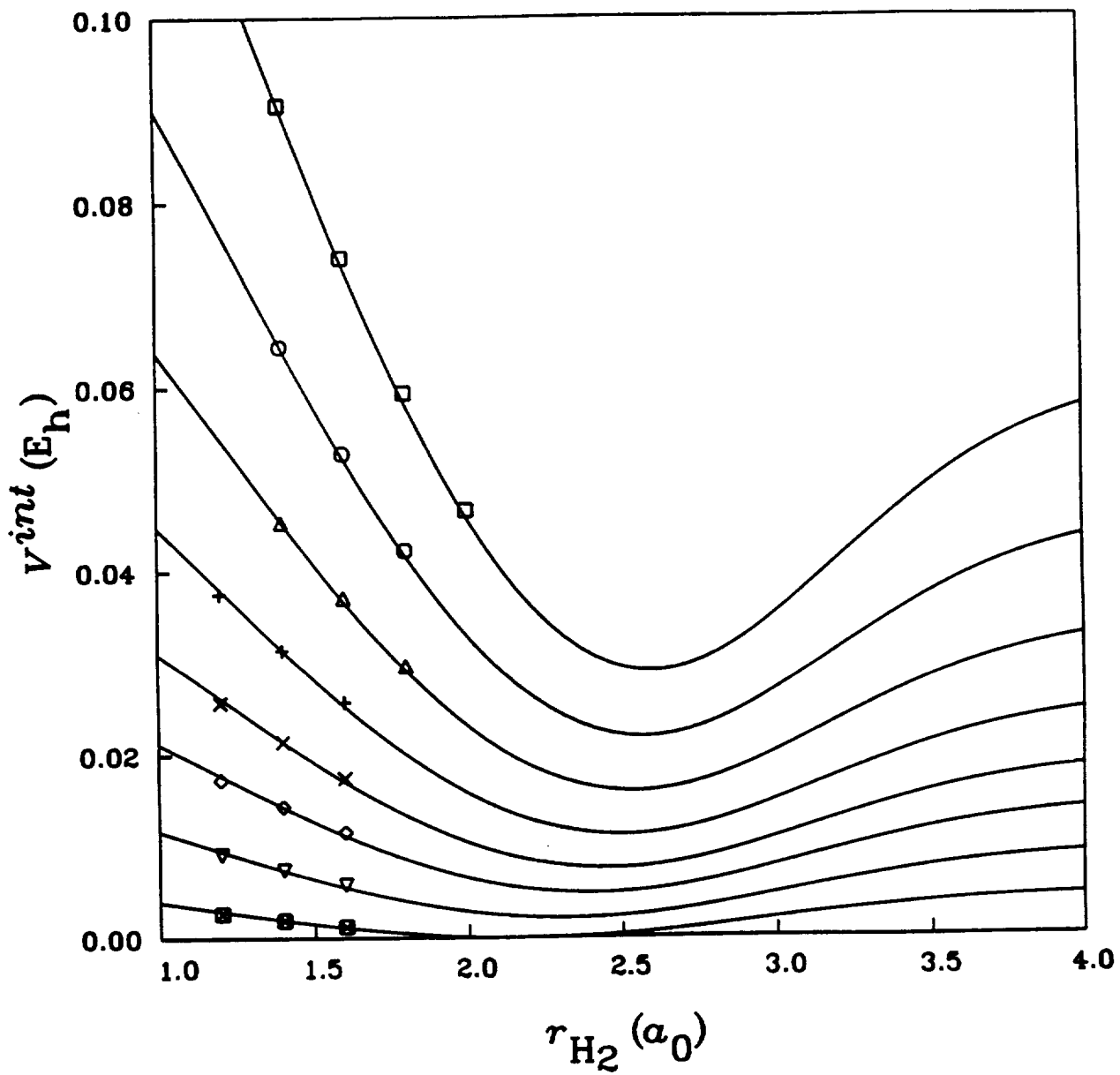

$$z+yx$$


Fig. 3



**Theoretical Characterization of the Potential Energy Surface  
for**



**III. Computed Points to Define a Global Potential for H + O<sub>2</sub>**

Stephen P. Walch<sup>a</sup> and Ronald J. Duchovic<sup>a</sup>

ELORET Institute

Sunnyvale, Ca. 94087

Abstract. Recent calculations on the H + O<sub>2</sub> surface have focused on the minimum energy path region of the surface ( J. Chem. Phys., 88, 6273(1988) I ) and on the saddle point region for H atom exchange via a T-shaped HO<sub>2</sub> complex ( J. Chem. Phys., 91, 2373(1989) II ). In this paper, additional computed points are reported which, when combined with previously reported points, permit a global representation of the H + O<sub>2</sub> and HO<sub>2</sub> regions of the potential energy surface. The calculations are complete active space SCF/ externally contracted configuration interaction (CASSCF/CCI) using the same wavefunction as in II. The new points characterize the potential for all angles of approach ranging from perpendicular to collinear with the OO bond, for H to center of mass of O<sub>2</sub> distances ranging from 5.0 a<sub>0</sub> in to a distance corresponding to greater than 30 kcal/mol up the inner wall. A new collinear exchange saddle point is reported.

<sup>a</sup>Mailing Address: NASA Ames Research Center, Moffett Field, CA 94035.

## I. Introduction

The reaction



is an important reaction in combustion. In addition, as part of a program to model combustion processes important in the design of the high-speed civil transport, rate constants for H atom diffusion in air are needed. Computation of these rate constants requires a global potential for  $H + O_2$ . Recently, calculated points have been reported for the minimum energy path (MEP) region of the potential energy surface for reaction (1) [1]. (Hereafter, referred to as I.) Also, additional calculations have been reported which characterize the pathway for exchange of an H atom of  $HO_2$  via a T-shaped  $HO_2$  saddle point [2]. (Hereafter, referred to as II.) In the present paper, additional points are computed which, together with the points previously computed in II, provide the data needed to produce a global representation of the  $H + O_2$  interaction.

The computational method is discussed in Section II, the results are presented in Section III, and the conclusions are given in Section IV.

## II. Computational Details.

The coordinate system for these calculations is the same as that used in II. The coordinates used are the OO distance ( $r_{OO}$ ), the H to center of mass of  $O_2$  distance ( $r_{H-OO}$ ), and the angle ( $\theta$ ) between a line connecting H to the center of mass of  $O_2$  and a normal to the OO bond at the bond midpoint ( $\theta$  is  $0^\circ$  for T-shaped H- $O_2$  and  $90^\circ$  for collinear H- $O_2$ ).

The calculations were carried out in the same way as in I. A problem which was encountered in designing the calculations in II was that in the vicinity of the T-

shaped HO<sub>2</sub> saddle point a 5a'2a'' CASSCF active space was needed while in the remainder of the surface a 4a'1a'' active space was more appropriate. The way in which this was handled was to use the larger active space for  $\theta = 0^\circ, 10^\circ,$  and  $20^\circ$  and the smaller active space for larger  $\theta$  values. In the current calculations the smaller active space was used for all points except those having  $\theta = 0^\circ, 10^\circ,$  and  $20^\circ$  and  $r_{H-OO}$  smaller than the values considered in II. The orbitals obtained using these two active space sizes are similar enough that there has been no indication of discontinuities in the subsequent CCI energies which are CASSCF/CCI with a 5a'2a'' CASSCF wavefunction as reference space for the CI. All of the calculations were carried out in C<sub>s</sub> symmetry. Some of the calculations in II were carried out in C<sub>2v</sub> symmetry and where these were combined with the present calculations this is indicated in the tables.

Most of the calculations were carried out with the [4s3p2d1f/3s\*2p1d] basis set described in II. As discussed in II, the notation s\* indicates that the contraction of the first natural orbital for H is based on the atomic SCF orbital, while in the original basis of Almlöf and Taylor [3] this contraction is based on natural orbitals from a CI calculation on H<sub>2</sub>. Additional calculations were carried out along the MEP defined with the [4s3p2d1f/3s\*2p1d] basis set using a larger [5s4p3d2f/4s\*3pd2d] basis set [3].

Calculations were carried out for  $\theta$  values of  $0^\circ$  through  $90^\circ$  in  $10^\circ$  increments. For each  $\theta$  value a grid was carried out over  $r_{H-OO}$  and  $r_{OO}$  to obtain minimum energy cuts at fixed  $\theta$  values.

The calculations were carried out on the NASA Ames Cray Y-MP/832. These calculations used the MOLECULE[4]-SWEDEN[5] system of programs.

### III. Results and Discussion

The computed energies are given in Table AI of the appendix. In order to aid

in visualizing the surface, the energy was evaluated along fixed  $\theta$  minimum energy cuts. For each  $\theta$  and  $r_{H-OO}$ ,  $r_{OO}$  was varied and the energy at the minimum and the optimal  $r_{OO}$  are given in Table I. These minimum energy cuts are shown graphically in Figs. 1 and 2.

A number of features of the surface are evident in Figs. 1 and 2. These features include a very small entrance channel barrier, a minimum  $\approx 51$  kcal/mol below  $H + O_2$ , a T-shaped ( $\theta = 0^\circ$ ) H exchange saddle point  $\approx 13$  kcal/mol below  $H + O_2$ , and a collinear ( $\theta = 0^\circ$ ) H exchange saddle point  $\approx 9$  kcal/mol above  $H + O_2$ . It is also evident from Figs. 1 and 2 that for each  $\theta$  value there is a maximum and subsequent minimum as  $r_{H-OO}$  is decreased. This leads to additional stationary points which are maxima on the global surface for  $\theta = 0^\circ$  and  $90^\circ$ . In addition to these features there is also an  $OH + O$  product channel which is discussed below. The MEP for this process corresponds approximately to increasing  $r_{OO}$  while varying the other two geometrical parameters.

In order to define the MEP for the reactants channel, polynomial fits ( six-term quadratic in  $r_{OO}$  and  $\theta$ ) were obtained at each  $r_{H-OO}$  distance using the three  $\theta$  values nearest the minimum and three values of  $r_{OO}$  (9 points). At the  $HO_2$  minimum a ten-term quadratic polynomial in all three coordinates was obtained to define the stationary points. These results are given in Table II. Additional calculations were carried out along this MEP using the [5s4p3d2f/4s\*3p2d] basis set. These results are also given in Table II.

In Fig. 3, the energy along the MEP with the [4s3p2d1f/3s\*2p1d] basis set is compared with the energy along the MEP of I (using the basis set of I). Both curves are referenced to the respective  $H + O_2$  asymptotic energy, therefore they coincide at large  $r_{H-OO}$ . From Fig. 3 it is seen that the curves essentially coincide up to  $r_{H-OO} \approx 3.5a_0$ . For shorter  $r_{H-OO}$  the comparison is more difficult since

the MEP of I was determined on a coarser  $r_{H-OO}$  grid than in the present work. For I only the energy at the minimum is shown near the bottom of the well. The saddle point geometries and relative energies for the H-O<sub>2</sub> entrance channel saddle point and HO<sub>2</sub> minimum are given in Table III. Here it is seen that the geometry at the HO<sub>2</sub> minimum is in good agreement with that obtained in I (maximum error is 0.02 a<sub>0</sub> in  $r_{OH}$ ) but the H-O<sub>2</sub> well depth is 1.9 kcal/mol smaller with the [4s3p2d1f/3s\*2p1d] basis set and 0.2 kcal/mol smaller with the [5s4p3d2f/4s\*3p2d] basis set. The H-O<sub>2</sub> entrance saddle point geometry differs more between the two calculations (maximum error 0.18 a<sub>0</sub> in  $r_{HO}$ , but the difference in the barrier height is only 0.04 kcal/mol for the larger basis set).

Using the computed HO<sub>2</sub> well depth, the computed HO<sub>2</sub> and O<sub>2</sub> vibrational frequencies from I, and the experimental H atom  $\Delta H_f^0$  of 51.6 kcal/mol [6], gives a  $\Delta H_f^0$  of 5.3 kcal/mol for HO<sub>2</sub>. This value may be compared to the value of  $3.5_{-0.5}^{+1.0}$  kcal/mol recommended by Benson [7]. Using the error limits quoted by Benson, the error in the computed HO<sub>2</sub> well depth is between 0.8 and 2.3 kcal/mol. This error range is quite reasonable for the basis set and level of calculation used here, and thus these calculations are consistent with the  $\Delta H_f^0$  for HO<sub>2</sub> recommended by Benson.

Fig. 4 and Fig. 5 compare the variation of  $\theta$  and  $r_{OO}$  along the MEP as a function of  $r_{H-OO}$  for the present work and the calculations in I. The general features of the  $\theta$  and  $r_{OO}$  variations are similar but there are some significant variations in detail. It is interesting that these geometrical parameters seem to coincide at the stationary points but vary in between. This may result from the non-rigorous method of defining the MEP which is used here. It should be noted that the MEP as defined here is mainly for purposes of visualizing the surface. A more accurate definition of these features must await the development of an accurate analytic representation

of the surface.

Table IV shows three fixed  $\theta$  minimum energy cuts in which  $r_{H-OO}$  is varied for each  $r_{OO}$ . These cuts are for motion orthogonal to the reactant channel and represent the intersection of the product channel MEP and the HOO minimum. These curves are plotted in the inset to Fig. 1.

Fig. 1 also shows higher energy regions of the surface corresponding to  $\theta$  values near  $0^\circ$  and  $90^\circ$ . It is evident from Fig. 1 that there are saddle points for H atom exchange along cuts with  $\theta = 0^\circ$  and  $90^\circ$ . For these two choices of  $\theta$  the actual symmetry is  $C_{2v}$  and the barrier (maximum on the surface) prior to the saddle point corresponds to a curve crossing ( ${}^2B_1 \rightarrow {}^2A_2$  for  $\theta = 0^\circ$  and  ${}^2\Sigma^- \rightarrow {}^2\Pi$  for  $\theta = 90^\circ$ ). Table III also shows the saddle point geometries and barriers for the two exchange saddle points. Here it is seen that the T-shaped exchange saddle point is 13 kcal/mol below  $H + O_2$ , while the collinear saddle point is 9 kcal/mole above  $H + O_2$ . Both of these barriers are below the  $OH + O$  product channel. Given the barriers to dissociation for  $\theta = 90^\circ$  and also possible centrifugal barriers, it is possible that a complete circular motion of H around  $O_2$  could occur for energies greater than 9 kcal/mol. In any case, the T-shaped H exchange saddle point is accessible to all  $H + O_2$  collisions, since it is below the  $H + O_2$  asymptote. It is anticipated that these previously uncharacterized features of the  $H + O_2$  potential will have significant dynamical consequences.

#### IV. Conclusions.

Computed points are reported which, when combined with previously published points from II, permit a global representation of the  $H + O_2$  and  $HO_2$  regions of the potential energy surface for the reaction:



The new points characterize the potential for all angles of approach of H to O<sub>2</sub> and for the inner repulsive wall region. In addition to connecting the points for the T-shaped H-O<sub>2</sub> exchange saddle point ( previously characterized in II ) to the reactant minimum energy path and inner wall regions, this work also characterizes a new collinear H-O<sub>2</sub> exchange saddle point which is only 9 kcal/mol above H + O<sub>2</sub>. It is anticipated that these new features of the potential energy surface will have significant dynamical consequences.

#### ACKNOWLEDGMENTS

S.P. Walch was supported by a NASA grant(NCC2-478).

## References

1. S.P. Walch, C.M. Rohlfiing, C.F. Melius, and C.W. Bauschlicher, Jr, J. Chem. Phys., **88**, 6273(1988).
2. S.P. Walch and C.M. Rohlfiing, J. Chem. Phys., **91**, 2373(1989).
3. J. Almlöf and P.R. Taylor, J. Chem. Phys. **86**, 4070(1987).
4. J. Almlöf, MOLECULE, a vectorized Gaussian integral program.
5. SWEDEN is a vectorized SCF-MCSCF-direct CI- conventional CI-CPF-MCPF program written by P.E.M. Siegbahn, C.W. Bauschlicher, Jr., B. Roos, P.R. Taylor, A. Heiberg, J. Almlöf, S.R. Langhoff, and D.P. Chong.
6. JANAF tables
7. L.G.S. Shum and S.W. Benson, J. Phys. Chem., **87**, 3479(1983).

Table I. H + O<sub>2</sub> Energy Along Fixed  $\Theta$  Cuts.

$r_{H-O}$	$r_{O-O}$	$\theta$	Energy	$\delta E$
1.4	2.878	0.0	-0.46948	-3.56
1.2	3.101	0.0	-0.44941	9.04
5.0	2.28	10.0	-0.46208	1.09
4.5	2.28	10.0	-0.45963	2.62
4.0	2.28	10.0	-0.45435	5.94
3.5	2.283	10.0	-0.44366	12.64
3.0	2.335	10.0	-0.42631	23.53
2.5	2.603	10.0	-0.45009	8.61
2.0	2.627	10.0	-0.48636	-14.15
1.8	2.670	10.0	-0.49069	-16.87
1.6	2.745	10.0	-0.48507	-13.34
1.4	2.903	10.0	-.46851	-2.85
1.2	3.164	10.0	-.44622	11.04
5.0	2.28	20.0	-0.46254	0.80
4.5	2.28	20.0	-0.46078	1.90
4.0	2.28	20.0	-0.45737	4.04
3.5	2.300	20.0	-0.45235	7.19
3.0	2.412	20.0	-0.45429	5.97
2.5	2.545	20.0	-0.48478	-13.16
2.2	2.509	20.0	-0.50633	-26.68

2.0	2.594	20.0	-0.50976	-28.83
1.8	2.664	20.0	-0.50461	-25.60
1.6	2.802	20.0	-0.48671	-14.37
1.4	3.060	20.0	-0.45957	2.66
1.2	3.653	20.0	-0.43836	15.97
5.0	2.28	30.0	-0.46308	0.46
4.5	2.28	30.0	-0.46227	0.97
4.0	2.284	30.0	-0.46168	1.34
3.5	2.324	30.0	-0.46479	-0.61
3.0	2.444	30.0	-0.48378	-12.5
2.8	2.494	30.0	-0.49779	-21.3
2.6	2.521	30.0	-0.51274	-30.7
2.4	2.543	30.0	-0.52515	-38.5
2.2	2.555	30.0	-0.53097	-42.1
2.0	2.557	30.0	-0.52470	-38.2
1.8	2.666	30.0	-0.50064	-23.1
1.6	2.974	30.0	-0.45961	2.64
5.0	2.28	40.0	-0.46329	0.33
4.5	2.28	40.0	-0.46315	0.41
4.0	2.294	40.0	-0.46499	-0.74
3.5	2.36	40.0	-0.47546	-7.31
3.0	2.487	40.0	-0.50753	-27.4
2.8	2.516	40.0	-0.52402	-37.8

2.6	2.530	40.0	-0.53803	-46.6
2.4	2.528	40.0	-0.54451	-50.6
2.2	2.523	40.0	-0.53653	-45.6
2.0	2.533	40.0	-0.50476	-25.7
1.8	2.648	40.0	-0.43845	15.9
5.0	2.28	50.0	-0.46262	0.75
4.5	2.28	50.0	-0.46208	1.09
4.0	2.357	50.0	-0.46450	-0.43
3.5	2.416	50.0	-0.48006	-10.2
3.0	2.435	50.0	-0.52048	-35.6
2.8	2.537	50.0	-0.53564	-45.1
2.6	2.515	50.0	-0.54252	-49.4
2.4	2.472	50.0	-0.53321	-43.5
2.2	2.405	50.0	-0.49595	-20.2
2.0	2.303	50.0	-0.41303	31.9
5.0	2.28	60.0	-0.46076	1.91
4.5	2.28	60.0	-0.45806	3.61
4.0	2.313	60.0	-0.45677	4.42
3.5	2.491	60.0	-0.47462	-6.78
3.0	2.559	60.0	-0.51669	-33.2
2.5	2.404	60.0	-0.50224	-24.1
2.2	2.252	60.0	-0.39683	42.0
5.0	2.28	70.0	-0.45805	3.61

4.5	2.28	70.0	-0.45152	7.71
4.0	2.297	70.0	-0.44194	13.72
3.5	2.588	70.0	-0.45769	3.84
3.0	2.543	70.0	-0.49354	-18.66
2.5	2.296	70.0	-0.43458	18.34
5.0	2.28	80.0	-0.45545	5.25
4.5	2.28	80.0	-0.44514	11.72
4.0	2.255	80.0	-0.42539	24.11
3.5	2.674	80.0	-0.43334	19.12
3.0	2.503	80.0	-0.46114	1.68
2.5	2.222	80.0	-0.37282	57.1
5.0	2.28	90.0	-0.45456	5.80
4.5	2.28	90.0	-0.44269	13.25
4.0	2.28	90.0	-0.41797	28.77
3.5	2.723	90.0	-0.41288	31.96
3.25	2.617	90.0	-0.43737	16.6
3.0	2.493	90.0	-0.44634	10.96
2.75	2.352	90.0	-0.42450	24.7

Table II. Computed MEP for H Atom Addition to O<sub>2</sub>.

$r_{H-O}$	$r_{O-O}$	$\theta$	Energy(bs 1 <sup>a</sup> )		Energy(bs 2 <sup>b</sup> )	
10.0	2.28		(-0.46381)	0.0	-150.46219(-.47133)	0.0
5.0	2.28	37.4	(-0.46332)	0.31	-150.46134(-.47068)	0.41
4.60	2.28	40.6	(-0.46325)	0.35	-150.46110(-.47060)	0.46
4.5	2.28	39.5	(-0.46315)	0.41		
4.0	2.30	43.2	(-0.46520)	-0.87	-150.46287(-.47304)	-1.07
3.5	2.41	49.6	(-0.48008)	-10.21	-150.47626(-.48805)	-10.49
3.0	2.54	52.7	(-0.52111)	-35.96	-150.51830(-.53019)	-36.9
2.8	2.55	52.8	(-0.53612)	-45.38	-150.53274(-.54445)	-45.9
2.6	2.52	47.2	(-0.54331)	-49.89	-150.54244(-.55393)	-51.8
2.49	2.52	43.5	(-0.54546)	-51.24	-150.54415(-.55557)	-52.9
2.4	2.51	41.3	(-0.54462)	-50.71	-150.54393(-.55529)	-52.7
2.2	2.52	36.1	(-0.53994)	-47.77	-150.53760(-.54886)	-48.7

<sup>a</sup> [4s3p2d1f/3s\*2p] ANO basis set.

<sup>b</sup> [5s4p3d2f/4s\*3p2d] ANO basis set.

Table III. Stationary Points on the H + O<sub>2</sub> Surface.

	H-O <sub>2</sub>	HO <sub>2</sub>	H-O <sub>2</sub> ( $\theta=0^\circ$ ) <sup>c</sup>	H-O <sub>2</sub> ( $\theta=90^\circ$ )
$r_{OO}$	2.28	2.52	2.70	2.51
$r_{H-OO}$	4.60	2.49	1.74	3.06
$\theta$	46.3	43.5	0.0	90.0
$r_{OH}$	3.96	1.86		
$\theta'^a$	118	104.2		
E(bs 1)	0.35	-51.2	-13	9.2
E(bs 2)	0.46	-52.9		
$r_{OO}^b$	2.29	2.52		
$r_{OH}^b$	4.14	1.84		
$\theta'^b$	116.4	104.4		
$E^b$	0.5	-53.1		

<sup>a</sup>  $\angle$  HOO.

<sup>b</sup> values from ref. I.

<sup>c</sup> from ref. II.

Table IV. H + O<sub>2</sub> Energy Along Fixed  $\Theta$  Cuts.

$r_{O-O}$	$r_{H-OO}$	$\theta$	Energy	$\delta E$
2.4	2.410	40.0	-0.54100	-48.4
2.5	2.410	40.0	-0.54436	-50.4
2.6	2.412	40.0	-0.54341	-49.9
2.7	2.415	40.0	-0.53944	-47.5
2.4	2.228	30.0	-0.52560	-38.8
2.5	2.212	30.0	-0.53031	-41.7
2.6	2.199	30.0	-0.53050	-41.8
2.7	2.176	30.0	-0.52758	-40.0
2.4	2.599	50.0	-0.53967	-47.6
2.5	2.614	50.0	-0.54251	-49.4
2.6	2.630	50.0	-0.54116	-48.5
2.7	2.646	50.0	-0.53693	-45.9

## Figure Captions.

Fig. 1. Potential surface for  $\text{H} + \text{O}_2$ . The figure shows ten fixed  $\theta$  minimum energy cuts. For each  $r_{\text{H}-\text{OO}}$ ,  $r_{\text{OO}}$  was varied and the minimum energy is shown in the figure. These cuts are for the reactant ( $\text{H} + \text{O}_2$ ) channel. The inset shows three fixed  $\theta$  minimum energy cuts. Here  $r_{\text{H}-\text{OO}}$  is varied for each  $r_{\text{OO}}$ . These cuts are for motion orthogonal to the reactant channel and represent the intersection of the product channel MEP and the HOO minimum.

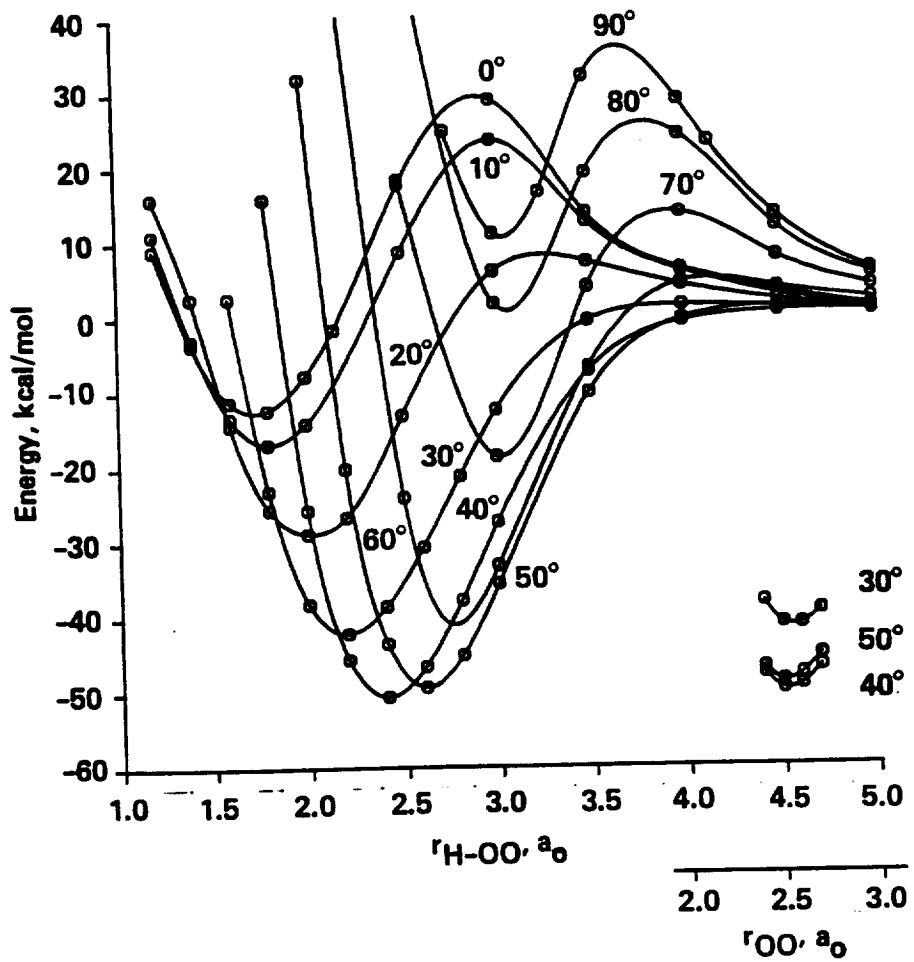
Fig. 2. Potential surface for  $\text{H} + \text{O}_2$ . This figure shows the same information as Fig. 1 in the format of a perspective plot.

Fig. 3. Comparison of energy as a function of  $r_{\text{H}-\text{OO}}$  along the MEP from I and the present calculations. For the present calculations results are shown with both basis sets.

Fig. 4. Comparison of  $\theta$  as a function of  $r_{\text{H}-\text{OO}}$  for the MEP from I and the present work.

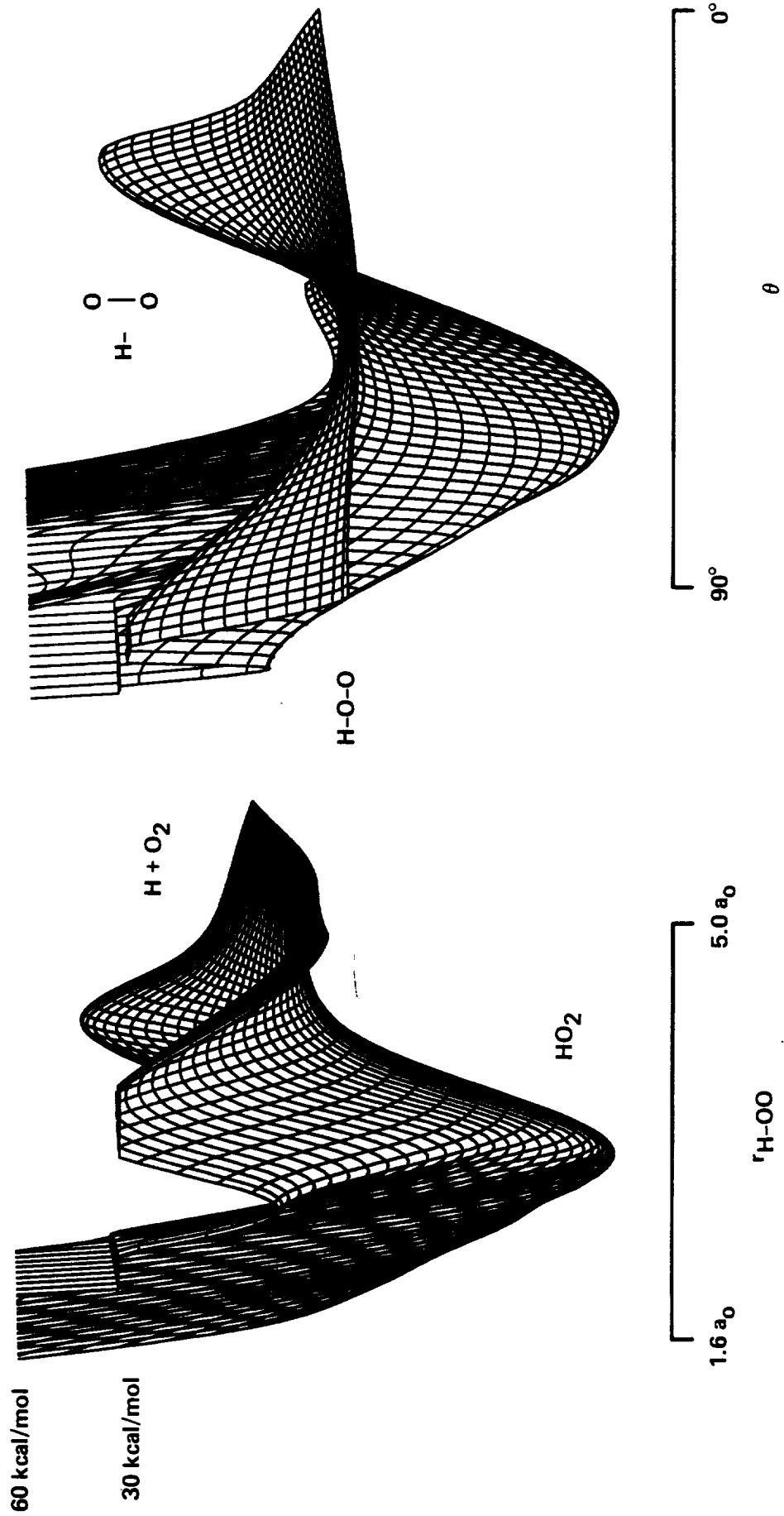
Fig. 5. Comparison of  $r_{\text{OO}}$  as a function of  $r_{\text{H}-\text{OO}}$  for the MEP from I and the present work.

Fig. 1



Walch-1

# THE H + O<sub>2</sub> SURFACE



Walch

Fig. 2

U

HOO

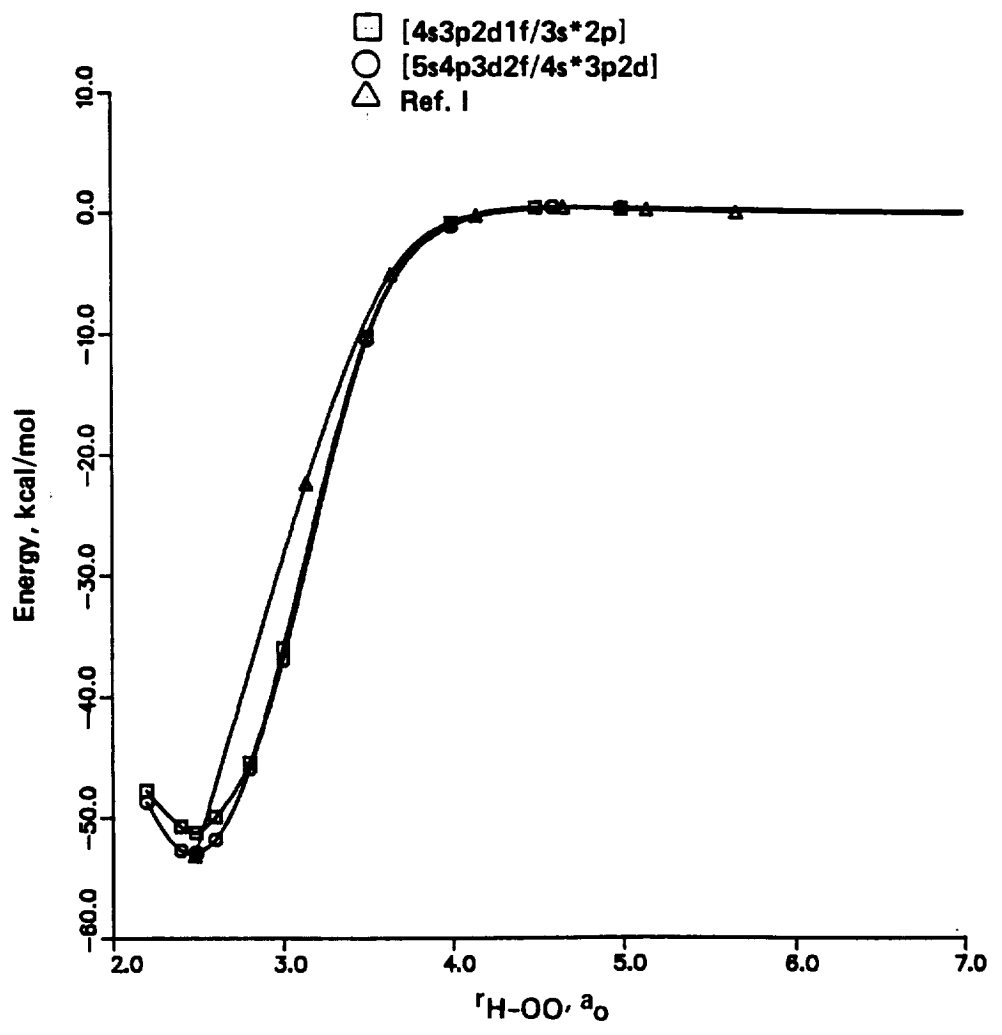
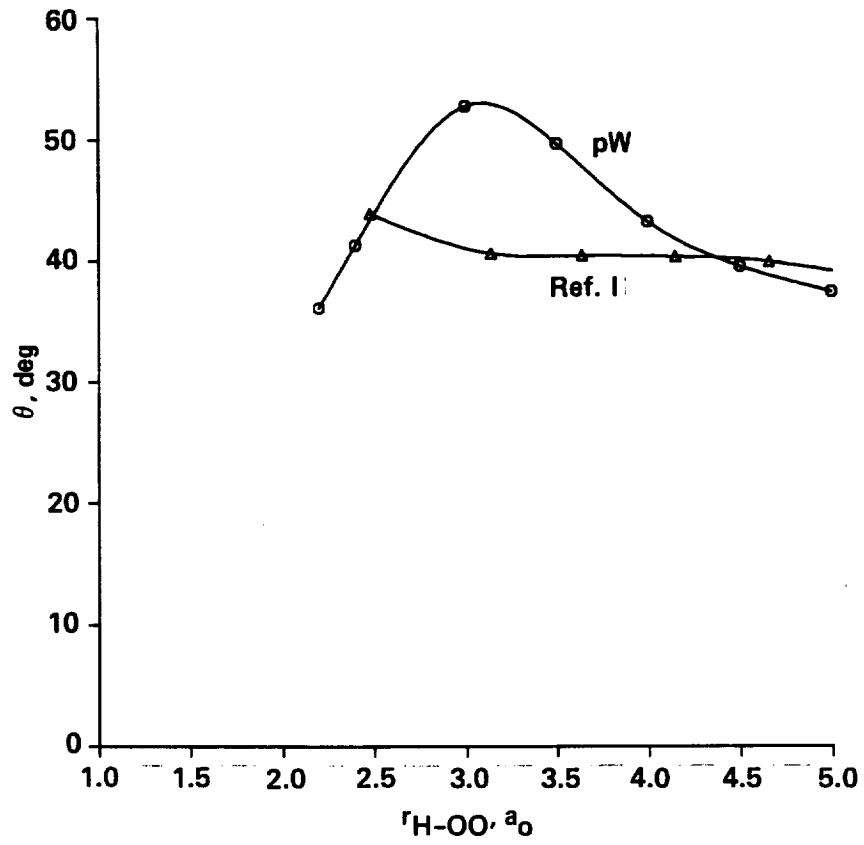
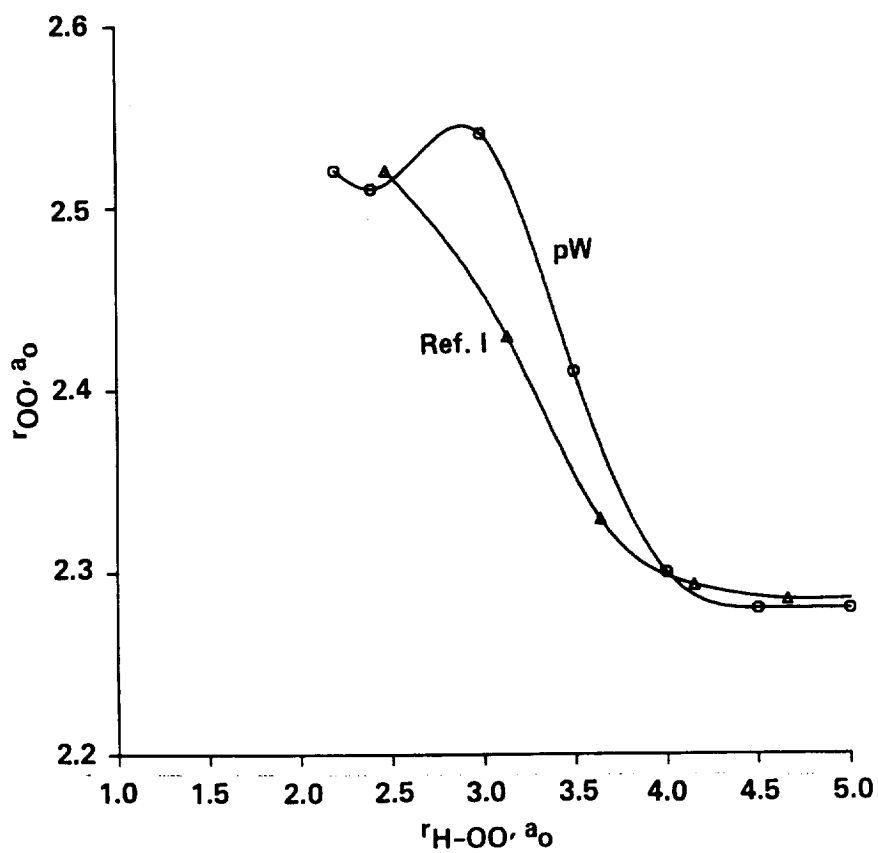


Fig. 4



Walch-4

Fig. 5



Walch-5



Appendix. The appendix contains a table of all the computed CASSCF/CCI energies. The energies are in the form CCI(CCI + Q). Note that for the CCI + Q energies -150. is not repeated. Thus, for the first point the CCI energy is -150.45491 and the CCI+Q energy is -150.46381. Distances are in  $a_0$ , angles are in degrees, and energies are in  $E_H$ .

Table AI. H + O<sub>2</sub> Long Range Points.

$r_{H-O-O}$	$r_{O-O}$	$\theta$	Energy
10.0	2.28		-150.45491(-.46381)
11.15	2.3	90.0	-150.45482(-.46385) <sup>a</sup>
6.15	2.3	90.0	-150.45364(-.46269) <sup>a</sup>
5.15	2.3	90.0	-150.44734(-.45656) <sup>a</sup>
4.15	2.3	90.0	-150.41740(-.42687) <sup>a</sup>
5.0	2.28	90.0	-150.44542(-.45456)
4.5	2.28	90.0	-150.43341(-.44269)
4.0	2.28	90.0	-150.40842(-.41797)
3.5	2.4	90.0	-150.38260(-.39467)
3.5	2.5	90.0	-150.39275(-.40517)
3.5	2.6	90.0	-150.39803(-.41083)
3.5	2.7	90.0	-150.39960(-.41281)
3.5	2.8	90.0	-150.39837(-.41206)
3.25	2.5	90.0	-150.42224(-.43441)
3.25	2.6	90.0	-150.42481(-.43731)
3.25	2.7	90.0	-150.42299(-.43588)
3.0	2.4	90.0	-150.43172(-.44341)
3.0	2.5	90.0	-150.43434(-.44632)
3.0	2.6	90.0	-150.43021(-.44251)
3.0	2.7	90.0	-150.42044(-.43310)
2.75	2.3	90.0	-150.41175(-.42306)
2.75	2.4	90.0	-150.41165(-.42325)

2.75	2.5	90.0	-150.40087(-.41273)
2.75	2.6	90.0	-150.38048(-.39260)
5.0	2.28	80.0	-150.44640(-.45545)
4.5	2.28	80.0	-150.43592(-.44514)
4.0	2.28	80.0	-150.41553(-.42522)
4.0	2.3	80.0	-150.41504(-.42483)
4.0	2.4	80.0	-150.40886(-.41950)
3.5	2.28	80.0	-150.39797(-.41069)
3.5	2.3	80.0	-150.40051(-.41324)
3.5	2.4	80.0	-150.41073(-.42345)
3.5	2.5	80.0	-150.41696(-.42971)
3.5	2.6	80.0	-150.41991(-.43278)
3.5	2.7	80.0	-150.42030(-.43327)
3.5	2.8	80.0	-150.41872(-.43168)
3.0	2.4	80.0	-150.44633(-.45797)
3.0	2.5	80.0	-150.44927(-.46114)
3.0	2.6	80.0	-150.44627(-.45833)
3.0	2.7	80.0	-150.43848(-.45071)
2.5	2.1	80.0	-150.34869(-.35939)
2.5	2.2	80.0	-150.36147(-.37237)
2.5	2.3	80.0	-150.35636(-.36744)
2.5	2.4	80.0	-150.33626(-.34751)
2.5	2.5	80.0	-150.30295(-.31437)
5.0	2.28	70.0	-150.44899(-.45805)
4.5	2.28	70.0	-150.44221(-.45152)

4.0	2.28	70.0	-150.43188(-.44187)
4.0	2.3	70.0	-150.43181(-.44194)
4.0	2.4	70.0	-150.42845(-.43937)
3.5	2.28	70.0	-150.43284(-.44477)
3.5	2.3	70.0	-150.43473(-.44677)
3.5	2.4	70.0	-150.44153(-.45387)
3.5	2.5	70.0	-150.44479(-.45720)
3.5	2.6	70.0	-150.44536(-.45768)
3.5	2.7	70.0	-150.44456(-.45689)
3.0	2.4	70.0	-150.47718(-.48871)
3.0	2.5	70.0	-150.48143(-.49310)
3.0	2.6	70.0	-150.48094(-.49270)
3.0	2.7	70.0	-150.47690(-.48865)
2.5	2.2	70.0	-150.41862(-.42911)
2.5	2.3	70.0	-150.42388(-.43457)
2.5	2.4	70.0	-150.41739(-.42823)
2.5	2.5	70.0	-150.40149(-.41242)
5.0	2.28	60.0	-150.45167(-.46076)
4.5	2.28	60.0	-150.44871(-.45806)
4.0	2.28	60.0	-150.44649(-.45649)
4.0	2.3	60.0	-150.44661(-.45673)
4.0	2.4	60.0	-150.44399(-.45473)
3.5	2.28	60.0	-150.45585(-.46717)
3.5	2.3	60.0	-150.45732(-.46875)
3.5	2.4	60.0	-150.46175(-.47358)
3.5	2.5	60.0	-150.46258(-.47461)

3.5	2.6	60.0	-150.46107(-.47310)
3.0	2.3	60.0	-150.49059(-.50188)
3.0	2.4	60.0	-150.50007(-.51146)
3.0	2.5	60.0	-150.50446(-.51597)
3.0	2.6	60.0	-150.50480(-.51634)
2.5	2.3	60.0	-150.48774(-.49838)
2.5	2.4	60.0	-150.49144(-.50223)
2.5	2.5	60.0	-150.48810(-.49898)
2.2	2.2	60.0	-150.38533(-.39542)
2.2	2.3	60.0	-150.38534(-.39559)
2.2	2.4	60.0	-150.37485(-.38521)
2.2	2.5	60.0	-150.35665(-.36707)
5.0	2.28	50.0	-150.45354(-.46262)
4.5	2.28	50.0	-150.45276(-.46208)
4.0	2.28	50.0	-150.45418(-.46407)
4.0	2.3	50.0	-150.45427(-.46425)
4.0	2.4	50.0	-150.45131(-.46179)
4.0	2.5	50.0	-150.44439(-.45534)
4.0	2.6	50.0	-150.43532(-.44663)
3.5	2.28	50.0	-150.46541(-.47630)
3.5	2.3	50.0	-150.46646(-.47745)
3.5	2.4	50.0	-150.46860(-.48001)
3.5	2.5	50.0	-150.46703(-.47869)
3.5	2.6	50.0	-150.46319(-.47493)
3.0	2.3	50.0	-150.49815(-.50933)

3.0	2.4	50.0	-150.50602(-.51735)
3.0	2.5	50.0	-150.50888(-.52027)
3.0	2.6	50.0	-150.50834(-.51976)
2.8	2.4	50.0	-150.52075(-.53186) <sup>c</sup>
2.8	2.5	50.0	-150.52416(-.53537) <sup>c</sup>
2.8	2.6	50.0	-150.52359(-.53484) <sup>c</sup>
2.6	2.4	50.0	-150.52875(-.53967) <sup>c</sup>
2.6	2.5	50.0	-150.53146(-.54247) <sup>c</sup>
2.6	2.6	50.0	-150.52991(-.54096) <sup>c</sup>
2.4	2.4	50.0	-150.52137(-.53206) <sup>c</sup>
2.4	2.5	50.0	-150.52225(-.53304) <sup>c</sup>
2.4	2.6	50.0	-150.51875(-.52958) <sup>c</sup>
2.2	2.3	50.0	-150.48128(-.49161)
2.2	2.4	50.0	-150.48548(-.49595) <sup>c</sup>
2.2	2.5	50.0	-150.48344(-.49399) <sup>c</sup>
2.2	2.6	50.0	-150.47714(-.48772) <sup>c</sup>
2.0	2.3	50.0	-150.40079(-.41089)
2.0	2.4	50.0	-150.40111(-.41133) <sup>c</sup>
2.0	2.5	50.0	-150.39575(-.40604) <sup>c</sup>
2.0	2.6	50.0	-150.38684(-.39716) <sup>c</sup>
1.8	2.6	50.0	-150.22628(-.23634) <sup>c</sup>
1.8	2.5	50.0	-150.23443(-.24445) <sup>c</sup>
1.8	2.4	50.0	-150.24079(-.25074) <sup>c</sup>
1.6	2.6	50.0	-149.98075(-.99050) <sup>c</sup>
1.6	2.5	50.0	-149.97765(-.98735) <sup>c</sup>

1.6	2.4	50.0	-149.97579(-.98544) <sup>c</sup>
5.0	2.28	40.0	-150.45423(-.46329)
4.5	2.28	40.0	-150.45391(-.46315)
4.0	2.28	40.0	-150.45524(-.46493)
4.0	2.3	40.0	-150.45521(-.46498)
4.0	2.4	40.0	-150.45152(-.46173)
4.0	2.5	40.0	-150.44363(-.45425)
4.0	2.6	40.0	-150.43332(-.44430)
3.5	2.28	40.0	-150.46344(-.47399)
3.5	2.3	40.0	-150.46409(-.47473)
3.5	2.4	40.0	-150.46411(-.47515)
3.5	2.5	40.0	-150.46028(-.47159)
3.5	2.6	40.0	-150.45418(-.46562)
3.0	2.3	40.0	-150.48923(-.50028)
3.0	2.4	40.0	-150.49505(-.50626)
3.0	2.5	40.0	-150.49619(-.50750)
3.0	2.6	40.0	-150.49407(-.50541)
2.8	2.4	40.0	-150.51051(-.52162) <sup>c</sup>
2.8	2.5	40.0	-150.51279(-.52397) <sup>c</sup>
2.8	2.6	40.0	-150.51153(-.52276) <sup>c</sup>
2.6	2.4	40.0	-150.52366(-.53460) <sup>c</sup>
2.6	2.5	40.0	-150.52680(-.53785) <sup>c</sup>
2.6	2.6	40.0	-150.52592(-.53704) <sup>c</sup>
2.4	2.4	40.0	-150.53019(-.54098) <sup>c</sup>
2.4	2.5	40.0	-150.53343(-.54434) <sup>c</sup>

2.4	2.6	40.0	-150.53241(-.54338) <sup>c</sup>
2.2	2.4	40.0	-150.52262(-.53324) <sup>c</sup>
2.2	2.5	40.0	-150.52569(-.53641) <sup>c</sup>
2.2	2.6	40.0	-150.52448(-.53526) <sup>c</sup>
2.0	2.4	40.0	-150.49070(-.50112) <sup>c</sup>
2.0	2.5	40.0	-150.49402(-.50454) <sup>c</sup>
2.0	2.6	40.0	-150.49326(-.50384) <sup>c</sup>
1.8	2.8	40.0	-150.42584(-.43624)
1.8	2.6	40.0	-150.42786(-.43823) <sup>c</sup>
1.8	2.5	40.0	-150.42605(-.43636) <sup>c</sup>
1.8	2.4	40.0	-150.42065(-.43086) <sup>c</sup>
1.6	2.6	40.0	-150.31825(-.32841) <sup>c</sup>
1.6	2.5	40.0	-150.30895(-.31903) <sup>c</sup>
1.6	2.4	40.0	-150.29676(-.30674) <sup>c</sup>
5.0	2.28	30.0	-150.45406(-.46308)
4.5	2.28	30.0	-150.45312(-.46227)
4.0	2.28	30.0	-150.45219(-.46167)
4.0	2.3	30.0	-150.45205(-.46160)
4.0	2.4	30.0	-150.44768(-.45760)
4.0	2.5	30.0	-150.43888(-.44920)
4.0	2.6	30.0	-150.42747(-.43815)
3.5	2.28	30.0	-150.45401(-.46423)
3.5	2.3	30.0	-150.45431(-.46462)
3.5	2.4	30.0	-150.45244(-.46317)
3.5	2.5	30.0	-150.44664(-.45766)

3.5	2.6	30.0	-150.43856(-.44975)
3.0	2.3	30.0	-150.46833(-.47922)
3.0	2.4	30.0	-150.47228(-.48336)
3.0	2.5	30.0	-150.47187(-.48308)
3.0	2.6	30.0	-150.46851(-.47976)
2.8	2.4	30.0	-150.48517(-.49622) <sup>c</sup>
2.8	2.5	30.0	-150.48661(-.49778) <sup>c</sup>
2.8	2.6	30.0	-150.48456(-.49578) <sup>c</sup>
2.6	2.4	30.0	-150.49880(-.50978) <sup>c</sup>
2.6	2.5	30.0	-150.50155(-.51265) <sup>c</sup>
2.6	2.6	30.0	-150.50031(-.51147) <sup>c</sup>
2.4	2.4	30.0	-150.51004(-.52093) <sup>c</sup>
2.4	2.5	30.0	-150.51376(-.52477) <sup>c</sup>
2.4	2.6	30.0	-150.51338(-.52447) <sup>c</sup>
2.2	2.4	30.0	-150.51472(-.52548) <sup>c</sup>
2.2	2.5	30.0	-150.51940(-.53029) <sup>c</sup>
2.2	2.6	30.0	-150.51953(-.53050) <sup>c</sup>
2.0	2.4	30.0	-150.50681(-.51743) <sup>c</sup>
2.0	2.5	30.0	-150.51256(-.52332) <sup>c</sup>
2.0	2.6	30.0	-150.51374(-.52458) <sup>c</sup>
1.8	2.8	30.0	-150.48787(-.49866)
1.8	2.7	30.0	-150.48976(-.50051)
1.8	2.6	30.0	-150.48948(-.50016) <sup>c</sup>
1.8	2.5	30.0	-150.48602(-.49660) <sup>c</sup>
1.8	2.4	30.0	-150.47799(-.48845) <sup>c</sup>

1.6	3.2	30.0	-150.44722(-.45793)
1.6	3.0	30.0	-150.44885(-.45959)
1.6	2.9	30.0	-150.44871(-.45943)
1.6	2.8	30.0	-150.44747(-.45815)
1.6	2.7	30.0	-150.44463(-.45524)
1.6	2.6	30.0	-150.43952(-.45003) <sup>c</sup>
1.6	2.5	30.0	-150.43119(-.44160) <sup>c</sup>
1.6	2.4	30.0	-150.41833(-.42860) <sup>c</sup>
5.0	2.28	20.0	-150.45356(-.46254)
4.5	2.28	20.0	-150.45171(-.46078)
4.0	2.28	20.0	-150.44810(-.45737)
3.5	2.28	20.0	-150.44237(-.45223)
3.5	2.3	20.0	-150.44238(-.45235)
3.5	2.4	20.0	-150.43891(-.44935)
3.0	2.3	20.0	-150.44106(-.45183)
3.0	2.4	20.0	-150.44329(-.45426)
3.0	2.5	20.0	-150.44167(-.45275)
2.5	2.4	20.0	-150.46918(-.48023)
2.5	2.5	20.0	-150.47314(-.48434)
2.5	2.6	20.0	-150.47284(-.48414)
2.5	2.7	20.0	-150.46949(-.48084)
2.2	2.8	20.0	-150.48701(-.49756) <sup>c</sup>
2.2	2.7	20.0	-150.49198(-.50255) <sup>c</sup>
2.2	2.6	20.0	-150.49487(-.50547) <sup>c</sup>
2.0	2.8	20.0	-150.49399(-.50439) <sup>c</sup>

2.0	2.7	20.0	-150.49796(-.50834) <sup>c</sup>
2.0	2.6	20.0	-150.49940(-.50976) <sup>c</sup>
1.8	2.8	20.0	-150.49191(-.50214) <sup>c</sup>
1.8	2.7	20.0	-150.49424(-.50444) <sup>c</sup>
1.8	2.6	20.0	-150.49390(-.50406) <sup>c</sup>
1.6	3.0	20.0	-150.47234(-.48250) <sup>d</sup>
1.6	2.8	20.0	-150.47664(-.48671) <sup>c</sup>
1.6	2.6	20.0	-150.47239(-.48235) <sup>c</sup>
1.4	3.2	20.0	-150.44828(-.45846) <sup>d</sup>
1.4	3.1	20.0	-150.44936(-.45948) <sup>d</sup>
1.4	3.0	20.0	-150.44932(-.45937) <sup>d</sup>
1.2	3.8	20.0	-150.42758(-.43790) <sup>d</sup>
1.2	3.6	20.0	-150.42788(-.43830) <sup>d</sup>
1.2	3.4	20.0	-150.42671(-.43700) <sup>d</sup>
1.2	3.3	20.0	-150.42507(-.43528) <sup>d</sup>
1.2	3.2	20.0	-150.42233(-.43247) <sup>d</sup>
1.2	3.1	20.0	-150.41812(-.42819) <sup>d</sup>
5.0	2.28	10.0	-150.45313(-.46208)
4.5	2.28	10.0	-150.45063(-.45963)
4.0	2.28	10.0	-150.44523(-.45435)
3.5	2.28	10.0	-150.43420(-.44366)
3.5	2.3	10.0	-150.43401(-.44357)
3.5	2.4	10.0	-150.42934(-.43941)
3.0	2.3	10.0	-150.41506(-.42612)
3.0	2.4	10.0	-150.41441(-.42564)

3.0	2.5	10.0	-150.41082(-.42200)
2.5	2.3	10.0	-150.41874(-.42984)
2.5	2.4	10.0	-150.43054(-.44196)
2.5	2.5	10.0	-150.43654(-.44826)
2.5	2.6	10.0	-150.43810(-.45009)
2.5	2.7	10.0	-150.43630(-.44849)
2.2	2.8	10.0	-150.45917(-.46980) <sup>c</sup>
2.2	2.6	10.0	-150.46435(-.47497) <sup>c</sup>
2.0	2.8	10.0	-150.47161(-.48214) <sup>c</sup>
2.0	2.7	10.0	-150.47510(-.48561) <sup>c</sup>
2.0	2.6	10.0	-150.47576(-.48625) <sup>c</sup>
1.8	2.8	10.0	-150.47780(-.48820) <sup>c</sup>
1.8	2.7	10.0	-150.48019(-.49056) <sup>c</sup>
1.8	2.6	10.0	-150.47964(-.48997) <sup>c</sup>
1.6	2.8	10.0	-150.47433(-.48460) <sup>c</sup>
1.6	2.7	10.0	-150.47453(-.48475) <sup>c</sup>
1.6	2.6	10.0	-150.47161(-.48178) <sup>c</sup>
1.4	3.0	10.0	-150.45726(-.46754) <sup>d</sup>
1.4	2.9	10.0	-150.45830(-.46851) <sup>d</sup>
1.4	2.8	10.0	-150.45729(-.46743) <sup>d</sup>
1.4	2.7	10.0	-150.45360(-.46367) <sup>d</sup>
1.2	3.2	10.0	-150.43572(-.44611) <sup>d</sup>
1.2	3.1	10.0	-150.43556(-.44586) <sup>d</sup>
1.2	3.0	10.0	-150.43366(-.44387) <sup>d</sup>
1.2	2.9	10.0	-150.42961(-.43972) <sup>d</sup>

5.0	2.0	0.0	-150.40941(-.41785) <sup>b</sup>
5.0	2.2	0.0	-150.45111(-.45990) <sup>b</sup>
5.0	2.3	0.0	-150.45345(-.46236) <sup>b</sup>
5.0	2.4	0.0	-150.44854(-.45754) <sup>b</sup>
4.0	2.2	0.0	-150.44257(-.45144) <sup>b</sup>
4.0	2.3	0.0	-150.44494(-.45392) <sup>b</sup>
4.0	2.4	0.0	-150.44010(-.44917) <sup>b</sup>
3.5	2.2	0.0	-150.43014(-.43916) <sup>b</sup>
3.5	2.3	0.0	-150.43272(-.44189) <sup>b</sup>
3.5	2.4	0.0	-150.42810(-.43736) <sup>b</sup>
3.0	2.2	0.0	-150.40491(-.41429) <sup>b</sup>
3.0	2.3	0.0	-150.40815(-.41769) <sup>b</sup>
3.0	2.4	0.0	-150.40416(-.41381) <sup>b</sup>
2.5	2.4	0.0	-150.41135(-.42244) <sup>b</sup>
2.5	2.5	0.0	-150.42059(-.43164) <sup>b</sup>
2.5	2.6	0.0	-150.42431(-.43533) <sup>b</sup>
2.5	2.7	0.0	-150.42401(-.43499) <sup>b</sup>
2.15	2.5	0.0	-150.45182(-.46259) <sup>b</sup>
2.15	2.6	0.0	-150.45537(-.46613) <sup>b</sup>
2.15	2.7	0.0	-150.45486(-.46562) <sup>b</sup>
2.0	2.5	0.0	-150.46131(-.47194) <sup>b</sup>
2.0	2.6	0.0	-150.46517(-.47580) <sup>b</sup>
2.0	2.7	0.0	-150.46494(-.47559) <sup>b</sup>
1.8	2.5	0.0	-150.46714(-.47757) <sup>b</sup>

1.8	2.6	0.0	-150.47205(-.48251) <sup>b</sup>
1.8	2.7	0.0	-150.47280(-.48329) <sup>b</sup>
1.8	2.8	0.0	-150.47049(-.48102) <sup>b</sup>
1.6	2.5	0.0	-150.46109(-.47132) <sup>b</sup>
1.6	2.6	0.0	-150.46822(-.47850) <sup>b</sup>
1.6	2.7	0.0	-150.47104(-.48137) <sup>b</sup>
1.6	2.8	0.0	-150.47065(-.48104) <sup>b</sup>
1.4	3.0	0.0	-150.45702(-.46743) <sup>d</sup>
1.4	2.8	0.0	-150.45839(-.46863) <sup>d</sup>
1.4	2.6	0.0	-150.44870(-.45879) <sup>d</sup>
1.2	3.2	0.0	-150.43782(-.44836) <sup>d</sup>
1.2	3.0	0.0	-150.43801(-.44832) <sup>d</sup>
1.2	2.8	0.0	-150.42961(-.43972) <sup>d</sup>
1.2	2.6	0.0	-150.40785(-.41778) <sup>d</sup>

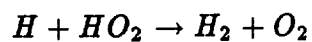
<sup>a</sup> Points run in  $C_{2v}$  (collinear) symmetry (from II).

<sup>b</sup> Points run in  $C_{2v}$  (edge-on) symmetry (from II.).

<sup>c</sup> Points from II.

<sup>d</sup> Points run in  $C_s$  symmetry with (52) active space to be compatible with the calculations in II.

**Computed Reaction Rate  
for**



Stephen P. Walch<sup>a</sup>  
ELORET Institute  
Sunnyvale, CA. 94087

and

Richard L. Jaffe  
NASA Ames Research Center  
Moffett Field, CA 94035

Abstract. The rate for the reaction  $H + HO_2 \rightarrow H_2 + O_2$  is computed using transition state theory based on energies which are derived from complete active space SCF(CASSCF)/ multireference contracted configuration interaction(CCI) calculations with a large atomic natural orbital(ANO) basis set. The saddle point is found to resemble  $H + HO_2$  and the computed barrier height is 3.6 kcal/mol.

<sup>a</sup>Mailing Address: NASA Ames Research Center, Moffett Field, CA 94035.

## I. Introduction

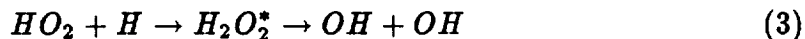
The reaction



is thought to be an important initiation reaction in  $H_2$  combustion. The only experimental determination [1] of the rate of reaction (1) derives from an indirect measurement of the rate of the reverse reaction.



The products of reaction (2) correspond to a triplet surface. However, the reactants also correlate with the ground state of  $H_2O_2$  for the singlet surface.



Here the product is OH radical. The rate of reaction (2) was inferred from the rate of disappearance of  $HO_2$  and the rate of formation of OH. This rate determination was carried out at only two temperatures ( $\approx 300K$  and  $\approx 500K$ ). Thus, it is difficult to extrapolate the rate to flame temperatures ( $\approx 2000K$ ). Current kinetics models [2,3] differ significantly in the rate which is used for reaction (2). The uncertainty in this rate is sufficient that a theoretical estimate of the rate, even one with some severe approximations, would be useful.

Reaction (2) is exoergic by 58 kcal/mol. In accord with this, the saddle point is expected to resemble  $H + HO_2$  and a small barrier is expected to this H abstraction process. In the present calculations the force constant matrix at the saddle point for reaction (2) is computed from ab-initio calculations and the rate of reaction (2)

is computed using transition state theory (TST) with a one-dimensional tunneling correction based on an Eckart barrier [4].

The computational method is discussed in Section II, the results are presented in Section III, and the conclusions are given in Section IV.

## II. Computational Details.

The basis sets used in the present study are atomic natural orbital(ANO) basis sets [5]. These basis sets are optimal for describing the atomic correlation and have very small basis set superposition errors, but are sufficiently flexible to be used in molecular calculations at both the SCF and CI level. The O basis set is (13s8p6d4f)/[4s3p2d1f] and is described in detail in Ref. 5. The H basis set is (8s6p4d)/[3s2p1d], and is that developed by Almlöf and Taylor [5].

Most of the calculations were carried out in  $C_s$  symmetry. The CASSCF active space had 6 active electrons distributed among five  $a'$  and one  $a''$  orbitals. The qualitative character of the CASSCF orbitals is: 1-4 $a'$  correspond to the O 1s and O 2s levels, which are not correlated in these calculations. The 5 $a'$  orbital is a 2p lone pair localized mainly on the far oxygen. 6 $a'$  and 7 $a'$  are the OO and OH bond orbitals. 8 $a'$  is the H 1s orbital. 9 $a'$  and 10 $a'$  are correlating orbitals for the OO and OH bonds. The 1 $a''$  orbital is an O 2p lone pair localized mainly on the near oxygen and the 2 $a''$  orbital is a singly occupied O 2p orbital localized mainly on the far oxygen.

Ten electrons were correlated in the CCI calculations. The reference configurations for the CCI consisted of following 29 spatial occupations formed from the 5-10  $a'$  and the 1-2  $a''$  orbitals:

$$\left. \begin{array}{l} 5a'^2 6a'^2 7a'^2 8a'^1 9a'^0 10a'^0 \\ 5a'^1 6a'^2 7a'^2 8a'^2 9a'^0 10a'^0 \end{array} \right\}$$

$$\left. \begin{array}{l}
 5a'^1 6a'^2 7a'^2 8a'^1 9a'^1 10a'^0 \\
 5a'^1 6a'^2 7a'^2 8a'^1 9a'^0 10a'^1 \\
 5a'^2 6a'^1 7a'^2 8a'^2 9a'^0 10a'^0 \\
 5a'^2 6a'^1 7a'^2 8a'^1 9a'^1 10a'^0 \\
 5a'^2 6a'^1 7a'^2 8a'^1 9a'^0 10a'^1 \\
 5a'^2 6a'^2 7a'^1 8a'^2 9a'^0 10a'^0 \\
 5a'^2 6a'^2 7a'^1 8a'^1 9a'^1 10a'^0 \\
 5a'^2 6a'^2 7a'^1 8a'^1 9a'^0 10a'^1
 \end{array} \right\} \times \left. \begin{array}{l}
 1a'^2 2a'^1 \\
 1a'^1 2a'^2
 \end{array} \right\}$$

$$\left. \begin{array}{l}
 5a'^2 6a'^2 7a'^0 8a'^1 9a'^2 10a'^0 \\
 5a'^2 6a'^1 7a'^1 8a'^1 9a'^2 10a'^0 \\
 5a'^2 6a'^0 7a'^2 8a'^1 9a'^2 10a'^0 \\
 5a'^2 6a'^2 7a'^0 8a'^1 9a'^1 10a'^1 \\
 5a'^2 6a'^1 7a'^1 8a'^1 9a'^1 10a'^1
 \end{array} \right\} \times 1a'^2 2a'^1$$

$$\left. \begin{array}{l}
 5a'^2 6a'^0 7a'^2 8a'^1 9a'^1 10a'^1 \\
 5a'^2 6a'^2 7a'^0 8a'^1 9a'^0 10a'^2 \\
 5a'^2 6a'^1 7a'^1 8a'^1 9a'^0 10a'^2 \\
 5a'^2 6a'^0 7a'^2 8a'^1 9a'^0 10a'^2
 \end{array} \right\}$$

The first group of configurations includes products of single excitations among the

$a'$   $\text{HO}_2$  like orbitals and single excitations among the  $a''$  orbitals. While the second group of configurations includes double excitations among the  $a'$   $\text{HO}_2$  like orbitals. These groups of configurations were found to be the most important classes of configurations for this system for the  $\text{H} + \text{HO}_2$  and  $\text{H} - \text{HO}_2$  saddle point regions of the surface, and included all the configurations with expansion coefficient greater than 0.05 in the CASSCF wavefunction.

The multireference analog of Davidson's correction [6] was computed to estimate the importance of higher excitations. The correction used in the CCI [7] is  $\Delta E (1 - C_0^2)/C_0^2$ , where  $\Delta E$  is the CI energy minus the reference energy and  $C_0^2$  is the sum of the squares of the coefficients of the reference configurations in the CI wavefunction. In the CCI program two different estimates of  $C_0$  are used. The second is obtained as defined above as the dot product of the valence portion of the CI vector with itself, while the first is the dot product of the valence CI vector with the valence portion of the CI vector. In most cases these two estimates of  $C_0^2$  give very similar results and we have normally reported the first estimate. In the present case, there is enough difference that we have chosen to use the second estimate, which we believe to be more reliable.

The electronic structure calculations were carried out on the NASA Cray XMP-48 and the NAS Cray Y-MP/8-32. All the calculations used the MOLECULE[8]-SWEDEN[9] system of programs. The normal mode analysis at the saddle point for reaction (2) was carried out using the program SURVIB[10], while the TST theory calculations were carried out using code written locally.

### III. Results and Discussion.

The computed energies are tabulated in the appendix [10]. The computed points are adequate to define both the diagonal and off diagonal components of the force constant matrix at the saddle point. A polynomial was fit to the computed points

using the SURVIB program [10]. This polynomial contained 45 terms through cubic in the in plane coordinates ( $r_{OO}$ ,  $r_{OH}$ ,  $\angle$  HOO,  $r_{HH}$ , and  $\angle$  HHO) and a quadratic and quartic term in the dihedral angle defined by the HOO plane of the HO<sub>2</sub> species and the HHO plane formed by the two hydrogens and the near O. This fit had an RMS error  $< 0.1$  kcal/mol. The saddle point geometry, vibrational frequencies, and barrier height are given in Table I. From Table I it is seen that the saddle point  $r_{OH}$ ,  $r_{OO}$ , and  $\angle$  HOO are  $0.15 a_0$  longer,  $-0.06 a_0$  shorter, and  $2.7^\circ$  larger than the geometry obtained for free HOO [12] using the same basis set and a similar CCI calculation. The changes in  $r_{OO}$  and  $\theta$  are consistent with the slightly elongated OH bond, based on the computed minimum energy path for H atom addition to O<sub>2</sub> [12]. The  $r_{HH}$  on the other hand is  $\approx 0.8 a_0$  longer than in free OH. The latter result is consistent with an early saddle point as expected for a very exothermic H abstraction process. The saddle point is coplanar with the far H atom  $3.8^\circ$  from being collinear with the OH bond (in a direction away from the far O atom). The computed barrier height is 3.63 kcal/mol before correction for zero-point energy.

Table II shows the potential for varying the angles  $\alpha$  and the dihedral angle  $\beta$  between the HOO and HHO planes. From Table II it is seen that the most stable structure has the HH bond trans to the OO bond ( $\beta = 180^\circ$ ), with the  $90^\circ$  dihedral angle structure next, and the  $0^\circ$  dihedral angle structure (cis) highest. Fig. 2 shows the energy as a function of the variation of  $\beta$  for  $\alpha$  fixed at  $3.63^\circ$ . One interesting feature of Fig. 1 is a slight minimum at  $\beta = 0.0^\circ$ . This feature appears to be real. In particular it has been found that it is not an artifact of symmetry breaking effects, which are found to be negligible. In a hindered rotor model, the variation in energy for a full rotation of the dihedral angle with  $\angle$  HHO fixed at  $176.4^\circ$  ( $\alpha = 3.63^\circ$ ) is  $\approx 0.07$  kcal/mol ( $\approx 23 \text{ cm}^{-1}$ ). This energy change may be compared to an out of plane bending frequency of  $\approx 300 \text{ cm}^{-1}$  if the out of plane motion is treated

as a bend. This result reflects the near degeneracy of the bending modes i.e. the rotational barrier would be zero if the bend modes were degenerate. None the less two models were considered: i) a bend model in which the two bending modes of the HH group are nearly degenerate and ii) a hindered rotor model in which one bending mode remains, but the other vibration is treated as a hindered rotation. These two models lead to somewhat different rates within the transition state theory model, as discussed below.

The vibrational frequencies are also given in Table I. From examination of the normal mode coordinates,  $\omega_2$  and  $\omega_3$  are found to be OH stretch and OO stretch modes, respectively. The frequencies of these modes differ from those reported for free HOO [12] by  $-26$  and  $+6$   $\text{cm}^{-1}$ , respectively. This is consistent with the early saddle point for reaction (2).  $\omega_1$  is found to be an OH stretching mode. The frequency for this mode is  $1795$   $\text{cm}^{-1}$  smaller than for free HO<sub>2</sub>. Examination of the normal mode coordinates indicates that this mode involves motion of both H atoms of the H-HO<sub>2</sub> complex. Thus, the lower frequency results from a larger reduced mass as well as some decrease in the bond force constant due to the stretched OH bond. The remaining two real frequencies are  $347$  and  $333$   $\text{cm}^{-1}$  and these correspond to in plane and out of plane bending motion of the HH group. The near degeneracy of these two modes is consistent with the near collinear arrangement of the H-H-O atoms at the saddle point H-HO<sub>2</sub> geometry. It should be noted here that the out of plane bending mode is significantly anharmonic. The  $333$   $\text{cm}^{-1}$  frequency results from a quadratic-quartic fit of the dihedral angle. A quadratic term only leads to a frequency of  $887$   $\text{cm}^{-1}$ . Finally, the frequency corresponding to the reaction coordinate is  $1786$   $i$

Table I also shows the zero-point correction computed within the bend model using the HO<sub>2</sub> frequencies reported in Ref. 12. The frequencies in Ref. 12 were

obtained with the same basis set and comparable computational level to that used in the present work. There may be some inconsistency with the present work in that in Ref. 12 only a quadratic polynomial was used as compared to a cubic polynomial in the present work. These small effects will not be of great significance here since, within the transition state theory model, the reactant vibrational frequencies mainly effect the effective barrier, through the zero-point energy, and the computed barrier height is probably uncertain by  $\approx 1$  kcal/mol in the present calculation. Using the bend model the zero-point corrected barrier is 2.01 kcal/mol. In the hindered rotor model the out of plane vibration is removed, which reduces the zero-point energy by half of  $333\text{ cm}^{-1}$  or  $\approx 0.50$  kcal/mol, leading to an effective barrier of  $\approx 1.5$  kcal/mol. In the hindered rotor model the moment of inertia for the hindered rotation is very small leading to widely spaced rotational levels. Thus, the rigid rotor partition function is still used.

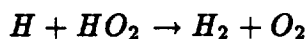
Fig. 2 compares the computed rates for reactions (1) and (2) to the experimental data [1] and to rate expressions used in combustion models [2,3]. In the transition state theory calculations the H atom and HO<sub>2</sub> each have an electronic degeneracy of 2 and a spatial degeneracy of 1, while H-HO<sub>2</sub> saddle point structure has an electronic degeneracy of 3 and a spatial degeneracy of 1. Computed rate curves are shown for the bend and hindered rotation models. In both cases the computed barrier heights are used without correction. The effect of tunneling is estimated using an Eckart potential. From Fig. 2 it is seen that at low temperatures the rigid rotor model gives a larger rate due to the lower effective barrier, but at higher temperatures the bend model shows a larger rate. This effect arises from the large contribution at high temperatures of the small out of plane bending frequency to the vibrational partition function. The bend model is expected to be more reliable, since the in-plane and out-of-plane bend frequencies are nearly degenerate - a result which is

consistent with the very small  $\alpha$  value (i.e. the H-H-O moiety is nearly collinear). Thus, to a first approximation the model is like a linear triatomic. Within this viewpoint, the very small barrier to “hindered rotation” shown in Fig. 1 is simply indicative of the close proximity of this system to the linear triatomic limit. Given this, only the rate predicted with the bend model is considered in the comparisons to experiment and current kinetic models.

Fig. 2 also shows the recommended experimental rate expression. At least at low temperatures, where experimental data exists, the experimental rate is larger than the theoretical rate. This result casts some doubt on the experimental rate, since the assumption of no recrossing and neglect of variational effects in the TST calculations should result in overestimating the rate. The rate used at 1000K by the Langley model [3] is in good agreement with the TST rate based on the bend model. The Lewis kinetic model [2] agrees well with the TST rate based on the bend model at high and low temperatures but is below the computed rate at intermediate temperatures. Also the TST rate shows a marked curvature which is not present in the Lewis model. Taking all this into consideration, the TST rate based on the bend model is recommended as the most reliable estimate of the rate for this reaction. The rate as a function of temperature computed with this model is given in Table III.

#### IV. Conclusions.

Transition state theory calculations including an estimate of tunneling through an Eckart barrier and based on an ab-initio potential energy surface have been carried out for the rate of the reaction



This reaction is found to have an early barrier with the H-H-O moiety very nearly collinear. Consistent with this the in-plane and out-of-plane HH bending modes are found to be nearly degenerate. TST theory calculations have been carried out for this model (bend model) and also for a model in which the bend motion of the H-H-O moiety is treated as a bend and hindered rotation (rotor model). It is concluded that the bend model is far more realistic in this system where the two components of the bend are nearly degenerate. The rate based on the bend model is recommended as the best estimate currently available for the rate of this reaction.

#### ACKNOWLEDGMENTS

S.P. Walch was supported by a NASA grant(NCC2-478). The calculations on the NAS YMP were made with a grant of computer time from the NAS facility.

## References

1. Baulch
2. Lewis kinetic model
3. Langley kinetic model
4. ref. for TST ( some review article)
5. J. Almlöf and P.R. Taylor, *J. Chem. Phys.* **86**, 4070(1987).
6. S.R. Langhoff and E.R. Davidson, *Int. J. Quantum Chem.*, **8**,61 (1974).
7. P.E.M. Siegbahn, *Int. J. Quant. Chem.*, **23**, 1869(1983).
8. J. Almlöf, MOLECULE, a vectorized Gaussian integral program.
9. SWEDEN is a vectorized SCF-MCSCF-direct CI- conventional CI-CPF-MCPF program written by P.E.M. Siegbahn, C.W. Bauschlicher,Jr., B. Roos, P.R. Taylor, A. Heiberg, J. Almlöf, S.R. Langhoff, and D.P. Chong.
10. L.B. Harding and W.C. Ermler, SURVIB, a normal mode analysis program for polyatomic molecules.
11. See AIP document no PAPS ..... for 5 pages of tables of energies. etc.
12. S.P. Walch, C.M. Rohlfing, C.F. Melius, and C.W. Bauschlicher,Jr., *J. Chem. Phys.* **88**, 6273(1988).

**Figure Captions.**

**Fig. 1. Energy for H-HO<sub>2</sub> as a function of the dihedral angle ( $\beta$ ) with the remaining geometrical parameters fixed at the computed H-HO<sub>2</sub> saddle point geometry.**

**Fig. 2. Comparison of TST calculations and "experimental" rate data for the reaction H<sub>2</sub> + O<sub>2</sub> → H + HO<sub>2</sub>.**

Fig. 1

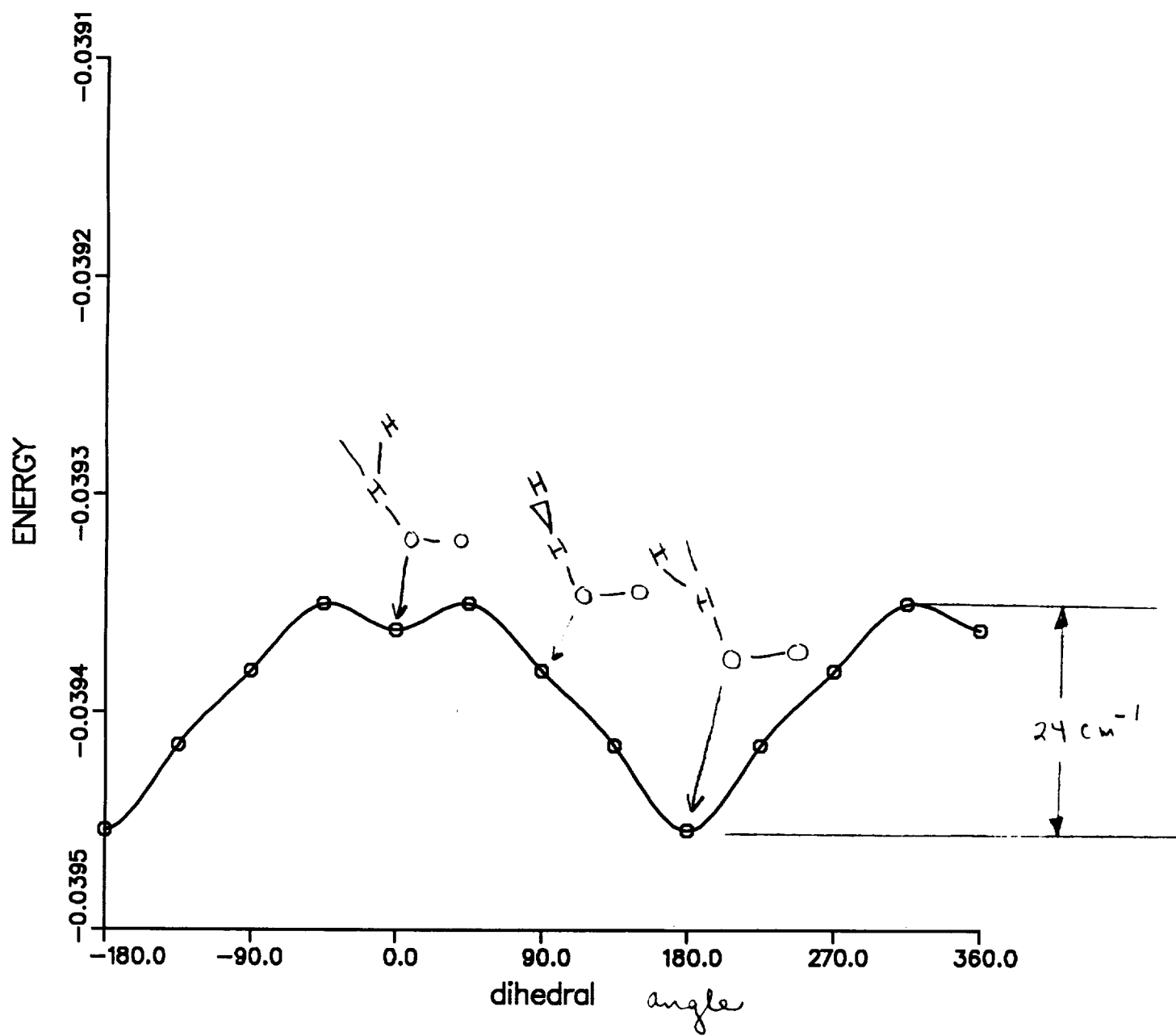


Fig. 2

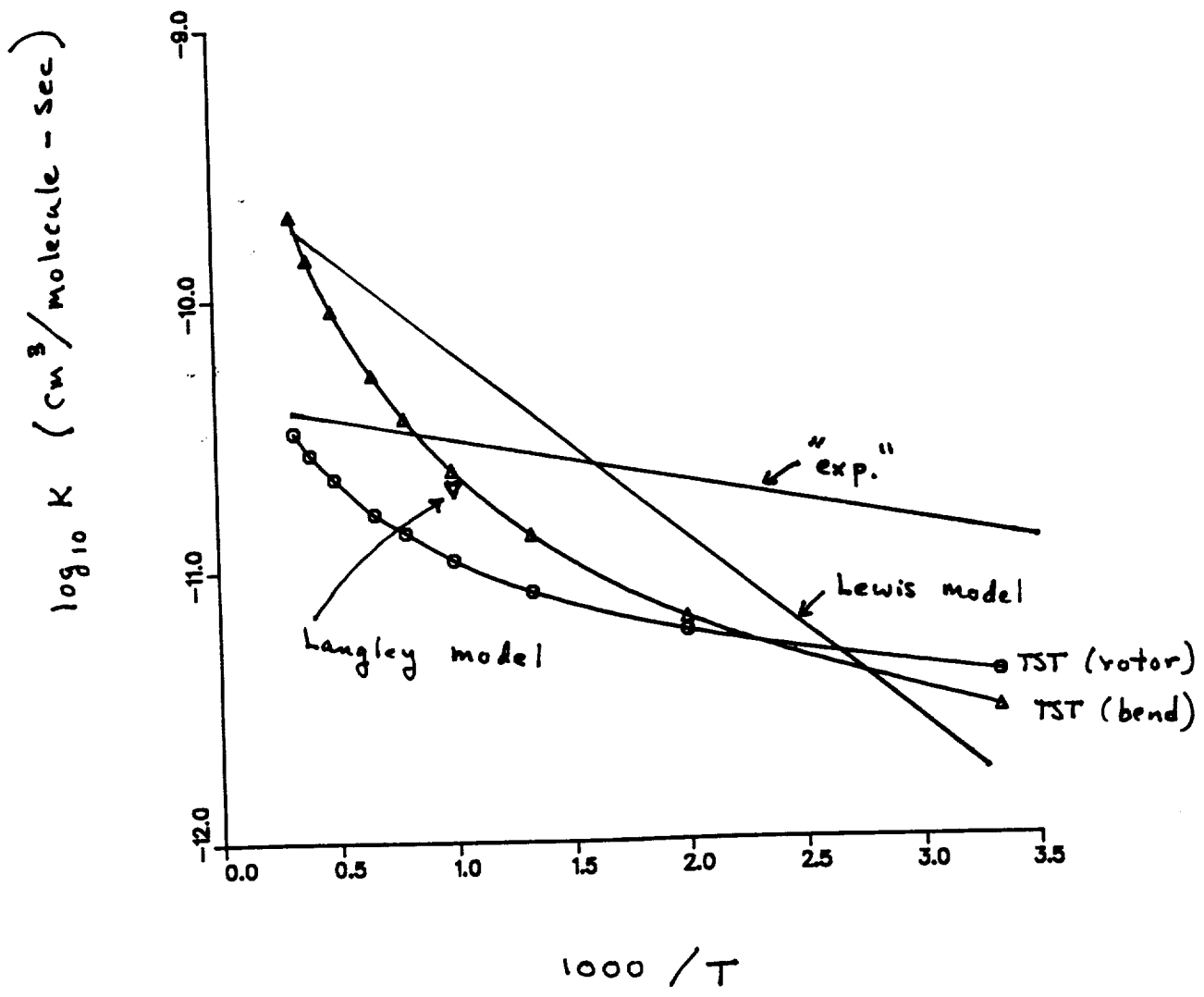


Table I. Computed Saddle Point Properties for H + HOO.

Geometry						
	$\alpha$	$r_{HH}$	$r_{OH}$	$r_{OO}$	$\theta$	
	-3.8	2.238	1.991	2.463	107.1	
Frequencies						
	$\omega_1$	$\omega_2$	$\omega_3$	$\omega_4$	$\omega_5$	$\omega_6$
$d^{2a}$	1736	1391	1226	347	887	1786 i
$d^2-d^{4b}$	1736	1391	1226	347	333	1786 i
Barrier Height						
$\Delta E_b$	3.63					
$\Delta$ ZPE	-1.62					
$\Delta E(\text{corr.})$	2.01					

<sup>a</sup> The dihedral angle is fit with a quadratic term.

<sup>b</sup> The dihedral angle is fit with a quadratic and a quartic term.

Table II. Computed Energies for H + HOO ( $\alpha$  and  $\beta$  variation).

$\alpha$	$\beta$	$r_{OO}$	$\theta$	$r_{HH}$	$r_{OH}$	D2
3.63	180.0	2.457	107.0	2.218	1.997	-151.039454
3.63	135.0	2.457	107.0	2.218	1.997	-151.039415
3.63	90.0	2.457	107.0	2.218	1.997	-151.039381
3.63	45.0	2.457	107.0	2.218	1.997	-151.039350
3.63	0.0	2.457	107.0	2.218	1.997	-151.039362
12.0	180.0	2.457	107.0	2.218	1.997	-151.03920
7.5	180.0	2.457	107.0	2.218	1.997	-151.03939
0.0	0.0	2.457	107.0	2.218	1.997	-151.03945
7.5	0.0	2.457	107.0	2.218	1.997	-151.03919
7.5	90.0	2.457	107.0	2.218	1.997	-151.03926

Table III. Computed Rate for Reaction (2).<sup>a</sup>

---

---

T	$\kappa^b$	rate
300	4.01	0.2976E-11
500	1.79	0.6586E-11
750	1.32	0.1355E-10
1000	1.17	0.2340E-10
1250	1.10	0.3625E-10
1500	1.07	0.5206E-10
2000	1.04	0.9216E-10
2500	1.02	0.1427E-09
3000	1.01	0.2026E-09

<sup>a</sup> Computed using the bend model (see text).

<sup>b</sup>  $\kappa$  is the tunneling correction

Table AI. Computed Energies for H + HOO<sup>a</sup>

$\alpha$	$r_{OO}$	$\theta$	$r_{HH}$	$r_{OH}$	E(hartree)	D1	D2
0.0	2.52	104.4	18.16	1.84 <sup>b</sup>	-151.03432	(-.04594)	(-.04528)
0.0	2.52	104.4	2.4	2.2	-151.01734	(-.03518)	(-.03194)
0.0	2.52	104.4	2.4	2.0	-151.02580	(-.04070)	(-.03913)
0.0	2.52	104.4	2.4	1.8	-151.02563	(-.03901)	(-.03807)
0.0	2.52	104.4	2.2	2.2	-151.02038	(-.04035)	(-.03579)
0.0	2.52	104.4	2.2	2.0	-151.02460	(-.04060)	(-.03854)
0.0	2.52	104.4	2.2	1.8	-151.02157	(-.03554)	(-.03445)
0.0	2.52	104.4	2.0	2.2	-151.02464	(-.04684)	(-.04081)
0.0	2.52	104.4	2.0	2.0	-151.02304	(-.04035)	(-.03764)
0.0	2.52	104.4	2.0	1.8	-151.01589	(-.03058)	(-.02926)
0.0	2.52	104.4	1.8	2.2	-151.02874	(-.05243)	(-.04544)
0.0	2.57	104.4	2.238	2.009	-151.02324	(-.03897)	(-.03708)
0.0	2.52	104.4	2.238	2.009	-151.02469	(-.04059)	(-.03857)
0.0	2.47	104.4	2.238	2.009	-151.02526	(-.04134)	(-.03917)
0.0	2.42	104.4	2.238	2.009	-151.02473	(-.04103)	(-.03867)
0.0	2.37	104.4	2.238	2.009	-151.02287	(-.03939)	(-.03682)
0.0	2.468	100.0	2.238	2.009	-151.02388	(-.03962)	(-.03767)
0.0	2.468	105.0	2.238	2.009	-151.02534	(-.04147)	(-.03926)
0.0	2.468	110.0	2.238	2.009	-151.02498	(-.04150)	(-.03905)

0.0	2.468	115.0	2.238	2.009	-151.02295	(-.03989)	(-.03719)
-10.0	2.468	106.9	2.238	2.009	-151.02525	(-.04164)	(-.03925)
-5.0	2.468	106.9	2.238	2.009	-151.02539	(-.04174)	(-.03938)
0.0	2.468	106.9	2.238	2.009	-151.02541	(-.04169)	(-.03938)
5.0	2.468	106.9	2.238	2.009			
10.0	2.468	106.9	2.238	2.009	-151.02506	(-.04113)	(-.03899)
-2.5	2.468	106.9	2.238	2.009	-151.02541	(-.04173)	(-.03940)
-2.5	2.37	117.	2.238	2.009	-151.02089	(-.03840)	(-.03522)
-2.5	2.37	97.	2.238	2.009	-151.01831	(-.03439)	(-.03211)
-2.5	2.57	117.	2.238	2.009	-151.01835	(-.03509)	(-.03258)
-2.5	2.57	97.	2.238	2.009	-151.02140	(-.03666)	(-.03508)
-2.5	2.37	106.9	2.238	2.1	-151.02326	(-.04199)	(-.03807)
-2.5	2.37	106.9	2.238	1.9	-151.02277	(-.03793)	(-.03610)
-2.5	2.57	106.9	2.238	2.1	-151.02071	(-.03807)	(-.03524)
-2.5	2.57	106.9	2.238	1.9	-151.02385	(-.03861)	(-.03716)
-2.5	2.468	117.	2.238	2.1	-151.02067	(-.03964)	(-.03570)
-2.5	2.468	117.	2.238	1.9	-151.02132	(-.03684)	(-.03490)
-2.5	2.468	97.	2.238	2.1	-151.02009	(-.03715)	(-.03443)
-2.5	2.468	97.	2.238	1.9	-151.02264	(-.03697)	(-.03576)
-2.5	2.37	106.9	2.34	2.009	-151.02333	(-.03931)	(-.03700)

-2.5	2.37	106.9	2.14	2.009	-151.02352	(-.04098)	(-.03789)
-2.5	2.57	106.9	2.34	2.009	-151.02367	(-.03906)	(-.03727)
-2.5	2.57	106.9	2.14	2.009	-151.02236	(-.03892)	(-.03660)
-2.5	2.468	117.	2.34	2.009	-151.02183	(-.03821)	(-.03578)
-2.5	2.468	117.	2.14	2.009	-151.02160	(-.03952)	(-.03627)
-2.5	2.468	97.	2.34	2.009	-151.02258	(-.03756)	(-.03599)
-2.5	2.468	97.	2.14	2.009	-151.02163	(-.03781)	(-.03567)
7.5	2.37	106.9	2.238	2.009	-151.02316	(-.03970)	(-.03714)
7.5	2.57	106.9	2.238	2.009	-151.02284	(-.03863)	(-.03672)
-12.5	2.37	106.9	2.238	2.009	-151.02307	(-.03986)	(-.03711)
-12.5	2.57	106.9	2.238	2.009	-151.02278	(-.03884)	(-.03672)
7.5	2.468	117	2.238	2.009	-151.02152	(-.03852)	(-.03581)
7.5	2.468	97	2.238	2.009	-151.02174	(-.03700)	(-.03538)
-12.5	2.468	117	2.238	2.009	-151.02139	(-.03856)	(-.03569)
-12.5	2.468	97	2.238	2.009	-151.02195	(-.03770)	(-.03573)
7.5	2.468	106.9	2.34	2.009	-151.02556	(-.04106)	(-.03918)
7.5	2.468	106.9	2.14	2.009	-151.02482	(-.04163)	(-.03910)
-12.5	2.468	106.9	2.34	2.009	-151.02548	(-.04122)	(-.03914)
-12.5	2.468	106.9	2.14	2.009	-151.02477	(-.04188)	(-.03912)
7.5	2.468	106.9	2.238	2.1	-151.02354	(-.04125)	(-.03812)
7.5	2.468	106.9	2.238	1.9	-151.02536	(-.04013)	(-.03865)

-12.5	2.468	106.9	2.238	2.1	-151.02352	(-.04154)	(-.03818)
-12.5	2.468	106.9	2.238	1.9	-151.02523	(-.04022)	(-.03857)
-2.5	2.468	106.9	1.8	2.1	-151.02735	(-.04882)	(-.04346)
-2.5	2.468	106.9	1.8	2.4	-151.04332	(-.06928)	(-.06103)
-2.5	2.468	106.9	2.0	2.009	-151.02452	(-.04257)	(-.03933)
-2.5	2.468	106.9	2.0	2.1	-151.02592	(-.04602)	(-.04145)
-2.5	2.468	106.9	2.0	2.4	-151.03369	(-.06055)	(-.05145)
-2.5	2.468	106.9	2.14	1.9	-151.02412	(-.03952)	(-.03772)
-2.5	2.468	106.9	2.14	2.1	-151.02459	(-.04342)	(-.03961)
-2.5	2.468	106.9	2.14	2.2	-151.02411	(-.04554)	(-.03998)
-2.5	2.468	106.9	2.14	2.4	-151.02616	(-.05296)	(-.04372)
-2.5	2.468	106.9	2.238	1.8	-151.02231	(-.03628)	(-.03512)
-2.5	2.468	106.9	2.238	2.2	-151.02192	(-.04230)	(-.03742)
-2.5	2.468	106.9	2.34	1.8	-151.02432	(-.03795)	(-.03689)
-2.5	2.468	106.9	2.34	1.9	-151.02682	(-.04126)	(-.03986)
-2.5	2.468	106.9	2.34	2.1	-151.02315	(-.04019)	(-.03739)
-2.5	2.468	106.9	2.34	2.2	-151.01998	(-.03922)	(-.03506)
-12.0	2.457	106.99	2.218	1.997	-151.02520	(-.04161)	(-.03920)
-7.5	2.457	106.99	2.218	1.997	-151.02539	(-.04177)	(-.03939)
-3.63	2.457	106.99	2.218	1.997	-151.02547	(-.04181)	(-.03945)
0.0	2.457	106.99	2.218	1.997	-151.02547	(-.04176)	(-.03945)
7.5	2.457	106.99	2.218	1.997	-151.02525	(-.04139)	(-.03919)

<sup>a</sup> [4s3p2d1f/3s2p1d] ANO basis set. CASSCF/CCI calculations correlating 10 electrons using a (52) CASSCF active space and selected reference configurations (see text).

<sup>b</sup> This geometry is taken as H + HO<sub>2</sub> at infinite separation.